Published in Applied Energy with doi: 10.1016/j.apenergy.2022.120560

An IoT-enabled hierarchical decentralized framework for multi-energy microgrids market management in the presence of smart prosumers using a deep learning-based forecaster

Seyed Amir Mansouri [1*], Ahmad Rezaee Jordehi [2], Mousa Marzband[1,3], Marcos Tostado-Véliz [4], Francisco Jurado [4], José A. Aguado[5]

[1] Northumbria University, Electrical Power and Control Systems Research Group, Ellison Place NE1 8ST, Newcastle upon Tyne, United Kingdom
[2] Department of Electrical Engineering, Rasht Branch, Islamic Azad University, Rasht, Iran
[3] Center of Research Excellence in Renewable Energy and Power Systems, King Abdulaziz University, Jeddah 21589, Saudi Arabia
[4] Department of Electrical Engineering, University of Jaén, 23700, EPS Linares, Jaén, Spain
[5] Department of Electrical Engineering, Escuela de Ingenierias Industriales, University of Malaga, Malaga, 29010, Spain

Abstract

The integrated exploitation of different energy infrastructures in the form of multi-energy systems (MESs) and the transformation of traditional prosumers into smart prosumers are two effective pathways to achieve net-zero emission energy systems in the near future. Managing different energy markets is one of the biggest challenges for the operators of MESs, since different carriers are traded in them simultaneously. Hence, this paper presents a hierarchical decentralized framework for the simultaneous management of electricity, heat and hydrogen markets among multi-energy microgrids (MEMGs) integrated with smart prosumers. The market strategy of MEMGs is deployed using a hierarchical framework and considering the programs requested by smart prosumers. A deep learning-based forecaster is utilized to predict uncertain parameters while a risk-averse information gap decision theory (IGDT)-based strategy controls the scheduling risk. A new prediction-based mechanism for designing dynamic demand response (DR) schemes compatible with smart prosumers' behavior is introduced, and the results illustrate that this mechanism reduces the electricity and heat clearing prices in peak hours by 17.5% and 8.78%, respectively. Moreover, the results reveal that the introduced structure for hydrogen

* Corresponding Author: Amir.mansouri24@gmail.com

exchange through the transportation system has the ability to be implemented in competitive markets. Overall, the simulation results confirm that the proposed hierarchical model is able to optimally manage the competitive markets of electricity, heat and hydrogen by taking advantage of the potential of smart prosumers.

Keywords: Multi-Energy Systems; Smart Prosumers; Machine Learning; Internet of Things; Power-to-Hydrogen Technologies; Electric and Fuel Cell Vehicles.

Nomenclature

Abbreviations	
ADMM	Alternating direction method of multipliers
AI	Artificial intelligence
CHP	Combined heat and power
CNN	Convolutional neural network
CVaR	Conditional value at risk
DR	Demand response
EV	Electric vehicle
FCV	Fuel cell vehicle
HEMS	Home energy management system
HVAC	Heating, ventilation and air conditioning
IGDT	Information gap decision theory
IoT	Internet-of-things
LSTM	Long short-term memory
MEMG	Multi-energy microgrid
MES	Multi-energy system
MI	Mutual information
MILP	Mixed-integer linear programming
MINLP	Mixed-integer non-linear programming
ML	Machine learning
P2G	Power-to-gas
P2H	Power-to-hydrogen
P2X	Power-to-x
PAR	Peak-to-average ratio
RG	Renewable generation
RReliefF	Regression ReliefF
UB	Uncertainty budget
V2I	Vehicle-to-infrastructure
Sets	
t	Time step index
r	Hydrogen refueling station index
c	Charging station index
u	Consumer index
i,j	Node index
e	Electric vehicle index
f	Fuel cell vehicle index
k/o	Buy / Sell bid index
n	Power-to-hydrogen unit index
m	Multi-energy microgrid index
v	Hydrogen transfer truck index

ss	Sub-station index
h	Combined heat and power unit index
b	Boiler index
g	Gas turbine index
w	Wind turbine index
s	Solar panel index
es/hs/gs	Electrical / Thermal / Gas storage devices
d1,d2	Type A/B appliances index
*	Predicted parameter index
^	Fixed schedule index
it	Iteration index
Scalars	
α^{R}	Share of EV / FCV users from DR bonus (%)
$\alpha^{Transfer}$ / $\beta^{Transfer}$	Hydrogen market starting/ending time (h)
α_a / β_a	Starting/Ending operation time of each appliance (h)
α^{Comp}	Compressor coefficient
C^{P}	Specific heat capacity of hot water [J/(g.C°)]
Δt	Time step (h)
ε^{P} / ε^{H}	Maximum deviation of electrical/thermal load from its predicted value (%)
η^{loss}	Loss coefficient of storage devices (%)
η^{Ch} / η^{Dch}	Charge / Discharge efficiency of storage devices (%)
η^{El}	Electrolyzer Efficiency (%)
η^{Solar}	Solar panel efficiency (%)
η^{GT}	Gas turbine efficiency (%)
$\eta^{P,CHP}$ / $\eta^{H,CHP}$	Power / Heat efficiency of CHP (%)
G^{STD}	Standard solar radiation (W/m^2)
$\underline{H2}^{Ch,Connector}$ / $\bar{H2}^{Ch,Connector}$	Min / Max transfer rate of hydrogen refueling station (kg/h)
it^{Max}	Max iteration number
K_{delay}	Thermal delay coefficient
κ	Deviation damping factor
LHV^{H2}	Low heat value of hydrogen (kWh/kg)
LHV^{G}	Low heat value of gas (MJ/kg)
M	Big positive number
M^{H2}	Molar mass of hydrogen (kg/mol)
M^{G}	Volume mass of gas (kg/m^3)
m_q^{HS} / m_q^{HE}	Mass flow rate of heat source / heat exchanger (kg/s)
$\bar{P}^{Ch,Connector}$	Maximum charge rate of charging station (kW)
P^{x} / H^{x}	Power / Heat operating point of the CHP unit (kW)
$\pi^{Avg,x,Market}$	Average cost of electricity / heat / hydrogen market ($/kWh – $/kWh – $/kg)
R^{H2}	Hydrogen constant [J/(mol.K)]
T^{H2}	Internal temperature of the hydrogen tank (K)
V_0	Base voltage of electricity network (V)
v	Velocity of water (m/s)
v_{ci} / v_r / v_{co}	Cut-in/Rated/Cut-out wind speed (m/s)
w^{P} / w^{H}	Weight coefficient indicating the electrical/thermal load importance
$\underline{x}^{Market}$ / $\bar{x}^{Market}$	Min / Max level of electricity / heat / hydrogen Market participation (kW – kW – kg)

Parameters	
$E_{u,d1}^{A} / E_{u,d2}^{B}$	Energy consumption of type A / B appliances (kWh)
$E_{x}^{Initial}$	Initial energy of storage devices (kW – kW – m^3)
$\underline{E}_{x} / \bar{E}_{x}$	Min / Max energy limit of storage devices (kWh – kWh – m^3)
$E_{x}^{H2,Initial}$	Initial pressure of hydrogen tank (Pa)
$\underline{E}_{x}^{H2} / \bar{E}_{x}^{H2}$	Min / Max pressure limit of hydrogen tank (Pa)
$E_{e}^{Ch,Require}$	Energy required by EVs (kW)
G_{t}	Solar radiation (W/m^2)
$G_{i,t}^{Load}$	Gas load (m^3)
$H_{x,t}^{Load}$	Heating load (kW)
$H2_{x,t}^{Load}$	Hydrogen load (kg)
$H_{u}^{Avg,Load}$	Average heating load (kW)
$H2_{r}^{Avg,Load}$	Average hydrogen load (kg)
$\bar{H}_{u,t}^{DR+} / \bar{H}_{u,t}^{DR-}$	Maximum up / down of heating loads by DR scheme (kW)
$\bar{H2}_{r,t}^{DR+} / \bar{H2}_{r,t}^{DR-}$	Maximum up / down of hydrogen loads by DR scheme (kg)
$H2_{f}^{Ch,Require}$	Hydrogen required by FCVs (kg)
$\bar{H2}_{x}^{Ch,Tank} / \bar{H2}_{n}^{Dch,Tank}$	Inflow / Outflow limit of hydrogen tank (kg/h)
$\bar{H2}_{v}^{Ch,Truck} / \bar{H2}_{v}^{Dch,Truck}$	Inflow / Outflow limit of hydrogen transfer truck (kg/h)
$H2_{v}^{Cap,Truck}$	Hydrogen truck capacity (kg)
K_{l}^{Pipe}	Pack constant of the pipeline
$\kappa_{ss,i}^{x,Grid}$	Sub-station mapping
$\kappa_{l,i}^{x,Line}$	Line mapping
L_{l}	Length of the pipeline (m)
$P_{u,t}^{Fix,Load}$	Fixed part of the electrical demand of smart homes (kW)
$\underline{P}_{d1}^{A} / \bar{P}_{d1}^{A}$	Min / Max power of type A appliances (kW)
$P_{d2}^{B,Fix}$	Load demand of type B appliances (kW)
$\bar{P}_{l,t}^{Line} / \bar{Q}_{l,t}^{Line}$	Maximum active/reactive power flow (kW/kVAr)
$P_{x}^{Avg,Load}$	Average electrical load (kW)
$\bar{P}_{x,t}^{DR+} / \bar{P}_{x,t}^{DR-}$	Maximum up / down of electrical loads by DR scheme (kW)
$\bar{P}_{x}^{Ch}$	Maximum charge limit of electrical / thermal / gas storage devices (kW – kW – m^3/h)
$\bar{P}_{x}^{Dch}$	Maximum discharge limit of electrical / thermal / gas storage devices (kW – kW – m^3/h)
$\underline{P}_{g}^{GT} / \bar{P}_{g}^{GT}$	Min / Max power limit of gas turbine (kW)
$\bar{P}_{w}^{Wind}$	Wind turbine capacity (kW)
$\bar{P}_{s}^{Solar}$	Solar panel capacity (kW)
$\underline{Pr}_{i} / \bar{Pr}_{i}$	Min / Max gas pressure (Pa)
π_{t}^{Pen}	Penalty for residents' dissatisfaction ($/kW^2$)
$\pi_{m,t}^{x,MC}$	Marginal cost of MEMGs ($/kWh)
$\pi_{x,t}^{R}$	Base reward for DR participation ($/kWh – $/kWh – $/kg)
$\pi_{x,t}^{P,DR+} / \pi_{x,t}^{P,DR-}$	Hourly reward for participating in the electrical DR scheme ($/kWh)

$\pi_{u,t}^{H,DR+} / \pi_{u,t}^{H,DR-}$	Hourly reward for participating in the heating DR scheme ($/kWh)
$\pi_{r,t}^{H2,DR+} / \pi_{r,t}^{H2,DR-}$	Hourly reward for participating in the hydrogen DR scheme ($/kg)
$\pi_t^{x,Market}$	Market price ($/kWh – $/kWh – $/kg)
π_t^G	Gas price ($/m^3)
π_s^{Solar}	Generation cost of solar panel ($/kWh)
π_w^{Wind}	Generation cost of wind turbine ($/kWh)
$\pi_{m,k,t}^{x,Buy} / \pi_{m,o,t}^{x,Sell}$	The price of buy / sell bids of MEMGs for electricity / heating / hydrogen ($/kWh – $/kWh – $/kg)
$\pi_x^{Storage}$	Operation cost of electrical / thermal / gas storage devices ($/kWh – $/kWh – $/m^3)
R_l / X_l	Resistance / Reactance of electrical Line (ohm)
$T_t^{s,min} / T_t^{s,max}$	Min / Max temperature of supply pipelines (C^o)
$T_i^{r,min} / T_i^{r,max}$	Min / Max temperature of return pipelines (C^o)
T_v^{Fill}	Require time for filling hydrogen truck (h)
$T_{n,x}^{Travel}$	Traveling time of hydrogen trucks (h)
T_v^{Empty}	Require time for emptying hydrogen truck (h)
U_x^{H2}	Hydrogen tank capacity (m^3)
v_t	Wind speed (m/s)
$\hat{x}_{m,k,t}^{Buy} / \hat{x}_{m,o,t}^{Sell}$	Buy / Sell bids created by MEMGs for electricity / heating / hydrogen ($/kWh – $/kWh – $/kg)
Variables	
$C_{u,t}^{SH}$	Operation cost of smart home ($)
$C_{c,t}^{SCS}$	Operation cost of smart charging station ($)
$C_{r,t}^{SRS}$	Operation cost of smart hydrogen refueling station ($)
$C_{g,t}^{GT}$	Operation cost of gas turbine ($)
$C_{n,t}^{P2H}$	Operation cost of power-to-hydrogen unit ($)
$C_{b,t}^{Boiler}$	Operation cost of boiler ($)
$C_{h,t}^{CHP}$	Operation cost of CHP ($)
$C_{w,t}^{Wind}$	Operation cost of wind turbine ($)
$C_{s,t}^{Solar}$	Operation cost of solar panel ($)
$C_{x,t}^{Storage}$	Operation cost of storage devices ($)
$C_{m,t}^{IL}$	Operation cost of industrial load ($)
DF_m	Dissatisfaction factor (%)
$E_{x,t}$	Stored energy in electrical / thermal / gas storage devices (kW – kW – m^3)
$E_{n,t}^{H2}$	Hydrogen tank pressure (Pa)
$G_{l,t}^{Line}$	Gas flow (m^3/h)
$G_{g,t}^{GT}$	Gas turbine gas consumption (m^3)
$G_{h,t}^{CHP}$	CHP gas consumption (m^3)
$G_{b,t}^{Boiler}$	Boiler gas consumption (m^3)
$H_{b,t}^{Boiler}$	Boiler heat generation (kW)
$H_{h,t}^{CHP}$	CHP heat generation (kW)

$H2_{f,t}^{Ch}$	Hydrogen usage of FCV (kg)
$H2_{f,t}^{DR+} / H2_{f,t}^{DR-}$	Upward / Downward level of hydrogen loads by DR scheme (kg)
$H2_{n,t}^{Sell}$	P2H hydrogen generation (kg)
$H2_{r,t}^{Buy} / H2_{m,t}^{Buy}$	Refueling station / Industrial load hydrogen Consumption (kg)
$H2_{n,v,t}^{Sell} / H2_{x,v,t}^{Buy}$	Inflow / Outflow of hydrogen truck (kg)
$H2_{n,t}^{El}$	Electrolyzer hydrogen generation (kg)
$P_{x,t}^{Load} / Q_{x,t}^{Load}$	Active / Reactive electrical load (kW/kVAr)
$P_{x,t}^{DR+} / P_{x,t}^{DR-}$	Upward / Downward level of electrical loads by DR scheme (kW)
$P_{ss,t}^{P,Grid} / Q_{ss,t}^{P,Grid}$	Active / Reactive power exchange with the main grid (kW/kVAr)
$P_{l,t}^{Loss}$	Power loss (kW)
$P_{u,d1,t}^{A} / P_{u,d2,t}^{B}$	Power consumption of Type A / B appliances (kW)
$P_{l,t}^{Line} / Q_{l,t}^{Line}$	Active / Reactive power flow (kW/kVAr)
$P_{x,t}^{Ch} / P_{x,t}^{Dch}$	Charge / Discharge value of storage devices (kW – kW – m^3/h)
$P_{g,t}^{GT} / Q_{g,t}^{GT}$	Active / Reactive power generation by gas turbine (kW/kVAr)
$P_{w,t}^{Wind}$	Wind power generation (kW)
$P_{s,t}^{Solar}$	Solar power generation (kW)
$P_{r,t}^{Sell} / P_{n,t}^{Sell}$	Surplus power of hydrogen refueling station / P2H unit (kW)
$P_{c,t}^{Exchange}$	Power exchange of smart charging station (kW)
$P_{n,t}^{El}$	Electrolyzer power consumption (kg)
$Pr_{i,t}$	Gas pressure (Pa)
$T_{i,t}^{s} / T_{i,t}^{r}$	Temperature of supply / return pipelines (C°)
$T_{l,t}^{s,out} / T_{l,t}^{r,out}$	Outlet temperature of supply / return pipeline (C°)
$V_{i,t}$	Voltage magnitude (V)
$x_{m,t,it}^{Market}$	The amount of power / heating / hydrogen exchange of MEMGs (kW – kW – kg)
$x_{m,k,t}^{Buy} / x_{m,o,t}^{Sell}$	Buy / Sell power by MEMGs for electricity / heating / hydrogen ($/kWh – $/kWh – $/kg)
Binary Variables	
$I_{x,t}^{arrival} / I_{x,t}^{departure}$	Arrival / Departure status of EV and FCV
$I_{m,o,t}^{x,Sell} / I_{m,k,t}^{x,Buy}$	Sell / Buy status of market bids
$I_{n,v,t}^{Start} / I_{x,v,t}^{End}$	Start / End work time of trucks
$I_{x,t}^{Ch} / I_{x,t}^{Dch}$	Charge / Discharge status of storage devices
$I_{g,t}^{GT}$	Gas turbine activity status
$I_{h,t}^{CHP}$	CHP unit activity status
$I_{u,d1,t}^{A} / I_{u,d2,t}^{B}$	Activity status of appliances type A / B
$I_{u,d1,t}^{A,Start} / I_{u,d2,t}^{B,Start}$	Starting flag status of type A / B appliances
$I_{u,d1,t}^{A,End} / I_{u,d2,t}^{B,End}$	Ending flag status of type A / B appliances

1. Introduction

1.1. Background and Motivation

The high speed of climate change and the increasing emission of greenhouse gases in recent decades have transformed energy supply policies, so that new policies have focused on replacing all fossil fuel sources with renewable generations (RGs). Despite the many environmental and economic advantages, these new policies have serious technical challenges [1]. Their main technical challenge is related to the intermittent output of RGs, which poses many threats to the stability and continuity of energy supply. Multi-energy systems are a very effective solution to deal with technical challenges, as energy conversion technologies have advanced significantly in recent years [2].

In multi-energy systems, the excess power of RGs can be converted to other forms of energy using advanced converters. With the progress of water electrolysis and fuel cell technologies, power-to-x (P2X) converters are an effective solution to convert the excess power of RGs to other forms of energy. Depending on their internal structure, P2X converters can convert the excess power of RGs into hydrogen, methanol, methane, and ammonia, which are used in transportation, aircraft, and heavy industries [3].

The management of energy markets in modern multi-energy systems consisting of several MEMGs is one of the main challenges for the operators of these systems. Note that in modern multi-energy systems, different carriers such as electricity, gas, heat, hydrogen, etc. are simultaneously exchanged between MEMGs. Energy markets in modern multi-energy systems, on the one hand, must guarantee the privacy of MEMGs, and on the other hand, must provide a fully competitive environment for the exchange of different forms of energy [4]. Moreover, maintaining energy balance in multi-energy systems is one of the important points that directly affects the price of different energy carriers [5]. DR schemes are a key way to control the energy balance in the network. In multi-energy systems, these schemes can be applied

to different loads and significantly improve the operational flexibility. It should be mentioned that DR schemes that are applied simultaneously to different loads are called integrated DR schemes [6,7].

Over the past years, Internet-of-things (IoT) technologies have been integrated with the home energy management system (HEMS) and play an important role in smart controlling and managing the end users of the system [8]. It should be stated that IoT-based HEMS is the basis of forming smart homes. In addition, modern smart homes are equipped with advanced artificial intelligence (AI) and machine learning (ML) technologies that can be trained and predict the near future [9]. The movement of ordinary buildings towards such an intelligent concept is an important pathway to achieve fully active and intelligent energy systems. In general, the optimal and intelligent energy management of buildings is essential since they account for more than 40% of energy consumption and carbon emissions in the world. This high share of energy consumption in buildings has led to their high impact on energy markets, so that MEMGs market strategies are designed based on their behavior. Therefore, any positive change in the behavior of buildings can lead to achieving more optimal market strategies for MEMGs.

1.2. Literature Review

During the last decade, several studies have proven that the successful participation of stakeholders in energy markets requires the design of an optimal market strategy [10,11]. In this regard, in [12] an optimal strategy for the participation of aggregators in electricity, heat and carbon markets in multi-energy systems under the high penetration of RGs has been introduced. To guarantee the least sharing of information, the problem is formulated using the alternating direction method of multipliers (ADMM) and the results reflect that the simultaneous participation in multi-energy markets significantly reduces the costs of aggregators compared to participation in the single-energy market. In [13] a new strategy for pricing different carriers in multi-energy systems is introduced. In this study, the price correlation between different carriers has been evaluated in detail and guidelines have been provided to reduce this correlation. In [14], a new strategy for the participation of stakeholders in electricity and heat markets is introduced, taking into account power-to-gas (P2G) technologies, in which the uncertainty budget (UB)

method is adopted to increase planning robustness against price uncertainties. The simulation results show that the use of P2G and power-to-hydrogen (P2H) technologies has created a proper linkage between the electricity and gas networks, resulting in 2.13% reduction in total costs. The authors in [15] have introduced a hybrid conditional value at risk (CVaR)-robust based strategy for the participants of an energy hub in day-ahead energy and reserve markets. The Monte Carlo method is utilized to model the uncertainties, whereas the planning risk is controlled by the CVaR method. The proposed strategy is formulated as mixed-integer non-linear programming (MINLP) and its goal is to minimize both operation costs and CO_2 emissions. The simulation results validate the optimality of the proposed strategy in this study.

Several researchers have studied the impact of implementing DR schemes on the management of energy markets in multi-energy systems. For instance, the authors in [16] presented a new strategy for managing day-ahead energy markets in regional multi-energy systems. This strategy is formulated in a bi-level format, where the profit of energy suppliers is maximized in the upper level and the cost of consumers is minimized in the lower level. An integrated DR scheme is applied to different loads and the simulation results prove its effect on improving the economic and environmental indicators of the system. In [17], a two-stage model for the management of energy markets in a multi-energy system is presented, which uses the conditional value-at-risk-based method to model the uncertainties associated with RGs output, EVs' behavior, and the load demand. Besides, the risk of uncertainties is controlled by the IGDT method in this study. The results reflect that a 2% increase in operating costs lowers planning risk by 1.3%. Also, the results demonstrate that the simultaneous consideration of storage devices, EVs and the integrated DR scheme reduced operating costs by 17.5%. In [18], the authors have used P2H technologies to reduce operating costs and CO_2 emissions in MEMGs. Integrated DR schemes and hydrogen storage devices have also been used to neutralize the effects of RGs output power uncertainties. The simulation results show that the proposed strategy not only makes more use of the capacity of RGs, but also reduces the consumption of fossil fuels in the network.

Smart buildings have a very high potential for improving energy efficiency due to the automatic control of their components. In recent years, many studies have been conducted with the aim of improving energy management models in smart buildings, while only a small number of studies have evaluated their effects on the technical and economic indicators of the system. In this regard, [19] introduces a multi-objective HEMS architecture for smart home scheduling, which goals are to reduce the electricity bill, increase the comfort level of residents and reduce peak-to-average ratio (PAR). The proposed HEMS is solved by multi-objective arithmetic optimization algorithm and the results prove its effect on reducing electricity cost and PAR. In [20], the authors presented an IoT-based HEMS for smart homes scheduling, which is programmed based on the non-intrusive load monitoring technique. The proposed system sends the real-time data of the appliances to the users through the ThingSpeak platform to remotely control the consumption of their appliances. The simulation results reveal that the proposed system improves the flexibility of energy management in smart homes. In [21], the authors discuss the importance of managing heating, ventilation and air conditioning (HVAC) systems in smart buildings and show that with the optimal management of these systems, energy consumption costs can be reduced in smart buildings, while the thermal comfort index is maintained in a proper range. [22] presents an optimal system for energy management in smart buildings in which an inverter-based air conditioner is used to control the temperature of the home. In the proposed concept, electrical storage devices are installed next to solar panels to reduce their output fluctuations. Also, an indoor-outdoor temperature model is introduced, which leads to more optimal operation of the air conditioner system. In [23], the impact of smart homes' program on the economic indicators of microgrids has been investigated. To this end, a centralized three-objective model is presented, where operating cost, emission and PAR are the objective functions. The problem is solved by the fuzzy method and the results reveal the high impact of smart consumers on modifying the system demand curve and also reducing the costs of microgrids. Contrary to [23], the authors in [24] introduced a decentralized model for the operation of microgrids, in which the effect of the comfort index of smart homes on the technical and economic indicators of the network

is investigated. The proposed concept is modeled in the form of mixed-integer linear programming (MILP), and the operating cost and the customers' comfort index are the optimization goals. The simulation results reflect that the relative reduction of comfort level leads to considerable improvement of technical and economic indicators.

The spread of RGs and demand side management technologies in recent years has turned a large number of traditional consumers into prosumers. Despite the many technical, economic and environmental advantages, these technologies have made it difficult to predict the behavior of end-users and have increased the number of operational uncertainties [25]. This problem has attracted the attention of researchers towards forecasting techniques. In this regard, the authors in [26] have introduced a new model based on the deep multi-task learning and ensemble method to predict the load demand of a multi-energy system. In this model, three different gated recurrent units are considered, which have high adaptability to different fluctuations of the load curve. The analysis of the simulation results shows that the proposed model can accurately predict the temporal and spatial correlation between different energy networks. In [27], the authors presented a method based on deep belief network for forecasting electrical, heating and gas demands in multi-energy systems. In order to facilitate prediction, first, different loads are numerically analyzed and then they are categorized into different groups. In order to identify hidden features of time series of energy systems, the deep belief network technique is utilized and the simulation results prove the high accuracy of the proposed technique to predict the behavior of systems with different prosumers. In [28], the authors have evaluated the effects of accurate forecasting of uncertain parameters such as the output power of RGs and load demand on the optimal operation of multi-energy systems. To this end, a model based on the multi-task learning method has been introduced and its impact on economic and reliability indicators has been analyzed. In the proposed technique, convolutional neural network (CNN) is used to identify useful aspects of the input data and the simulation results reveal the high accuracy of this model for short-term prediction of different loads in multi-energy systems.

The advancement of P2X converters in recent years has led to a significant increase in their influence in multi-energy systems. Many studies have shown that these converters lead to increased efficiency and flexibility of multi-energy systems while reducing operating costs. In [29], an optimal model for scheduling a distribution system in the presence of a hydrogen-based energy hub is introduced. The hub under study is equipped with a hydrogen storage device and P2H and H2P units. The harmony search algorithm is utilized to solve the model and the results illustrate that P2H and H2P units prevent the elimination of excess production of RGs and subsequently reduce the operating costs significantly. Also, the results reflect that the implementation of the integrated DR scheme leads to the modification of the consumption pattern of electrical and thermal loads. In [30], a multi-objective dynamic method is presented to investigate the short- and long-term effects of installing P2G technology in the energy hub from technical, economic and environmental perspectives. The results reveal that the installation of P2G in the hub consumes a significant part of the CO_2 released by the CHP and boiler units, and thus reduces the emissions of the hub by about 10%. In addition, the results substantiate that P2G installation reduces losses and operating costs perfectly. In [31], the authors have planned the operation of a multi-energy system in the presence of hydrogen storage devices and FCVs. Uncertainties related to production and demand are modeled in a stochastic format and the results reflect that the proposed model reduces operating costs while maintaining energy balance in the system. In addition, the results prove that the simultaneous consideration of hydrogen storage devices and FCVs leads to a significant reduction in system costs. In [32], a bi-objective framework for scheduling the day-ahead energy market of microgrids equipped with P2H units, hydrogen storage devices, fuel cells and EVs is presented. The goals of this model are cost and emission minimization, and the operational uncertainties are modeled by the hybrid robust-stochastic method. The simulation results reflect the high impact of hydrogen-based technologies on reducing costs and emissions. Also, the results reveal that the simultaneous consideration of hydrogen-based technologies and the DR scheme significantly increases the operational flexibility. In [33], the problem of optimal scheduling of MEMGs consisting of electricity, heating and hydrogen

carriers in the presence of EVs, solar panels and P2H and H2P units has been investigated. In this study, the hydrogen produced by the P2H unit is sold to industrial loads. The problem is modeled in MILP form and CVaR method is used to manage the risk arising from the uncertainties of solar panels, load and EVs' behavior. The simulation results confirm the effect of hydrogen-based converters on reducing the operating costs of MEMGs by 9.28%. The authors in [34] presented a multi-objective method for day-ahead scheduling of an integrated electricity-gas-hydrogen system consisting of P2G units and FCVs. In the proposed model, P2G units convert the excess power of RGs into hydrogen and natural-gas to supply the hydrogen needed by FCVs. The operating cost and CO_2 emission are the optimization goals, and the weighted sum method is adopted to solve the model. The results reflect that the presence of P2G and fuel cell vehicle (FCV) units has lowered the operation and emission costs by 8.04% and 9.8%, respectively.

Many researches have substantiated that dynamic thermal rating (DTR) systems lead to the improvement of the economic, reliability and security factors of the power transmission systems. It has been confirmed in [35] that DTR systems are necessary to achieve stable electrical networks. In [36] and [37], the authors have shown the effect of DTR and storage devices on improving the reliability of electrical networks. It has been shown in [38] that deep learning is an effective method for predicting DTR. [39–41] show the significant impact of DTR and information and communication technologies on improving the reliability of cyber-physical systems.

1.3. Research Gap and Contribution

The above literature review reflects that only a few studies have investigated the effects of smart prosumers' behavior at the system level. It can also be seen that there is a lack of a comprehensive model for managing electricity, heat and hydrogen markets among MEMGs in the presence of smart homes, smart electric vehicle (EV) charging stations and smart hydrogen refueling stations. Therefore, the authors of this paper present a hierarchical model consisting of six layers to bridge the above gap. In the proposed model, a fully competitive structure is designed for the simultaneous management of

electricity, heat and hydrogen markets among MEMGs. Also, in order to take advantage of the potential of smart prosumers including smart homes and smart charging and hydrogen refueling stations, incentive DR schemes compatible with their behavior are designed in the proposed model. The main innovations of this work are listed below:

- Presenting a six-layer hierarchical framework for managing energy markets of modern MESs, taking into account energy flow constraints of electricity, gas and heating networks
- Presenting a structure for the hydrogen exchange among MEMGs through the transportation system
- Introducing a novel deep learning-based mechanism for designing dynamic DR schemes with different rewards for smart prosumers
- Utilizing a deep learning-based forecaster and a risk-averse IGDT-based strategy, respectively, for predicting uncertain parameters and managing scheduling risk
- Accurate modeling of indoor consumption of IoT-based smart homes and evaluating the impact of comfortable lifestyle of their residents on energy markets
- Enhancing technical and economic aspects of the MES through modifying the behavior of smart prosumers, EVs, and FCVs

2. System Description

Figure 1 provides an overview of the structure of the studied MES. According to the figure, this system consists of a modified 118-bus electric network [42], a 20-node heating network [43], and a 20-node gas network [44]. It should be mentioned that in this system, hydrogen is delivered to consumption points through the transportation system. The proposed MES consists of 6 MEMGs that are operated in a decentralized framework. As can be seen, renewable and non-renewable generation sources as well as different storage devices are installed on electricity, heating and gas networks. In addition, P2H units, combined heat and power (CHP) units, boilers, and compressors are also considered in the system. It

should be noted that all MEMGs are equipped with smart charging stations and smart hydrogen refueling stations since the system is designed considering the high penetration of EVs and FCVs. Besides, it is assumed that smart stations and EVs /FCVs communicate through the vehicle-to-infrastructure (V2I) system. Therefore, using this system, smart stations send incentive programs to EVs / FCVs and receive their feedback. The locations of smart homes on the electricity grid are marked with green. These homes are connected to electricity and heating networks to supply their electrical and thermal loads, respectively. Therefore, they can change the pattern of their electricity and heat consumption by participating in electrical and thermal DR schemes. Note that smart homes have solar panels and electrical storage devices and supply a significant part of their loads by them.

Studied hydrogen refueling stations in this paper, provide hydrogen through their small-scale P2H units and also purchase from the hydrogen market. It is noteworthy that small-scale P2H units placed in hydrogen refueling stations receive their required power from solar panels. Moreover, it can be observed that P2H units are also considered in the proposed MES, which are powered by their adjacent RGs.

Note that electrolyzer and hydrogen tank are the main components of P2H units. The hydrogen produced by these units is exchanged between MEMGs and subsequently delivered to consumption points through the transportation system. It should be stated that in the studied MES, hydrogen-consuming loads are hydrogen refueling stations and industrial loads, and the hydrogen market is held only between 6 am and 8 pm.

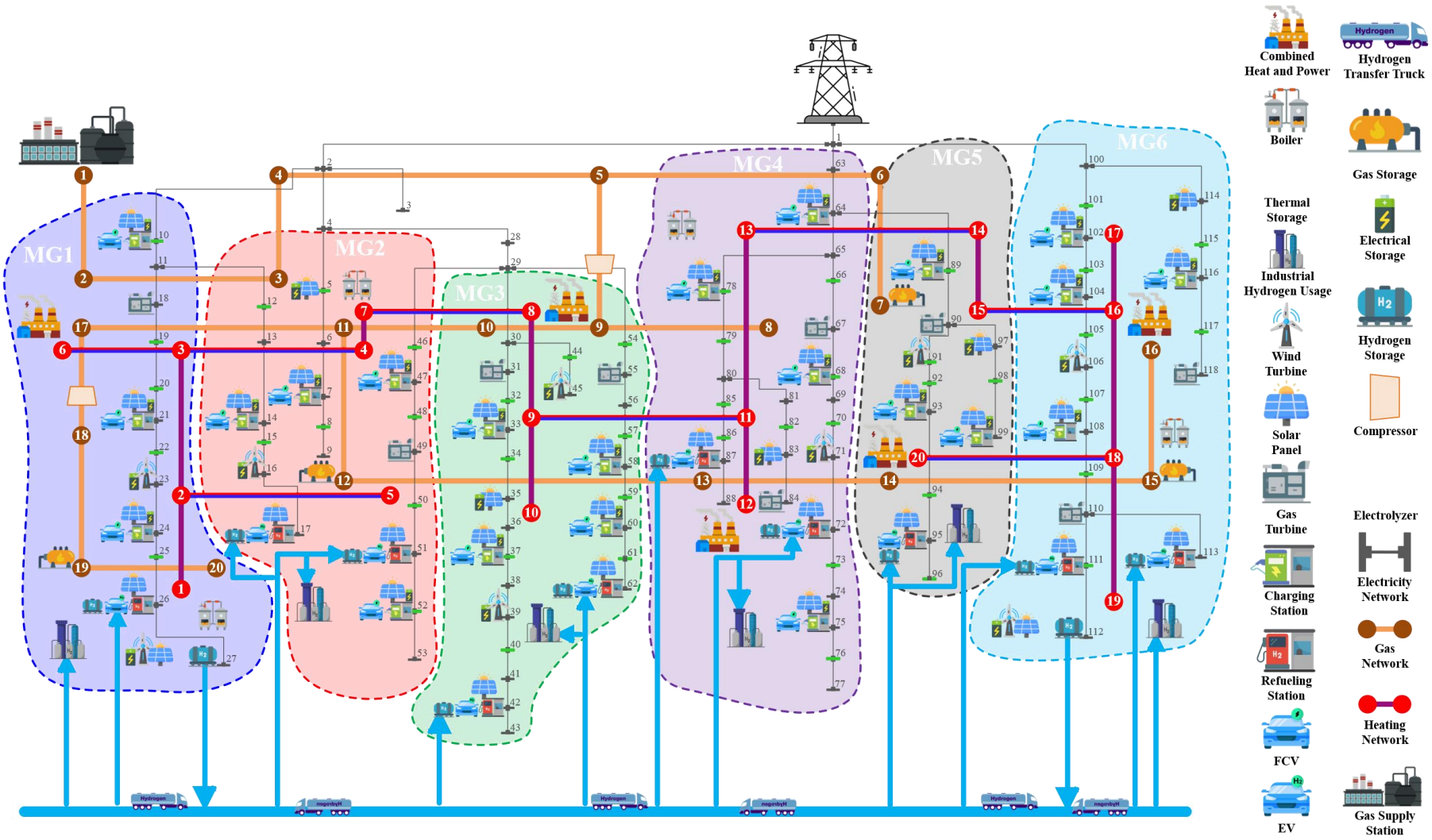

Fig. 1. The overview of the studied multi-energy system

3. Mathematical Modelling

The formulation of the proposed six-layer hierarchical model is introduced in this section. The first layer, which is related to prediction, is modeled in MATLAB, while layers 2 to 6 are formulated in a MILP form so that they can be solved by the powerful CPLEX solver in GAMS. It should be mentioned that the proposed model is designed for the simultaneous management of electricity, heat and hydrogen markets in a competitive and intelligent environment.

- **Layer 1**

In the first layer of the proposed hierarchical framework, a prediction technique based on deep learning is utilized to predict the price of different energy carriers, the demand of different loads, wind speed and solar irradiance. The details of this model are shown in Fig. 2. According to the figure, this technique completes the prediction process in three levels: data preprocessing, hybrid feature selection and prediction [45].

In the first level, data preprocessing is carried out in two steps. In the first step, all historical data related to prices, demands, wind speed and irradiance are merged in the form of a single dataset. Then, in the second step, the merged data is cleaned and normalized to prepare for advanced processing.

In the second level, hybrid feature selection is done in five steps. In the first step, normalized data are clustered where dissimilar samples are removed from them.

In the second step, regression Relieff (RReliefF) instance-based filter feature selection and information theoretic-based mutual information (MI) filter feature selection processes are performed with the aim of finding relevant features [45]. Note that RReliefF is an advanced version of the Relief family algorithms that has the ability to estimate the quality of features in regression problems.

Feature selection identifies relevant features in the dataset and discards everything else as irrelevant and redundant. Note that the feature selection improves the effectiveness and speed of learning algorithm as it reduces the dimensionality of the data. Generally, designing several feature subsets and then combining

them into a single subset leads to finding a better feature subset. Hence, in the third step, mutual information and RReliefF selected in the previous step are merged with the aim of identifying maximal relevant features. It is worth stating that the RReliefF and mutual information filter feature selection defines the relevant features by removing the irrelevant and noninformative features via statistical characteristics [45].

In the fourth step, wrapper feature selection is performed with the aim of tuning the selected features. Finally, In the fifth step, features optimum subset is generated.

In the third level, prediction is done in two steps. In the first step, the long short-term memory (LSTM) deep prediction model is constructed and trained by the features obtained from the previous steps. Ultimately, in the second step, the constructed model is tuned through rolling-based time series cross-validation.

The structure of LSTM cell is depicted in Fig. 2. According to the figure, this cell consists of three gates named forget gate, input gate and output gate. The forget gate specifies the information to be deleted. The input gate determines the information that should be used from the input to update the old cell state to the new cell state. The output gate specifies the information to be included in the output. Equations (a1)-(a6) model the LSTM cell. To this end, forget gate, input gate and output gate are calculated respectively by Eqs. (a1)-(a3). W_f , W_i and W_o denote the weight matrix associated with forget gate, input gate and output gate, respectively. Equations (a4) and (a5) determine the new cell state and candidate, respectively. c_{t-1} denotes the previous cell state. Lastly, hidden state is calculated via Eq. (a6).

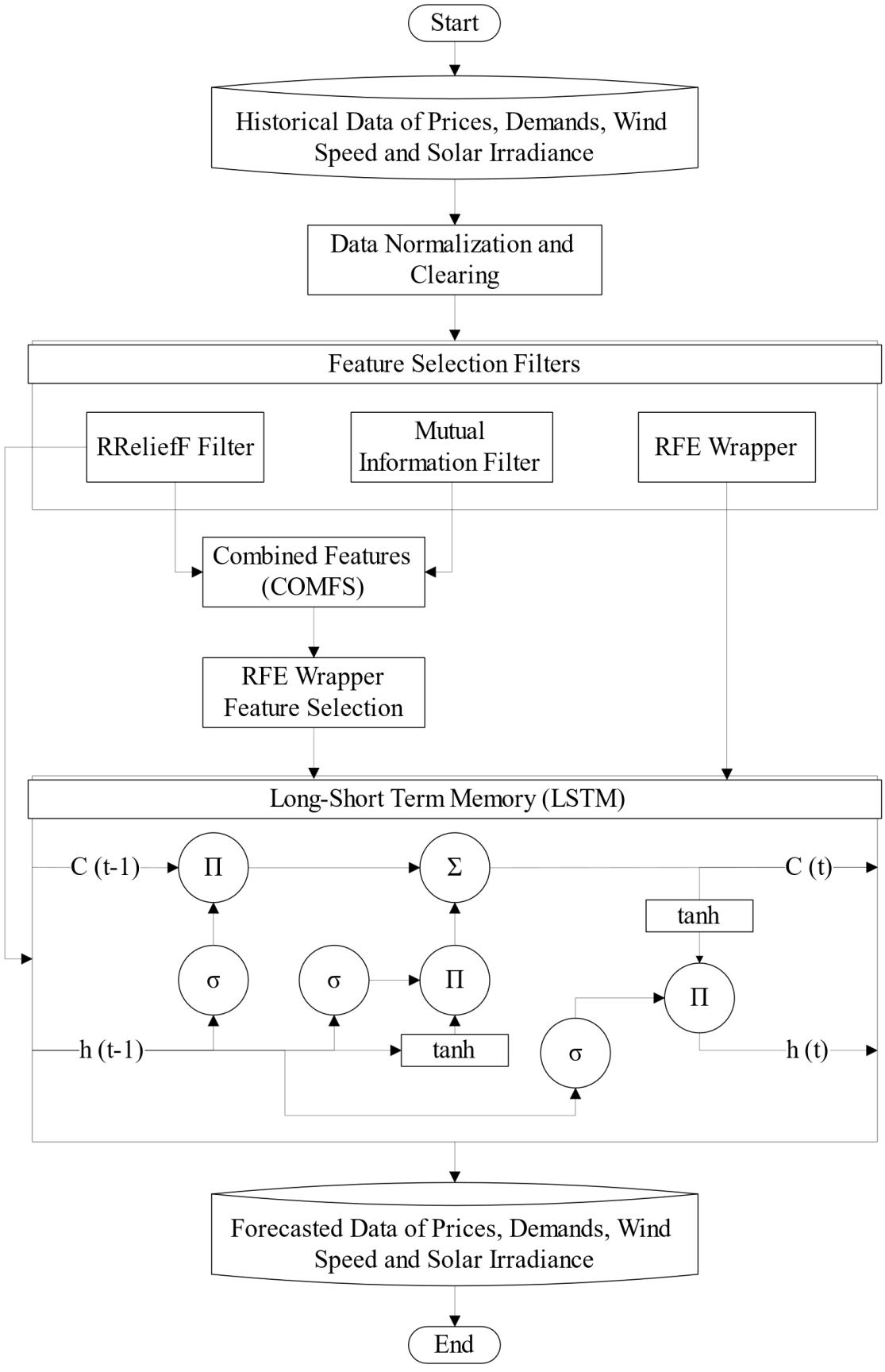

Fig. 2. Details of the deep learning-based forecaster

$$f_t = \sigma\left[W_f\left(h_{t-1}, x_t + b_f\right)\right] \quad \text{(a1)}$$
$$i_t = \sigma\left[W_i\left(h_{t-1}, x_t\right) + b_i\right] \quad \text{(a2)}$$
$$o_t = \sigma\left[W_o\left(h_{t-1}, x_t\right) + b_o\right] \quad \text{(a3)}$$
$$c_t = f_t \odot c_{t-1} + i_t \odot \tilde{c}_t \quad \text{(a4)}$$
$$\tilde{c}_t = \tanh\left[W_c\left(h_{t-1}, x_t\right) + b_c\right] \quad \text{(a5)}$$
$$h_t = o_t \odot \tanh\left(c_t\right) \quad \text{(a6)}$$

- **Layer 2**

In the second layer of the proposed model, using the prediction results, different DR schemes are designed for smart prosumers, including smart homes, smart charging stations, and smart hydrogen refueling stations. In this regard, the functions presented in Eqs. (b1)-(b3) respectively determine the hourly rewards for participation in electrical, heating and hydrogen DR schemes. These functions state that prosumers are rewarded for load reduction in periods above the average load level, and for load increase in periods below the average load level. The amount of reward is determined by an exponential function based on the difference between the average price and the predicted hourly price. Therefore, the amount of reward will be different for each customer and each hour.

$$P_{x,t}^{*Load} \geq P_x^{Avg,Load} \Rightarrow \begin{cases} \bar{P}_{x,t}^{DR-} = P_{x,t}^{*Load} - P_x^{Avg,Load} \\ \pi_{x,t}^{P,DR-} = \pi_{x,t}^{R} e^{\kappa\left|\pi^{Avg,P,Market} - \pi_t^{*P,Market}\right|} \end{cases}$$
$$P_{x,t}^{*Load} \leq P_x^{Avg,Load} \Rightarrow \begin{cases} \bar{P}_{x,t}^{DR+} = P_x^{Avg,Load} - P_{x,t}^{*Load} \\ \pi_{x,t}^{P,DR+} = \pi_{x,t}^{R} e^{\kappa\left|\pi^{Avg,P,Market} - \pi_t^{*P,Market}\right|} \end{cases} \quad x \in \{u,c,r\} \quad \text{(b1)}$$
$$H_{u,t}^{*Load} \geq H_u^{Avg,Load} \Rightarrow \begin{cases} \bar{H}_{u,t}^{DR-} = H_{u,t}^{*Load} - H_u^{Avg,Load} \\ \pi_{u,t}^{H,DR-} = \pi_{u,t}^{R} e^{\kappa\left|\pi^{Avg,H,Market} - \pi_t^{*H,Market}\right|} \end{cases}$$
$$H_{u,t}^{*Load} \leq H_u^{Avg,Load} \Rightarrow \begin{cases} \bar{H}_{u,t}^{DR+} = H_u^{Avg,Load} - H_{u,t}^{*Load} \\ \pi_{u,t}^{H,DR+} = \pi_{u,t}^{R} e^{\kappa\left|\pi^{Avg,H,Market} - \pi_t^{*H,Market}\right|} \end{cases} \quad \text{(b2)}$$
$$H2_{r,t}^{*Load} \geq H2_r^{Avg,Load} \Rightarrow \begin{cases} \bar{H}2_{r,t}^{DR-} = H2_{r,t}^{*Load} - H2_r^{Avg,Load} \\ \pi_{r,t}^{H2,DR-} = \pi_{r,t}^{R} e^{\kappa\left|\pi^{Avg,H2,Market} - \pi_t^{*H2,Market}\right|} \end{cases}$$
$$H2_{r,t}^{*Load} \leq H2_r^{Avg,Load} \Rightarrow \begin{cases} \bar{H}2_{r,t}^{DR+} = H2_r^{Avg,Load} - H2_{r,t}^{*Load} \\ \pi_{r,t}^{H2,DR+} = \pi_{r,t}^{R} e^{\kappa\left|\pi^{Avg,H2,Market} - \pi_t^{*H2,Market}\right|} \end{cases} \quad \text{(b3)}$$

- **Layer 3**

In this layer, smart charging / hydrogen refueling stations send incentive schemes to EVs / FCVs to motivate them to change their schedules. Note that these smart stations give a percentage of the reward received from the operator (α^R) to EVs / FCVs to encourage them to charge their schedules. Equation (c1) models the objective function of the third layer. This objective function is the minimization of EVs / FCVs costs, which is the difference between their charging costs and the rewards received for participating in incentive schemes. The load curve of charging / hydrogen refueling stations after EVs / FCVs participation in incentive programs is obtained through Eq. (c2). Constraint (c3) confines the minimum and maximum hourly charging / filling of each EV / FCV. Equation (c4) expresses that the power / hydrogen injected into each EV / FCV should be equal to its required value. Equation (c5) determines the arrival and departure flags of each EV / FCV. Constraint (c6) is provided to guarantee the continuity of the charging period. Note that the output of layer three is new charging schedule for EVs / FCVs. Constraints (c7) and (c8) limit the participation of EVs / FCVs in DR schemes.

$$\begin{aligned}\min F^3 = &\sum_c \left[\sum_{e\in\Omega_c^e} \sum_t \left(\pi_t^{*P,Market} P_{e,t}^{Ch} \right) - \alpha^R \left(\pi_{c,t}^{*P,DR+} P_{e,t}^{DR+} + \pi_{c,t}^{*P,DR-} P_{e,t}^{DR-} \right) \right] \Delta t \\ &+ \sum_r \left[\sum_{f\in\Omega_r^f} \sum_t \left(\pi_t^{*H2,Market} H2_{f,t}^{Ch} \right) - \alpha^R \left(\pi_{r,t}^{*H2,DR+} H2_{f,t}^{DR+} + \pi_{r,t}^{*H2,DR-} H2_{f,t}^{DR-} \right) \right] \Delta t \end{aligned} \quad \text{(c1)}$$

$$\begin{cases} \sum_{e\in\Omega_c^e} P_{e,t}^{Ch} = P_{c,t}^{*Load} + \sum_{e\in\Omega_c^e} \left(P_{e,t}^{DR+} - P_{e,t}^{DR-} \right) \\ \sum_{f\in\Omega_r^f} H2_{f,t}^{Ch} = H2_{r,t}^{*Load} + \sum_{f\in\Omega_r^f} \left(H2_{f,t}^{DR+} - H2_{f,t}^{DR-} \right) \end{cases} \quad \text{(c2)}$$

$$\begin{cases} 0 \le P_{e,t}^{Ch} \le \bar{P}^{Ch,Connector} I_{e,t}^{Ch} \\ 0 \le H2_{f,t}^{Ch} \le \bar{H2}^{Ch,Connector} I_{f,t}^{Ch} \end{cases} \quad \text{(c3)}$$

$$\begin{cases} \sum_t P_{e,t}^{Ch} \Delta t = E_e^{Ch,Require} \\ \sum_t H2_{f,t}^{Ch} \Delta t = H2_f^{Ch,Require} \end{cases} \quad \text{(c4)}$$

$$I_{x,t}^{arrival} - I_{x,t}^{departure} = I_{x,t}^{Ch} - I_{x,t-1}^{Ch} \qquad x \in \{e, f\} \quad \text{(c5)}$$

$$\sum_t \left(I_{x,t}^{arrival} + I_{x,t}^{departure} \right) \le 2 \qquad x \in \{e, f\} \quad \text{(c6)}$$

$$\begin{cases} \sum_{e\in\Omega_c^e} P_{e,t}^{DR-} \le \hat{\bar{P}}_{c,t}^{DR-} \\ \sum_{f\in\Omega_r^f} H2_{f,t}^{DR-} \le \hat{\bar{H}}2_{r,t}^{*DR-} \end{cases} \quad \text{(c7)}$$

$$\begin{cases} \sum_{e\in\Omega_c^e} P_{e,t}^{DR+} \le \widehat{\bar{P}}_{c,t}^{DR+} \\ \sum_{f\in\Omega_r^f} H2_{f,t}^{DR+} \le \widehat{\bar{H}}2_{r,t}^{DR+} \end{cases} \quad \text{(c8)}$$

- **Layer 4**

In the fourth layer, smart homes, smart charging stations and smart hydrogen refueling stations do their scheduling with the aim of minimizing daily costs and taking into account the DR schemes provided by the MEMG operator (in layer 2). It should be mentioned that EVs / FCVs charge schedule obtained in the third layer is given as input parameters to this layer so that stations can be planned based on them. In Eqs. (d1)-(d3), the objective functions of smart homes, smart charging stations and smart hydrogen refueling stations are given. As it can be observed, the objective functions of these prosumers consist of their operating cost and the reward received for participating in DR schemes. Note that at the end of the fourth layer and after determining the values of the variables related to the power exchange of smart homes, charging stations and hydrogen refueling stations, their hourly energy shortage / surplus values are sent to the MEMG operator.

$$\min F^{4,1} = \sum_u \left(\sum_t C_{u,t}^{SH} - \left(\pi_{u,t}^{P,DR+} P_{u,t}^{DR+} + \pi_{u,t}^{P,DR-} P_{u,t}^{DR-} + \pi_{u,t}^{H,DR+} H_{u,t}^{DR+} + \pi_{u,t}^{H,DR-} H_{u,t}^{DR-} \right) \right) \quad \text{(d1)}$$

$$\min F^{4,2} = \sum_c \left[\sum_t \left(C_{c,t}^{SCS} - \left(1-\alpha^R\right) \left(\pi_{c,t}^{P,DR+} P_{c,t}^{DR+} + \pi_{c,t}^{P,DR-} P_{c,t}^{DR-} \right) \right) \right] \quad \text{(d2)}$$

$$\min F^{4,3} = \sum_r \left[\sum_t \left(C_{r,t}^{SRS} - \left(1-\alpha^R\right) \left(\pi_{r,t}^{H2,DR+} H2_{r,t}^{DR+} + \pi_{r,t}^{H2,DR-} H2_{r,t}^{DR-} \right) \right) \right] \quad \text{(d3)}$$

- **Layer 5**

In the fifth layer, MEMGs make their market strategies according to the programs received from the fourth layer. To this end, each MEMG minimizes the daily costs of its service area through Eq. (e1). It should be stated that each MEMG only has access to the information of its area and this objective function is solved separately for each MEMG in to guarantee the decentralization of scheduling. Equations (e2)-(e4) ensure the balance of electrical, heating and hydrogen consumption within the

service area of each MEMG. The marginal price of each carrier (electricity, heating, hydrogen) is equal to the shadow price of its balance equation (e2-e4). Equation (e5) is used to calculate the amount of power, heating and hydrogen exchanges in each MEMG. This equation is solved in 10 repetitions for each hour, which results in obtaining 10 different values for the exchange variable related to each carrier in that hour. Note that putting each of these values in the power balance equations leads to obtaining a different marginal price. The functions presented in Eqs. (e6) and (e7) store the values obtained for the exchange variables and the marginal prices related to them in new parameters and form the bids. At the end of the fifth layer, each MEMG makes a number of buy/sell bids (10 bids per carrier per hour) and sends them to the pool market.

$$\min F_m^5 = \sum_t \left(\begin{array}{l} \sum_{g\in\Omega_m^g} C_{g,t}^{GT} + \sum_{u\in\Omega_m^u} C_{u,t}^{SH} + \sum_{c\in\Omega_m^c} C_{c,t}^{SCS} + \sum_{r\in\Omega_m^r} C_{r,t}^{SRS} + \sum_{n\in\Omega_m^n} C_{n,t}^{P2H} + \sum_{b\in\Omega_m^b} C_{b,t}^{Boiler} \\ + \sum_{h\in\Omega_m^h} C_{h,t}^{CHP} + \sum_{w\in\Omega_m^w} C_{w,t}^{Wind} + \sum_{s\in\Omega_m^s} C_{s,t}^{Solar} + \sum_{x\in\Omega_m^x}^{x\in\{es,hs,gs\}} C_{x,t}^{Storage} + C_{m,t}^{IL} \end{array} \right) \quad \text{(e1)}$$

$$\sum_{g\in\Omega_m^g} P_{g,t}^{GT} + \sum_{w\in\Omega_m^w} P_{w,t}^{Wind} + \sum_{s\in\Omega_m^s} P_{s,t}^{Solar} + \sum_{es\in\Omega_m^{es}} P_{es,t}^{Dch} + \sum_{r\in\Omega_m^r} P_{r,t}^{Sell} + \sum_{n\in\Omega_m^n} P_{n,t}^{Sell} + P_{m,t}^{Market} = \sum_{i\in\Omega_m^i} P_{i,t}^{Load} + \sum_{c\in\Omega_m^c} P_{c,t}^{Exchange} + \sum_{es\in\Omega_m^{es}} P_{es,t}^{Ch} \quad , \quad \pi_{m,t}^{P,MC} \quad \text{(e2)}$$

$$\sum_{b\in\Omega_m^b} H_{b,t}^{Boiler} + \sum_{h\in\Omega_m^h} H_{h,t}^{CHP} + \sum_{hs\in\Omega_m^{es}} P_{hs,t}^{Dch} + H_{m,t}^{Market} = \sum_{i\in\Omega_m^i} H_{i,t}^{Load} + \sum_{hs\in\Omega_m^{es}} P_{hs,t}^{Ch} \quad , \quad \pi_{m,t}^{H,MC} \quad \text{(e3)}$$

$$\sum_{n\in\Omega_m^n} H2_{n,t}^{Sell} + H2_{m,t}^{Market} = \sum_{i\in\Omega_m^i} H2_{i,t}^{Load} + \sum_{r\in\Omega_m^r} H2_{r,t}^{Buy} + H2_{m,t}^{Buy} \quad , \quad \pi_{m,t}^{H2,MC} \quad \text{(e4)}$$

$$x_{m,t,it}^{Market} = \underline{x}^{Market} + \left(\frac{it-1}{it^{Max}-1} \right) \left(\overline{x}^{Market} \right) \qquad x \in \{P, H, H2\} \quad \text{(e5)}$$

$$if \ x_{m,t,it}^{Market} \geq 0 \ \rightarrow \ \begin{cases} \widehat{x}_{m,k=it,t}^{Buy} = x_{m,t,it}^{Market} \\ \pi_{m,k=it,t}^{x,Buy} = \pi_{m,t}^{x,MC} \end{cases} \qquad x \in \{P, H, H2\} \quad \text{(e6)}$$

$$if \ x_{m,t,it}^{Market} \leq 0 \ \rightarrow \ \begin{cases} \widehat{x}_{m,o=it,t}^{Sell} = \left| x_{m,t,it}^{Market} \right| \\ \pi_{m,o=it,t}^{x,Sell} = \pi_{m,t}^{x,MC} \end{cases} \qquad x \in \{P, H, H2\} \quad \text{(e7)}$$

- **Layer 6**

In the sixth layer, the clearing of electricity, heat and hydrogen markets is done by the market manager. Equation (f1) shows that the goal of this layer is to maximize social welfare. Equation (f2) calculates the amount of power / heating / hydrogen exchange of MEMGs according to the approved bids. Equations (f3)-(f5) are provided to model power, heating and hydrogen limitations, respectively. $C^p m_q^{HS} \left(T_{i,t}^s - T_{i,t}^r \right)$

and $C^p m_q^{HE}\left(T_{i,t}^s - T_{i,t}^r\right)$ calculate the injected and consumed heating power in each node, respectively. $P_{l,t}^{Line}$ is the power flow in MEMG boundary lines; $H_{n,v,t}^{Sell}$ and $H_{x,v,t}^{Buy}$ are the exported and imported hydrogens from / to MEMG, respectively. Constraints (f6) and (f7) limit market transactions to bids sent by MEMGs. Finally, constraint (f8) only allows one bid to be accepted for each MEMG at time *t*.

$$\min F^6 = \sum_x \sum_t \sum_m \left(\sum_k \left(\pi_{m,k,t}^{x,Buy} x_{m,k,t}^{Buy} \right) - \sum_o \left(\pi_{m,o,t}^{x,Sell} x_{m,o,t}^{Sell} \right) \right) \quad \text{(f1)}$$

$$x_{m,t}^{Market} = \sum_o x_{m,o,t}^{Sell} - \sum_k x_{m,k,t}^{Buy} \quad \text{(f2)}$$

$$P_{m,t}^{Market} = \sum_{l \in \Delta_m^l} P_{l,t}^{Line} \quad \text{(f3)}$$

$$H_{m,t}^{Market} = \sum_{i \in \Omega_m^i} C^p m_q^{HS}\left(T_{i,t}^s - T_{i,t}^r\right) - \sum_{i \in \Omega_m^i} C^p m_q^{HE}\left(T_{i,t}^s - T_{i,t}^r\right) \quad \text{(f4)}$$

$$H2_{m,t}^{Market} = \sum_{n \in \Omega_m^n} \sum_v H2_{n,v,t}^{Sell} - \sum_{x \in \Omega_m^x} \sum_v H2_{x,v,t}^{Buy} \qquad x \in \{r, m\} \quad \text{(f5)}$$

$$0 \le x_{m,o,t}^{Sell} \le \hat{x}_{m,o,t}^{Sell} I_{m,o,t}^{x,Sell} \qquad x \in \{P, H, H2\} \quad \text{(f6)}$$

$$0 \le x_{m,k,t}^{Buy} \le \hat{x}_{m,k,t}^{Buy} I_{m,k,t}^{x,Buy} \qquad x \in \{P, H, H2\} \quad \text{(f7)}$$

$$\sum_o I_{m,o,t}^{x,Sell} + \sum_k I_{m,k,t}^{x,Buy} \le 1 \qquad x \in \{P, H, H2\} \quad \text{(f8)}$$

- **Electricity Network Constraints**

A linear power flow problem is presented in (g1)-(g7) to model the electricity network restrictions [46]. In (g1), the voltage magnitude at the end of the line *l* ($V_{j,t}$) is calculated, which is a function of the voltage magnitude at the beginning of this line ($V_{i,t}$) and the voltage drop along the line. $P_{l,t}^{Line}$ and $Q_{l,t}^{Line}$ are active and reactive power flows; V_0 is the base voltage of the 118-bus distribution network. Constraints (g2) and (g3) are provided to confine the flow of active and reactive powers, respectively. Similarly, the upper and lower limits of the voltage are confined by the constraint (g4). The power loss is calculated via Eq. (g5) and based on the flow of active and reactive powers. Finally, Eqs. (g6) and (g7) respectively guarantee the nodal balance of active and reactive powers. $P_{ss,t}^{PGrid}$ and $P_{l,t}^{Line}$ respectively represent the power purchased from the upstream grid and the power flow of the line *l*. $\kappa_{ss,i}^{PGrid}$ is a binary variable whose value is 1 only for the bus connected to the upstream grid. $\kappa_{l,i}^{Line}$ is the binary variable

related to the power passing through the line *l*, whose value can be 1 or -1 according to the flow direction [47].

$$V_{j,t} = V_{i,t} - \frac{R_l Q_{l,t}^{Line} + X_l P_{l,t}^{Line}}{V_0} \tag{g1}$$

$$-\bar{P}_{l,t}^{Line} \le P_{l,t}^{Line} \le \bar{P}_{l,t}^{Line} \tag{g2}$$

$$-\bar{Q}_{l,t}^{Line} \le Q_{l,t}^{Line} \le \bar{Q}_{l,t}^{Line} \tag{g3}$$

$$V_i^{\min} \le V_{i,t} \le V_i^{\max} \tag{g4}$$

$$P_{l,t}^{Loss} = R_l \left[\left(P_{l,t}^{Line} \right)^2 + \left(Q_{l,t}^{Line} \right)^2 \right] \tag{g5}$$

$$\begin{aligned} &\sum_{ss \in \Omega_i^{ss}} \kappa_{ss,i}^{P,Grid} P_{ss,t}^{P,Grid} + \sum_{l \in \Omega_i^l} \left(\kappa_{l,i}^{P,Line} P_{l,t}^{Line} + \frac{P_{l,t}^{Loss}}{2} \right) + \sum_{g \in \Omega_i^g} P_{g,t}^{GT} + \sum_{h \in \Omega_i^h} P_{h,t}^{CHP} + \sum_{w \in \Omega_i^w} P_{w,t}^{Wind} \\ &+ \sum_{s \in \Omega_i^s} P_{s,t}^{Solar} + \sum_{es \in \Omega_i^{es}} P_{es,t}^{Dch} + \sum_{r \in \Omega_i^r} P_{r,t}^{Sell} + \sum_{n \in \Omega_i^n} P_{n,t}^{Sell} = P_{i,t}^{Load} + \sum_{c \in \Omega_i^c} P_{c,t}^{Exchange} + \sum_{es \in \Omega_i^{es}} P_{es,t}^{Ch} \end{aligned} \tag{g6}$$

$$\sum_{ss \in \Omega_i^{ss}} \kappa_{ss,i}^{P,Grid} Q_{ss,t}^{P,Grid} + \sum_{l \in \Omega_i^l} \kappa_{l,i}^{P,Line} Q_{l,t}^{Line} + \sum_{g \in \Omega_i^g} Q_{g,t}^{GT} = Q_{i,t}^{Load} \tag{g7}$$

- **Heating Network Constraints**

The necessary relations for modeling the heating network are provided in (h1)-(h9) [43]. Note that this heating network has supply and return pipes for transferring hot water. The amount of heating power injected to each node is calculated by Eq. (h1). CHP, boiler and thermal storage device are components that inject heating power into the heating network. $T_{i,t}^s$ and $T_{i,t}^r$ are the temperature of the supply and return networks, respectively; m_q^{HS} and C^p denote the mass flow rate of the pipeline heat medium and specific heat capacity of the medium, respectively. Temperature changes in nodes with heating load are determined through Eq. (h2). Equations (h3) and (h4) show how to calculate the temperature of the supply and return networks, respectively. Constraints (h5) and (h6) are provided to confine the nodal supply and return temperatures, respectively. Equation (h7) denotes that the delay time of temperature change is a function of flow speed, pipe length and its thermal delay coefficient. K_{delay}, L_l and v denote thermal delay coefficient, pipe length and water velocity, respectively. Finally, Eq. (h8) is provided to calculate the temperature at the outlet of each pipe. This equation expresses that the outlet temperature

of each pipe is a function of its inlet temperature, delay time, heating losses. T_t^a represents the ambient temperature.

$$\sum_{h\in\Omega_i^h} H_{h,t}^{CHP} + \sum_{b\in\Omega_i^b} H_{b,t}^{Boiler} + \sum_{hs\in\Omega_i^{hs}} P_{hs,t}^{Dch} = C^p m_q^{HS}\left(T_{i,t}^s - T_{i,t}^r\right) \quad \text{(h1)}$$

$$H_{i,t}^{Load} + \sum_{hs\in\Omega_i^{hs}} P_{hs,t}^{Ch} = C^p m_q^{HE}\left(T_{i,t}^s - T_{i,t}^r\right) \quad \text{(h2)}$$

$$\sum_{l\in\Omega_i^l}\left(T_{l,t}^{s,out} m_{l,t}^s\right) = T_{i,t}^s \sum_{l\in\Omega_i^l} m_{l,t}^s \quad \text{(h3)}$$

$$\sum_{l\in\Omega_i^f}\left(T_{l,t}^{r,out} m_{l,t}^r\right) = T_{i,t}^r \sum_{l\in\Omega_i^f} m_{l,t}^r \quad \text{(h4)}$$

$$T_t^{s,min} \le T_{i,t}^s \le T_t^{s,max} \quad \text{(h5)}$$

$$T_i^{r,min} \le T_{i,t}^r \le T_i^{r,max} \quad \text{(h6)}$$

$$T_l^{delay} = K_{delay}\frac{L_l}{v} \quad \text{(h7)}$$

$$T_{l,t}^{s,out} = \left(T_{l,t-T_l^{delay}}^{s,in} - T_{t-T_l^{delay}}^a\right)e^{-\frac{\lambda L}{C^p m_q}} + T_t^a \quad \text{(h8)}$$

- **Gas Network Constraints**

Gas network operational restrictions are modeled by (i1)-(i3) [44]. In this regard, constraint (i1) is presented to confine the nodal gas pressure. Equation (i2) is provided to calculate the gas flow in each pipe. Note that to simplify the simulation, this equation is linearized by the piecewise method. $Pr_{i,t}$ and $Pr_{j,t}$ respectively indicate the pressures at the beginning and end of the pipe; K_l^{Pipe} is the constant coefficient of the pipe, which depends on its physical characteristics. Finally, the nodal balance of the gas network is ensured through Eq. (i3).

$$\underline{Pr}_i \le Pr_{i,t} \le \bar{Pr}_i \quad \text{(i1)}$$

$$G_{l,t}^{Line}\left|G_{l,t}^{Line}\right| = \left(K_l^{Pipe}\right)^2\left[\left(Pr_{i,t}\right)^2 - \left(Pr_{j,t}\right)^2\right] \quad \text{(i2)}$$

$$\sum_{ss\in\Omega_i^{ss}} \kappa_{ss,i}^{G,Grid} G_{ss,t}^{G,Grid} + \sum_{l\in\Omega_i^l} \kappa_{l,i}^{G,Line} G_{l,t}^{Line} + \sum_{gs\in\Omega_i^s} P_{gs,t}^{Dch} = G_{i,t}^{Load} + \sum_{g\in\Omega_i^g} G_{g,t}^{GT} + \sum_{h\in\Omega_i^h} G_{h,t}^{CHP} + \sum_{b\in\Omega_i^b} G_{b,t}^{Boiler} + \sum_{gs\in\Omega_i^s} P_{gs,t}^{Ch} \quad \text{(i3)}$$

- **Hydrogen Transfer Constraints**

In Eqs. (j1)-(j11) a linear model for hydrogen transport by truck is introduced. Equation (j1) is the limitation of hydrogen extraction from the P2H tank. $H2_{n,v,t}^{Sell}$ and $\bar{H2}_n^{Dch,Tank}$ are the output hydrogen from

the P2H tank at time *t* and the outflow limit of the tank, respectively. $I_{n,v,t}^{Start}$ is a binary variable that shows the time flag when the tanker truck starts to fill. This restriction is also implemented in the case of simultaneous injection of hydrogen to several trucks, as shown in (j2). Constraints (j3) and (j4) model the restrictions of hydrogen injection from the truck to the P2H tank. $I_{x,v,t}^{End}$ is a binary variable that indicates the flag of the loading completion time. Constraints (j5) and (j6) state that each truck can only connect to one source or sink at time *t*. Since the time of holding the hydrogen market is between 6 am and 8 pm, the start and end time of the trucks is limited via constraints (j7) and (j8). Equation (j9) determines the completion time of hydrogen injection from the truck to the sink. $I_{x,v,t}^{End} ord(t)$ is the end time of hydrogen injection into the sink. $I_{n,v,t}^{Start} ord(t)$ is the starting time of loading the truck tank. T_v^{Fill}, $T_{n,x}^{Travel}$ and T_v^{Empty} are the times required for loading, reaching the destination, and unloading, respectively. Note that travel times between different production and consumption points are considered different. The times required for loading and unloading the truck tank are calculated by Eqs. (j10) and (j11). Constraint (j12) expresses that the amount of hydrogen injected into the truck tank must be less than its capacity. Finally, constraint (j13) expresses that total loading and total unloading by trucks during the operation period should be equal.

$$H2_{n,v,t}^{Sell} \le I_{n,v,t}^{Start} \bar{H}2_n^{Dch,Tank} \Delta t \quad \text{(j1)}$$

$$\sum_v H2_{n,v,t}^{Sell} \le \bar{H}2_n^{Dch,Tank} \Delta t \quad \text{(j2)}$$

$$H2_{x,v,t}^{Buy} \le I_{x,v,t}^{End} \bar{H}2_x^{Ch,Tank} \Delta t \qquad x \in \{r,m\} \quad \text{(j3)}$$

$$\sum_k H2_{x,v,t}^{Buy} \le \bar{H}2_x^{Ch,Tank} \Delta t \qquad x \in \{r,m\} \quad \text{(j4)}$$

$$\sum_n \sum_t I_{n,v,t}^{Start} \le 1 \quad \text{(j5)}$$

$$\sum_x \sum_t I_{x,v,t}^{End} \le 1 \qquad x \in \{r,m\} \quad \text{(j6)}$$

$$I_{n,v,t}^{Start} ord(t) \ge \alpha^{Transfer} \quad \text{(j7)}$$

$$I_{x,v,t}^{End} ord(t) \le \beta^{Transfer} \qquad x \in \{r,m\} \quad \text{(j8)}$$

$$I_{x,v,t}^{End} ord(t) \ge I_{n,v,t}^{Start} ord(t) + T_v^{Fill} + T_{n,x}^{Travel} + T_v^{Empty} \qquad x \in \{r,m\} \quad \text{(j9)}$$

$$T_v^{Fill} = \frac{\sum_n \sum_t H2_{n,v,t}^{Sell}}{\bar{H}2_v^{Ch,Truck}} \quad \text{(j10)}$$

$$T_v^{Empty} = \frac{\sum_x \sum_t H_{x,v,t}^{Buy}}{\bar{H}2_v^{Dch,Truck}} \qquad x \in \{r,m\} \qquad \text{(j11)}$$

$$\sum_n \sum_t H2_{n,v,t}^{Sell} \le H2_v^{Cap,Truck} \qquad \text{(j12)}$$

$$\sum_n \sum_v \sum_t H2_{n,v,t}^{Sell} = \sum_x \sum_v \sum_t H2_{x,v,t}^{Buy} \qquad x \in \{r,m\} \qquad \text{(j13)}$$

- **Electrical, Thermal and Gas Storage Devices**

In (k1)-(k6) a formulation for modeling electrical, thermal and gas storage devices is presented [44]. In Eqs. (k1) and (k2), respectively, the variables related to the injection and extraction of power / heating / gas to / from the storage devices are limited. In order to determine the injection and extraction status, $I_{x,t}^{Ch}$ and $I_{x,t}^{Dch}$ decision variables are used. Equation (k3) denotes how to calculate the energy level of the storage at time *t*. The energy stored in storage devices is confined by constraint (k4). Constraint (k5) expresses that injection and extraction operations cannot be performed simultaneously. Equation (k6) models the equality of the energy level at the beginning and end of operation. Finally, equation (k7) is provided to calculate the operating cost of the storage device.

$$0 \le P_{x,t}^{Ch} \le \bar{P}_x^{Ch} I_{x,t}^{Ch} \qquad x \in \{es,hs,gs\} \qquad \text{(k1)}$$

$$0 \le P_{x,t}^{Dch} \le \bar{P}_x^{Dch} I_{x,t}^{Dch} \qquad x \in \{es,hs,gs\} \qquad \text{(k2)}$$

$$E_{x,t} = \left(1-\eta^{loss}\right) E_{x,t} + \left(\eta^{Ch} P_{x,t}^{Ch} - \frac{P_{x,t}^{Dch}}{\eta^{Dch}}\right) \Delta t \qquad x \in \{es,hs,gs\} \qquad \text{(k3)}$$

$$\underline{E}_x \le E_{x,t} \le \bar{E}_x \qquad x \in \{es,hs,gs\} \qquad \text{(k4)}$$

$$0 \le I_{x,t}^{Ch} + I_{x,t}^{Dch} \le 1 \qquad x \in \{es,hs,gs\} \qquad \text{(k5)}$$

$$E_{x,t=24} = E_{x,t=0} = E_x^{Initial} \qquad x \in \{es,hs,gs\} \qquad \text{(k6)}$$

$$C_{x,t} = \pi_x^{Storage} \left(P_{x,t}^{Ch} + P_{x,t}^{Dch}\right) \qquad x \in \{es,hs,gs\} \qquad \text{(k7)}$$

- **Distributed Energy Resources**

The operation of distributed energy resources is modeled according to Eqs. (l1)-(l17) . In this regard, gas turbines are formulated through the Eqs. (l1)-(l3) [44]. The active power produced by gas turbine *g* at time *t* is calculated via Eq. (l1). Besides, constraints (l2) and (l3) maintain the active and reactive output powers of gas turbines in a predetermined range. The function presented in (l4) shows that the wind

speed determines the output power of wind turbines. Moreover, Eq. (l5) illustrates the direct effect of radiation on the output power of solar panels. Figure 4 denotes the feasible operating region of CHP units used in this study. Constraints (l6)-(l10) are provided to keep the operating point of CHP within this region. In this regard, constraint (l6) keeps the operating point of CHP below the line AB while constraint (l7) keeps this operating point above the line BC. Besides, constraint (l8) keeps the CHP operating point above the line CD. $I_{h,t}^{CHP}$ is a binary variable that determines whether CHP is on / off. Finally, constraints (l9) and (l10) limit the boundaries of heat and power production in CHP [48]. Equations (l11) and (l12), respectively, calculate the gas consumed by the gas turbine and boiler. Equation 13 models the relationship between the inlet and outlet of compressors placed on the gas network. According to this equation, the compressor receives the gas at its inlet and injects it into the network at a higher pressure. Ultimately, Eqs. (l14) - (l18) calculate the operating cost of different network components.

$$P_{g,t}^{GT} = \frac{M^{G} LHV^{G} \eta^{GT} G_{g,t}^{GT}}{3.6} \tag{l1}$$

$$\underline{P}_{g}^{GT} I_{g,t}^{GT} \le P_{g,t}^{GT} \le \bar{P}_{g}^{GT} I_{g,t}^{GT} \tag{l2}$$

$$-\alpha_{g}^{GT} Q_{g,t}^{GT} \le Q_{g,t}^{GT} \le \alpha_{g}^{GT} Q_{g,t}^{GT} \tag{l3}$$

$$P_{w,t}^{Wind} = \begin{cases} 0 & , \ v_t < v_{ci} \quad \text{Or} \ \ v_t \ge v_{co} \\ \bar{P}_{w}^{Wind} \dfrac{v_t - v_{ci}}{v_r - v_{ci}} & , \ v_{ci} \le v_t < v_r \\ \bar{P}_{w}^{Wind} & , \ v_r \le v_t < v_{co} \end{cases} \tag{l4}$$

$$P_{s,t}^{Solar} = \eta^{Solar} \frac{G_t}{G^{STD}} \bar{P}_{s}^{Solar} \tag{l5}$$

$$P_{h,t}^{CHP} \le P^{A} - \frac{P^{A} - P^{B}}{H^{A} - H^{B}} (H_{h,t}^{CHP} - H^{A}) \tag{l6}$$

$$P_{h,t}^{CHP} \ge P^{B} - \frac{P^{B} - P^{C}}{H^{B} - H^{C}} (H_{h,t}^{CHP} - H^{B}) - \ (1 - I_{h,t}^{CHP}) M \tag{l7}$$

$$P_{h,t}^{CHP} \ge P_{C}^{CHP} - \frac{P^{C} - P^{D}}{H^{C} - H^{D}} (H_{h,t}^{CHP} - H^{C}) - \ (1 - I_{h,t}^{CHP}) M \tag{l8}$$

$$0 \le H_{h,t}^{CHP} \le H^{B} I_{h,t}^{CHP} \tag{l9}$$

$$P^{C} I_{h,t}^{CHP} \le P_{h,t}^{CHP} \le P^{A} I_{h,t}^{CHP} \tag{l10}$$

$$G_{b,t}^{CHP} = \frac{3.6}{M^{G} LHV^{G}} \left(\frac{P_{h,t}^{CHP}}{\eta^{P,CHP}} + \frac{H_{h,t}^{CHP}}{\eta^{H,CHP}} \right) \tag{l11}$$

$$G_{b,t}^{Boiler} = \frac{3.6H_{b,t}^{Boiler}}{M^{G} LHV^{G} \eta^{Boiler}} \quad (l12)$$

$$Pr_{j} = \alpha^{Comp} Pr_{i} \quad (l13)$$

$$C_{g,t}^{GT} = \pi_{t}^{G} G_{g,t}^{GT} \quad (l14)$$

$$C_{w,t}^{Wind} = \pi_{w}^{Wind} P_{w,t}^{Wind} \Delta t \quad (l15)$$

$$C_{s,t}^{Solar} = \pi_{s}^{Solar} P_{s,t}^{Solar} \Delta t \quad (l16)$$

$$C_{h,t}^{CHP} = \pi_{t}^{Gas} G_{h,t}^{CHP} \quad (l17)$$

$$C_{b,t}^{Boiler} = \pi_{t}^{Gas} G_{b,t}^{Boiler} \quad (l18)$$

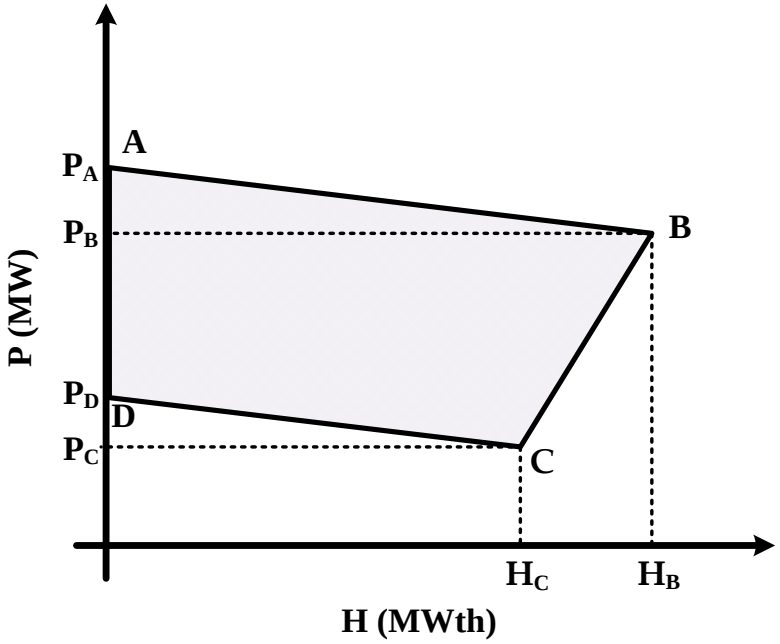

Fig. 3. Feasible operation area of CHP unit [48]

- **P2H Units**

In order to model P2H units, Eqs. (m1)-(m10) are presented. It is noteworthy to state that these units are integrated with wind and solar units to get their required power from them. Hydrogen produced in P2H units is calculated through Eq. (m1) [49]. LHV^{H2}, $P_{n,t}^{El}$ and η^{El} are the lower heat value, the electricity consumed by the electrolyzer and its efficiency, respectively. Constraint (m2) imposes a limit on the electrolyzer power consumption. Equation (m3) expresses that the level of hydrogen in the current hour depends on the injection and extraction of hydrogen to / from the tank, as well as the level of hydrogen in the previous hour. Constraint (m4) confines the hydrogen level during operation. Constraint (m5) sets the hydrogen level at a fixed value in the first and last hours of the operation. The power balance of P2H

units is modeled through Eq. (m6). This equation expresses that the total power produced by wind and solar units should be equal to the total power consumed in the electrolyzer and sold to the grid. It should be noted that only the surplus power of the mentioned renewable units is sold to the grid. It should be stated that only the surplus generation of these renewable units is sold to the grid. Finally, Eq. (m7) expresses that the hourly costs of P2H units includes the operating costs of their RGs, and the profit from selling hydrogen and power to the grid.

$$H2_{n,t}^{El} = \frac{\eta^{El} P_{n,t}^{El}}{LHV^{H2}} \quad \text{(m1)}$$

$$\underline{P}_n^{El} \le P_{n,t}^{El} \le \overline{P}_n^{El} \quad \text{(m2)}$$

$$E_{n,t}^{H2} = E_{n,t-1}^{H2} + \frac{R^{H2} T^{H2}}{U_n^{H2} M^{H2}} \left(H2_{n,t}^{El} - H2_{n,t}^{Sell} \right) \quad \text{(m3)}$$

$$\underline{E}_n^{H2} \le E_{n,t}^{H2} \le \overline{E}_n^{H2} \quad \text{(m4)}$$

$$E_{n,t=24}^{H2} = E_{n,t=0}^{H2} = E_n^{H2,Initial} \quad \text{(m5)}$$

$$\sum_{w \in \Omega_n^w} P_{w,t}^{Wind} + \sum_{s \in \Omega_n^s} P_{s,t}^{Solar} = P_{n,t}^{El} + P_{n,t}^{Sell} \quad \text{(m6)}$$

$$C_{n,t}^{P2H} = \sum_{w \in \Omega_n^w} C_{w,t}^{Wind} + \sum_{s \in \Omega_n^s} C_{s,t}^{Solar} - \pi_t^{*P,Market} P_{n,t}^{Sell} - \pi_t^{*H2,Market} H2_{n,t}^{Sell} \quad \text{(m7)}$$

- **Smart Hydrogen Refueling Stations**

Hydrogen refueling stations are operated according to Eqs. (n1)-(n6). Note that smart hydrogen refueling stations do their scheduling with the aim of minimizing daily costs and taking into account the schedule of FCVs (obtained from the third layer). These stations supply hydrogen through their small-scale P2H units and also purchase from the hydrogen market. Small-scale P2H units located in hydrogen refueling stations supply their required power through PV panels and also purchase from the electricity network. Equation (n1) calculates the hydrogen produced by small-scale P2H units, whereas constraint (n2) limits the power consumption of the electrolyzer. Eq. (n3) determines the hydrogen level of the tank in the current hour according to its level in the previous hour ($E_{r,t-1}^{H2}$) and the amount of hydrogen injection and extraction to / from it. R^{H2} and T^{H2} represent hydrogen constant and internal temperature of the hydrogen tank, respectively; U_r^{H2} and M^{H2} represent tank capacity and molar mass of hydrogen, respectively.

Constraints (n4) and (n5) confine the hydrogen level during the operation. Equation (n6) expresses that the power generated by solar panels can be injected into the electrolyzer or sold to the grid. Finally, Eq. (n7) calculates the hourly costs of hydrogen refueling stations.

$$H2_{r,t}^{El} = \frac{\eta^{El} P_{r,t}^{El}}{LHV^{H2}} \tag{n1}$$

$$\underline{P}_{\mathrm{r}}^{El} \le P_{r,t}^{El} \le \bar{P}_{r}^{El} \tag{n2}$$

$$E_{r,t}^{H2} = E_{r,t-1}^{H2} + \frac{R^{H2} T^{H2}}{U_{r}^{H2} M^{H2}} \left(H2_{r,t}^{El} + H2_{r,t}^{Buy} - \sum_{f \in \Omega_r^f} \widehat{H2}_{f,t}^{Ch} - H2_{r,t}^{DR+} + H2_{r,t}^{DR-} \right) \tag{n3}$$

$$E_{r,t=24}^{H2} = E_{r,t=0}^{H2} = E_{r,t}^{H2,Initial} \tag{n4}$$

$$\underline{E}_{r}^{H2} \le E_{r,t}^{H2} \le \bar{E}_{r}^{H2} \tag{n5}$$

$$\sum_{s \in \Omega_r^s} P_{s,t}^{Solar} = P_{r,t}^{El} + P_{r,t}^{Sell} \tag{n6}$$

$$C_{r,t}^{SRS} = \sum_{s \in \Omega_r^s} C_{s,t}^{Solar} + \pi_t^{*H2,Market} H2_{r,t}^{Buy} - \pi_t^{*P,Market} P_{r,t}^{Sell} - \pi_t^{*H2,Market} \sum_{f \in \Omega_r^f} \widehat{H2}_{f,t}^{Ch} \tag{n7}$$

- **Industrial Hydrogen Loads**

Industrial hydrogen loads are modeled by Eqs. (o1)-(o5). It should be noted that every hydrogen industrial load is equipped with a hydrogen tank. The level of available hydrogen in the tank is calculated via Eq. (o1). $H2_{m,t}^{Buy}$ and $H2_{m,t}^{Load}$ are hydrogen injected and extracted to / from the tank, respectively. The equality of the level of hydrogen stored in the tank during the first and last hours of operation is guaranteed by (o2). The upper and lower limits of the hydrogen stored in the tank are confined by constraint (o3). Equation (o4) states that the total amount of hydrogen purchased from trucks must be equal to the amount of hydrogen injected into the tank ($H2_{m,t}^{Buy}$). Finally, the cost of hydrogen purchased by the industrial hydrogen load is calculated in Eq. (o5).

$$E_{m,t}^{H2} = E_{m,t-1}^{H2} + \frac{R^{H2} T^{H2}}{U_{m}^{H2} M^{H2}} \left(H2_{m,t}^{Buy} - H2_{m,t}^{Load} \right) \tag{o1}$$

$$E_{m,t=24}^{H2} = E_{m,t=0}^{H2} = E_{m,t}^{H2,Initial} \tag{o2}$$

$$\underline{E}_{m}^{H2} \le E_{m,t}^{H2} \le \bar{E}_{m}^{H2} \tag{o3}$$

$$H2_{m,t}^{Buy} = \sum_{v} H2_{m,v,t}^{Buy} \tag{o4}$$

$$C_{m,t}^{IL} = \pi_t^{*H2,Market} H2_{m,t}^{Buy} \tag{o5}$$

- **Smart Charging Stations**

The relations needed for modeling charging stations are presented in Eqs. (p1) and (p2). These stations receive the schedule of EVs as input data and perform their scheduling according to them with the aim of minimizing daily costs. Note that charging stations are equipped with PV panels and electrical storage devices. Equation (p1) ensures power balance in charging stations. The daily cost of charging stations is calculated according to the Eq. (p2), which is the difference between their income and expenses.

$$P_{c,t}^{Exchange} + P_{c,t}^{PV} + \sum_{es \in \Omega_c^{es}} P_{es,t}^{Dch} + P_{c,t}^{DR-} = \sum_{es \in \Omega_c^{es}} P_{es,t}^{Ch} + \sum_{e \in \Omega_c^{e}} \widehat{P}_{e,t}^{Ch} + P_{c,t}^{DR+} \quad \text{(p1)}$$

$$C_{r,t}^{SCS} = \sum_{s \in \Omega_r^{s}} C_{s,t}^{Solar} + \pi_t^{P,Market} P_{c,t}^{Exchange} - \pi_t^{P,Market} \sum_{e \in \Omega_c^{e}} \widehat{P}_{e,t}^{Ch} \quad \text{(p2)}$$

- **Smart Homes**

IoT-based smart homes are modeled according to Eqs. (q1)-(q12). In the proposed model, two types of appliances are considered for these houses; Type A and type B. In type A appliances, both operating time and load consumption can be controlled, while in type B appliances, only operating time can be controlled. $P_{u,d1,t}^{A}$ and $P_{u,d2,t}^{B}$ denote the load consumption of type A and type B appliances, respectively. Equation (q1) states that the load of each smart home consists of a fixed amount ($P_{u,t}^{Fix,Load}$), the load of type A appliances ($P_{u,d1,t}^{A}$), the load of type B appliances ($P_{u,d2,t}^{B}$) and the amount of participation in DR programs. Constraints (q2) and (q3) ensure the complete operation of these appliances. Constraint (q4) is provided to confine the upper and lower borders of the power consumption in the type A appliances. Constraint (q5) expresses that if type B appliances are active, their power consumption will be equal to a fixed value. The activation of appliances types A and B is determined by the binary variables $I_{u,d1,t}^{A}$ and $I_{u,d2,t}^{B}$, respectively. Constraint (q6) does not allow appliances to be operated outside the allowed range. The flags of start and stop times of appliances are determined by Eqs. (q7) and (q8). Constraint (q9) prohibits simultaneous start and stop of an appliance. Constraint (q10) prevents interrupting the operation of appliances. Equation (q11) is introduced to make sure of the electricity balance in the smart

home. Equation 12 enables the participation of smart homes in thermal DR schemes. Equation (q13) calculates the hourly cost of the smart home, which consists of power and heat exchange with the networks, the penalty for residents' dissatisfaction (due to deviation from the preferred electrical and heating demands), the operating costs associated with the solar panel and the electrical storage device. The restrictions presented in (q14) limit the range of changes in electrical and heating loads of smart homes. ε^P and ε^H are the values of the maximum changes of electrical and heating loads, respectively, and their value is equal to 15%. Ultimately, the dissatisfaction factor is calculated through Eq. (q15). w^P and w^H are weight coefficients to determine the importance of electrical and thermal loads and their values are assumed to be 1 and 0.9, respectively.

$$P_{u,t}^{Load} = P_{u,t}^{Fix,Load} + \sum_{d1} P_{u,d1,t}^{A} + \sum_{d2} P_{u,d2,t}^{B} + P_{u,t}^{DR+} - P_{u,t}^{DR-} \tag{q1}$$

$$E_{u,d1}^{A} = \sum_{t\in[\alpha_a,\beta_a]} P_{u,d1,t}^{A}\Delta t \tag{q2}$$

$$E_{u,d2}^{B} = \sum_{t\in[\alpha_a,\beta_a]} P_{u,d2,t}^{B}\Delta t \tag{q3}$$

$$\underline{P}_{d1}^{A} I_{u,d1,t}^{A} \le P_{u,d1,t}^{A} \le \bar{P}_{d1}^{A} I_{u,d1,t}^{A} \tag{q4}$$

$$P_{u,d2,t}^{B} = P_{d2}^{B,Fix} I_{u,d2,t}^{B} \tag{q5}$$

$$\begin{cases} P_{u,d1,t}^{A} = 0 \\ P_{u,d2,t}^{B} = 0 \end{cases} \qquad t \notin [\alpha_a, \beta_a] \tag{q6}$$

$$-\bar{P}_{d1}^{A} I_{u,d1,t}^{A,End} \le P_{u,d1,t}^{A} - P_{u,d1,t-1}^{A} \le \underline{P}_{d1}^{A} I_{u,d1,t}^{A,Start} \tag{q7}$$

$$-P_{d2}^{B,Fix} I_{u,d2,t}^{B,End} \le P_{u,d2,t}^{B} - P_{u,d2,t-1}^{B} \le P_{d2}^{B,Fix} I_{u,d2,t}^{B,Start} \tag{q8}$$

$$\begin{cases} \sum_{t} I_{u,d1,t}^{A,Start} = 1 \\ \sum_{t} I_{u,d2,t}^{B,Start} = 1 \end{cases} \tag{q9}$$

$$\begin{cases} \sum_{t} I_{u,d1,t}^{A,End} = 1 \\ \sum_{t} I_{u,d2,t}^{B,End} = 1 \end{cases} \tag{q10}$$

$$\sum_{s\in\Omega_u^s} P_{s,t}^{Solar} + P_{u,t}^{Buy} + \sum_{es\in\Omega_u^{es}} P_{es,t}^{Dch} = P_{u,t}^{Load} + \sum_{es\in\Omega_u^{es}} P_{es,t}^{Ch} \tag{q11}$$

$$H_{u,t}^{Load} = H_{u,t}^{*Load} + H_{u,t}^{DR+} - H_{u,t}^{DR-} \tag{q12}$$

$$C_{u,t}^{SH} = \pi_t^{P,Market} P_{u,t}^{Buy} + \pi_t^{H,Market} H_{u,t}^{Load} + \pi_t^{P,Pen}\left(P_{u,t}^{Load} - P_{u,t}^{*Load}\right)^2 + \pi_t^{H,Pen}\left(H_{u,t}^{Load} - H_{u,t}^{*Load}\right)^2 + \sum_{s\in\Omega_n^s} C_{s,t}^{Solar} + \sum_{es\in\Omega_n^s} C_{es,t}^{Storage} \tag{q13}$$

$$\begin{cases} \left(1-\varepsilon^p\right) P_{u,t}^{*Load} \le P_{u,t}^{Load} \le \left(1+\varepsilon^p\right) P_{u,t}^{*Load} \\ \left(1-\varepsilon^H\right) H_{u,t}^{*Load} \le H_{u,t}^{Load} \le \left(1+\varepsilon^H\right) H_{u,t}^{*Load} \end{cases} \tag{q14}$$

$$DF_m = \frac{\sum_{u\in\Omega_m^u}\sum_t\left[w^P\left(P_{u,t}^{Load}-P_{u,t}^{*Load}\right)^2+w^H\left(H_{u,t}^{Load}-H_{u,t}^{*Load}\right)^2\right]}{\sum_{u\in\Omega_m^u}\sum_t\left[w^P\left(\varepsilon^P P_{u,t}^{*Load}\right)^2+w^H\left(\varepsilon^H H_{u,t}^{*Load}\right)^2\right]} \quad \text{(q15)}$$

- **Risk Management Constraints**

In the proposed model, an IGDT-based risk-averse strategy has been used to manage the scheduling risk of MEMGs [50]. Equation (r1) specifies the permissible range of fluctuations of the uncertain parameters from the prediction value. This range is different for each parameter. In (r2)-(r6) the relationships required for risk-averse scheduling of MEMGs (in fifth layer) are presented. As can be seen from these equations, in the risk-averse strategy, the operator spends more money to make MEMG scheduling robust against uncertainties. To investigate the effect of the risk management technique in the worst-case condition, underestimated load and price and overestimated generation are considered.

$$U\left(\alpha_x, x_t^*\right)=\left\{x_t:\frac{\left|x_t-x_t^*\right|}{x_t}\le\alpha_x\right\} \qquad x\in\left\{P_{m,t}^{Load}, H_{m,t}^{Load}, H2_{m,t}^{Load}, P_{w,t}^{Wind}, P_{s,t}^{Solar}, \pi_t^{P,Market}, \pi_t^{H,Market}, \pi_t^{H2,Market}\right\} \quad \text{(r1)}$$

$$\widehat{\alpha}_x\left(F_{mg}^{5,R}\right)=\max\left\{\alpha_x^R:\min F_{mg}^5\le F_{mg}^{5,R}\right\} \quad \text{(r2)}$$

$$F_{mg}^{5,R}=\left(1+\rho\right)F_{mg}^{5,predict} \quad \text{(r3)}$$

$$x_t=x_t^*\pm\alpha_x x_t^*\Rightarrow\begin{cases}x_t^*+\alpha_x x_t^* & , \ x\in\{load, price\}\\ x_t^*-\alpha_x x_t^* & , \ x\in\{generation\}\end{cases} \quad \text{(r4)}$$

$$0\le\rho\le1 \quad \text{(r5)}$$

$$\alpha_x\ge0 \quad \text{(r6)}$$

4. Methodology

Figure 4 provides the details required to implement the proposed six-layer hierarchical model. First, it should be noted that the first layer of the proposed model is modeled in MATLAB, while the second to sixth layers are modeled in GAMS. The optimization problem is solved in all six layers for the day-ahead horizon (24 hours) and the time sequence is 1 hour. According to the figure, in the first layer, the operator of each MEMG predicts the price of different energies, the load demands, wind speed and solar irradiance by a deep learning-based forecaster. The operator makes these predictions based on the

historical data of the last month. In the second layer, the operator designs incentive-based DR schemes according to the prediction results and sends them to smart prosumers including smart homes and smart charging / hydrogen refueling stations. In the third layer, smart charging / hydrogen refueling stations design their own incentive programs based on the DR schemes received from the operator and send them to EVs / FCVs. Subsequently, EVs / FCVs determine their new charging schedules according to the received incentive programs from stations. In the fourth layer, smart homes and smart charging / hydrogen refueling stations perform their scheduling in a decentralized environment and according to the designed DR schemes in layer 2. The outcome of the fourth layer is the energy shortage / surplus values of smart prosumers, which are sent to the MEMG operator. In the fifth layer, the MEMG operator plans its area according to the schedules received from smart prosumers, and subsequently makes buy / sell bids to participate in energy markets. Ultimately, in the sixth layer, the operators of MEMGs put their bids in pool markets, where the system operator calculates the clearing prices for different markets with the aim of maximizing social welfare. Table 1 presents the pseudocode to facilitate the simulation of the proposed hierarchical model.

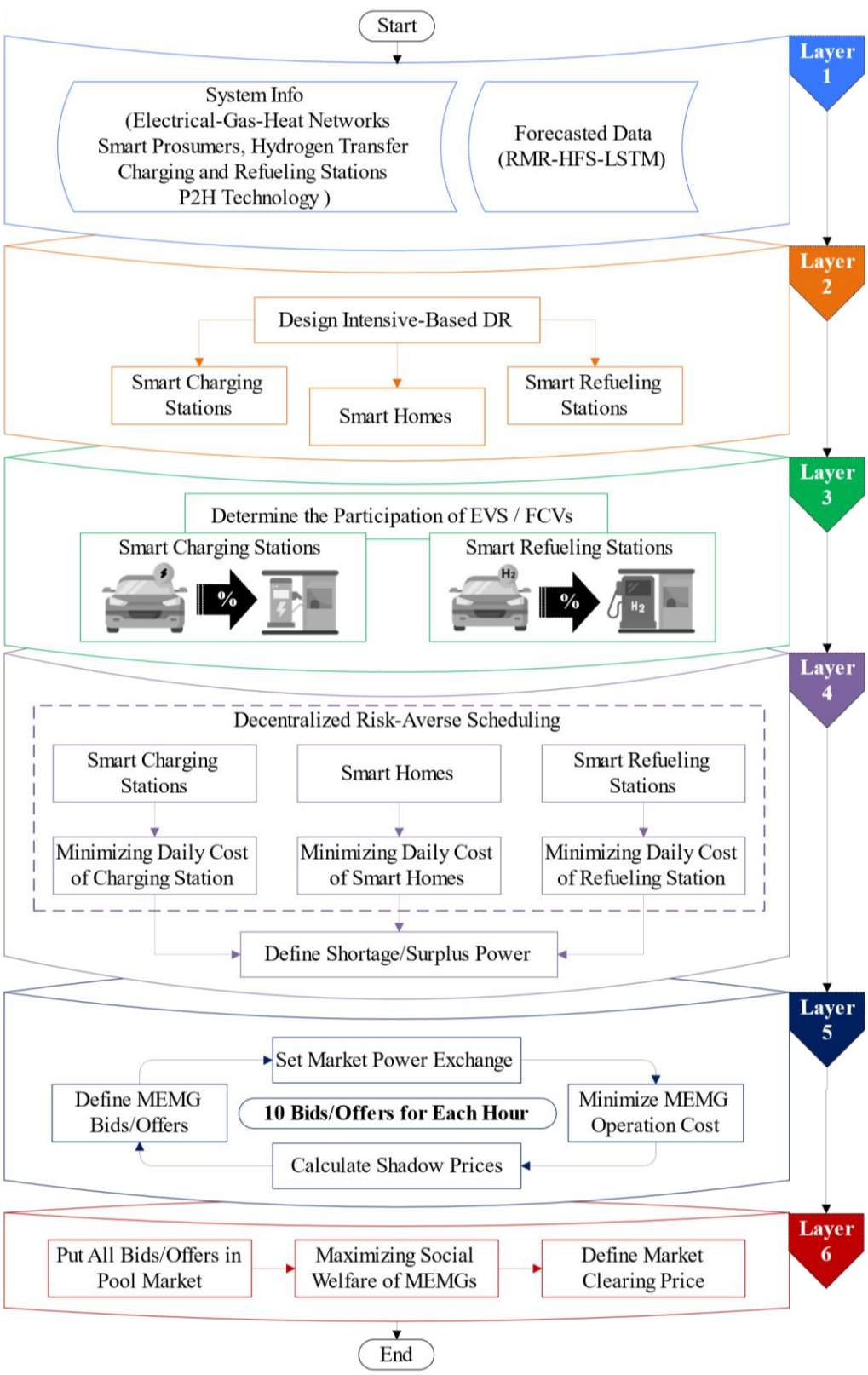

Fig. 4. Details of the proposed hierarchical framework

Table 1. Pseudocode to illustrate the implementation details of the proposed model

Layer 1	**Data Preprocessing**	01. Input all historical data for uncertain parameters. (Energy prices, demands, wind speed and irradiance) 02. Make single dataset based on input parameters. 03. Clean dataset and **do** normalization process.
	Hybrid Feature Selection	04. Removing dissimilar samples and clustering the dataset. 05. Find relevant features using RReliefF by distance function. 06. Calculate weight matrix for forget gate, input gate and output gate [Eqs. (a1)-(a3)]. 07. Calculates the correlation exist between features by mutual information filter. 08. Find maximal relevant features by merging selected features. 09. Tune selected features using wrapper feature selection. 10. Make optimum subset of features.
	Prediction	11. Determine useful information to update old cells. 12. Determine information should be included in the output. 13. Calculate hidden state [Eqs. (a4)-(a6)].
Layer 2	**Incentive-Based DR Schemes**	14. **For** each prosumer ***p***, **do**: 15. Design DR schemes for applying on electrical, heating and hydrogen networks [Eqs. (b1)-(b3)]. 16. **end** 17. Inform optimal DR schemes to smart prosumers.
Layer 3	**Vehicles Participation**	18. **For** each charging station ***c***, **do**: 19. Design incentive programs to motivate EV users to change their charging schedule. 20. Inform incentive programs to EV users through V2I technology. 21. Find participation rate of EVs in DR scheme [Eqs. (c1)-(c8)]. 22. Save schedules of EVs. 23. **end** 24. **For** each refueling station ***r***, **do**: 25. Design incentive programs to motivate FCV users to change their charging schedule. 26. Inform incentive programs to FCV users through V2I technology. 27. Find participation rate of FCVs in DR scheme [Eqs. (c1)-(c8)]. 28. Save schedules of FCVs. 29. **end**
Layer 4	**Smart Prosumers**	30. **For** each smart prosumer ***p***, **do**: 31. **If**, prosumer ***p*** is a smart home, **do**: 32. Consider DR schemes provided by the MEMG operator (designed in layer 2). 33. Solve scheduling problem of smart prosumer ***p*** [Eq. (d1)]. 34. **else** 35. load EV's / FCV's saved schedules (in layer 3). 36. Solve scheduling problem of smart prosumer ***p*** [Eqs. (d2)-(d3)]. 37. **end** 38. Save obtained schedule for smart prosumer ***p***. 39. **end**

Layer 5	**MEMG Scheduling**	40. **For** each MEMG ***m***, **do**: 41. Load obtained schedules for smart prosumers. 42. **For** each hour ***t***, **do**: 43. **For** each buy/sell bid ***it***, **do**: 44. Set exchange variables related to each carrier [Eq. (e5)]. 45. Solve scheduling problem of MEMG ***m*** with the aim of minimizing daily cost [Eqs. (e1)-(e4)]. 46. Find marginal prices of electricity, heating and hydrogen carriers [Eqs. (e6)-(e7)]. 47. Define buy/sell bids for hour ***t*** based on exchange variables and marginal prices. 48. **end** 49. **end** 50.**end**
Layer 6	**Market Clearing**	51. Add all buy/sell bids for each carrier to pool markets. 52. Find suitable buy/sell bids for each hour to maximize social welfare. 53. Limit exchange variables of each carrier to accepted offers. 54. Calculate clearing prices for each market [Eqs. (f1)-(f8)].

5. Simulation Results

5.1. Initializing

The six-layer hierarchical concept proposed in this study is tested in five different case studies (CSs) to be validated. Table 2 illustrates the assumptions of these CS. The data of the last months related to wind speed, radiation, price and different loads are provided in Figs. 5a-5l, since these data are needed to predict uncertain parameters. Fig. 5i shows that the industrial hydrogen load is considered deterministic as its behavior is assumed to be constant in all days. Therefore, there is no need to predict the day-ahead behavior of industrial hydrogen loads. It can also be seen from Figs. 5d-5f that three different demand curves are considered for the charging stations (Types A, B and C). Table 3 provides information regarding the location and specifications of the system components. Information on smart charging and hydrogen refueling stations are provided in Table 4. Besides, details about the location of smart homes and P2H units are presented in Table 5. The information on IoT-based appliances of smart homes is tabulated in Table 6. Lastly, the values of other input parameters are also presented in Table 7.

Table 2. Assumptions of studied cases

Case Studies	Risk-Neutral Strategy	Risk-Averse Strategy	Applying Integrated DR Schemes	Incentive Schemes for EVs / FCVs	Residents' Comfortable Lifestyle
1	✓	×	×	×	×
2	×	✓	×	×	×
3	×	✓	✓	×	×

4	×	✓	✓	✓	×
5	×	✓	✓	✓	✓

Table 3. Information on location and specifications of system components

Gas Turbines					
Number	**Connection Points**		**Capacity (kW)**	**Owner**	
	Electricity Grid	**Gas Network**			
1	18	2	400	MEMG 1	
2	49	12	300	MEMG 2	
3	31	10	350	MEMG 3	
4	55	9	300	MEMG 3	
5	67	8	300	MEMG 4	
6	84	13	400	MEMG 4	
7	90	7	350	MEMG 5	
8	110	15	350	MEMG 6	
9	118	16	300	MEMG 6	
Wind Turbines					
Number	**Connection Point**		**Capacity (kW)**	**Generation Bid ($/kW$)**	**Owner**
1	23		500	0.016	MEMG 1
2	16		550	0.015	MEMG 2
3	39		500	0.012	MEMG 3
4	45		550	0.015	MEMG 3
5	71		600	0.013	MEMG 4
6	91		500	0.013	MEMG 5
7	106		700	0.017	MEMG 6
Solar Panels					
Number	**Connection Point**		**Capacity (kW)**	**Generation Bid ($/kW$)**	**Owner**
1	5		150	0.018	MEMG 2
2	35		200	0.021	MEMG 3
3	83		250	0.019	MEMG 4
4	97		150	0.015	MEMG 5
5	114		150	0.018	MEMG 6

Table 4. Information on charging and hydrogen refueling stations

Smart Charging Stations					
Number	**Connection Point (Type)**	**Number of EVs**	**Components Capacity**		**Owner**
			Solar Panels (kW)	**Storage device (kWh)**	
1	10 (A)	95	170	60	MEMG1
2	21 (B)	45	100	50	MEMG1
3	24 (C)	130	250	80	MEMG1
4	7 (A)	100	200	60	MEMG2
5	14 (B)	55	100	50	MEMG2
6	47 (C)	100	200	60	MEMG2
7	52 (C)	150	300	100	MEMG2
8	33 (A)	130	250	85	MEMG3
9	37 (B)	85	150	50	MEMG3
10	58 (C)	120	220	70	MEMG3
11	60 (C)	170	320	100	MEMG3
12	64 (A)	125	250	80	MEMG4
13	68 (B)	80	150	50	MEMG4
14	75 (C)	110	200	60	MEMG4

15	78 (C)	160	310	100	MEMG4
16	89 (A)	100	200	60	MEMG5
17	93 (B)	40	80	50	MEMG5
18	99 (C)	110	210	60	MEMG5
19	102 (A)	110	200	60	MEMG6
20	104 (B)	70	140	50	MEMG6
21	108 (C)	125	250	80	MEMG6
22	114 (C)	155	300	100	MEMG6
Smart Hydrogen Refueling Stations					
Number	**Connection Point**	**Number of FCVs**	**Components Capacity**		**Owner**
			Solar Panels (kW)	**Hydrogen Tank (m^3)**	
1	26	125	100	5500	MEMG1
2	17	70	70	2700	MEMG2
3	51	130	100	4500	MEMG2
4	42	135	150	4700	MEMG3
5	62	90	100	3000	MEMG3
6	72	90	100	3000	MEMG4
7	87	80	70	2900	MEMG4
8	95	125	100	4500	MEMG5
9	111	100	150	3500	MEMG6
10	113	110	100	4500	MEMG6

Table 5. Information of P2H units and smart homes

P2H Units					
Number	**Connection Point**	**Components Capacity**			**Owner**
		Wind Turbine (kW)	**Solar Panels (kW)**	**Hydrogen Tank (m^3)**	
1	27	3200	1500	16000	MEMG1
2	112	4000	2000	20000	MEMG6
Smart Homes					
Number	**Connection Point**		**Number of Consumers**		**Owner**
	Electricity Grid	**Heating Network**			
1	10 – 19 – 20	3	40 – 37 – 109		MEMG1
2	22 – 25	2	35 – 47		MEMG1
3	5 – 12	7	32 – 55		MEMG2
4	8 – 15 – 50 – 52	5	21 – 17 – 184 – 22		MEMG2
5	46 – 48	4	44 – 72		MEMG2
6	32 – 34 – 57	9	95 – 47 – 22		MEMG3
7	37 – 40 – 59 – 61	10	88 – 79 – 18 – 49		MEMG3
8	44 – 54	8	37 – 87		MEMG3
9	66 - 78	13	78 – 53		MEMG4
10	68 – 70 – 79 – 85	11	21 – 94 – 59 – 22		MEMG4
11	73 – 76 – 86	12	22 – 45 – 77		MEMG4
12	89	14	54		MEMG5
13	91 – 92 – 98	15	25 – 61 – 20		MEMG5
14	94 – 96	20	43 – 29		MEMG5
15	101 – 103 – 115	17	91 – 82 – 26		MEMG6
16	105 – 107 – 117	16	33 – 99 – 27		MEMG6
17	109 – 111	18	102 – 184		MEMG6

Table 6. Details required for the operation of smart home appliances

Appliances	**Power Usage (kW)**			**Time Window (h)**		**Duration (h)**
	Min	**Nominal**	**Max**	**Start**	**End**	
Washing Machine	0.6	2.5	3.9	1	11	2

Clothes Dryer	0.2	2.2	3	1	19	1
Dishwasher	0.1	1.5	3.1	12	19	2
Refrigerator	0.01	0.1	0.1	1	24	24
Television	0.1	0.2	0.4	17	24	4
Lights	0.17	0.17	0.17	5	24	16
Rice Cooker	0.02	0.02	0.02	10	15	1
Kettle	0.95	1.89	0.95	5	10	2
Toaster	0.65	2.6	0.65	6	10	1
Microwave	0.45	2.7	0.45	11	20	2
Iron	1.1	1.1	1.1	1	10	1

Table 7. Values of input parameters required for simulation

Parameter	Value	Parameter	Value	Parameter	Value
LHV^{H2}	39.72 (kWh/kg)	v_{ci} / v_r / v_{co}	2 / 10 / 20 (m/s)	α^R	90%
LHV^G	50 (MJ/kg)	η^{El}	80%	α^{Comp}	1.2
M^{H2}	0.002 (kg/mol)	η^{Solar}	95%	C^p	4.186 [J/(g.C°)]
M^G	0.829 (kg/m^3)	G^{STD}	1000 (W/m^2)	Δt	1 (h)
R^{H2}	8.314 [J/(mol.K)]	$\alpha^{Transfer}$	6:00 (h)	η^{loss}	1%
T^{H2}	313 (K)	$B^{Transfer}$	23:00 (h)	η^{Ch} / η^{Dch}	95%

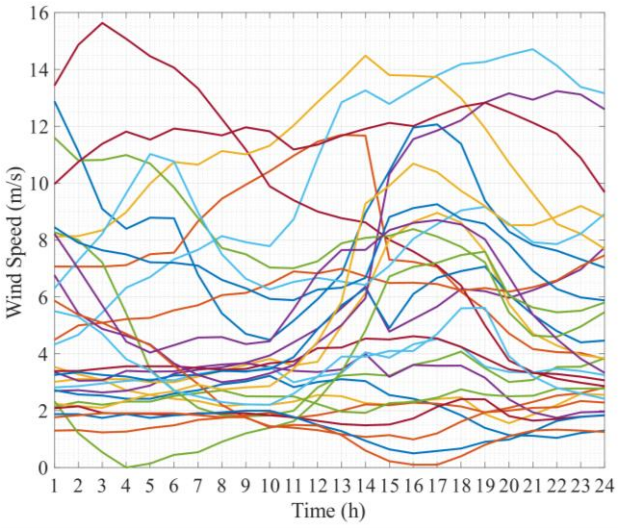

(a) Wind speed

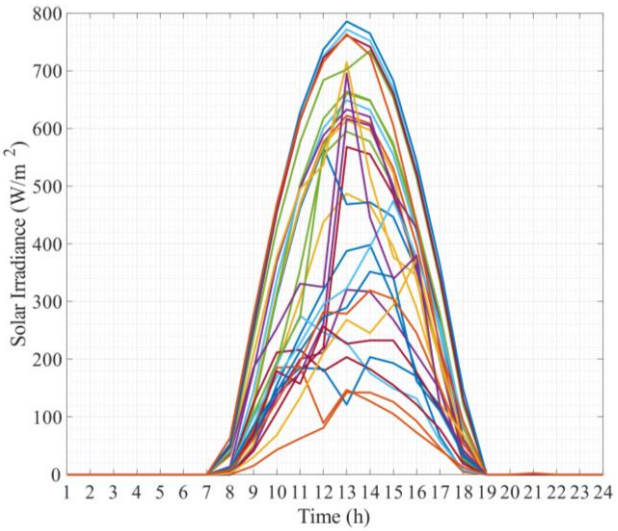

(b) Solar irradiance

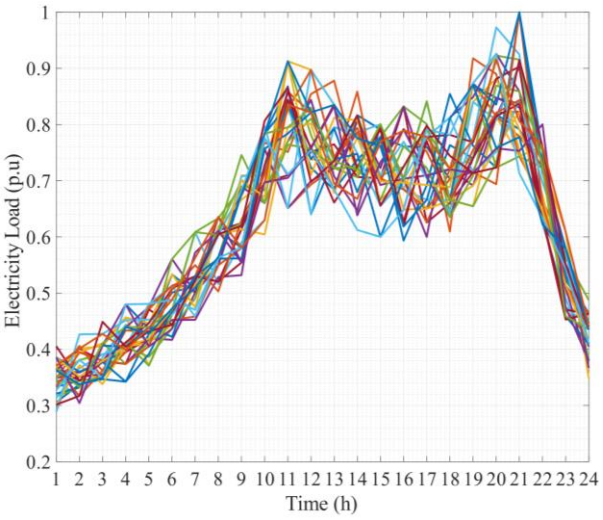

(c) Electricity load (Smart Homes)

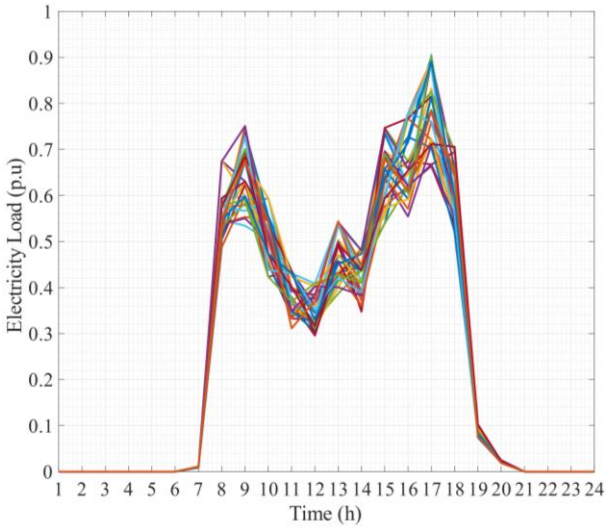

(d) Electricity load of the charging station type A

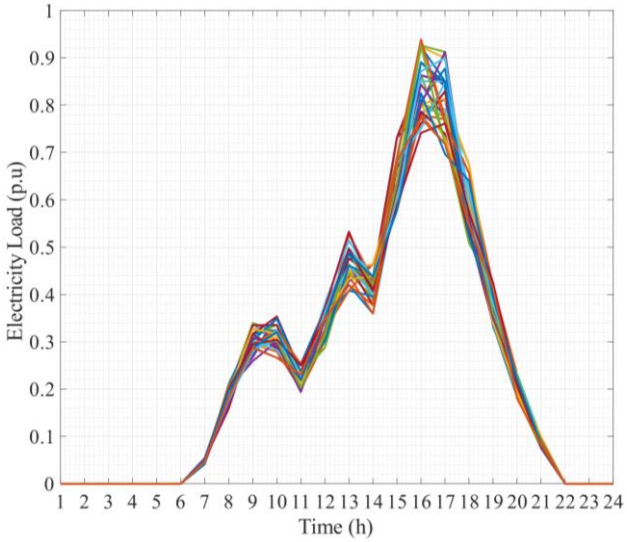

(e) Electricity load of the charging station type B

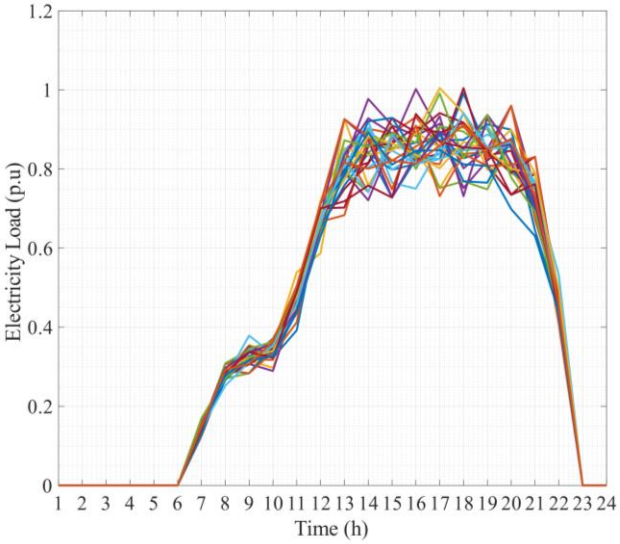

(f) Electricity load of the charging station type C

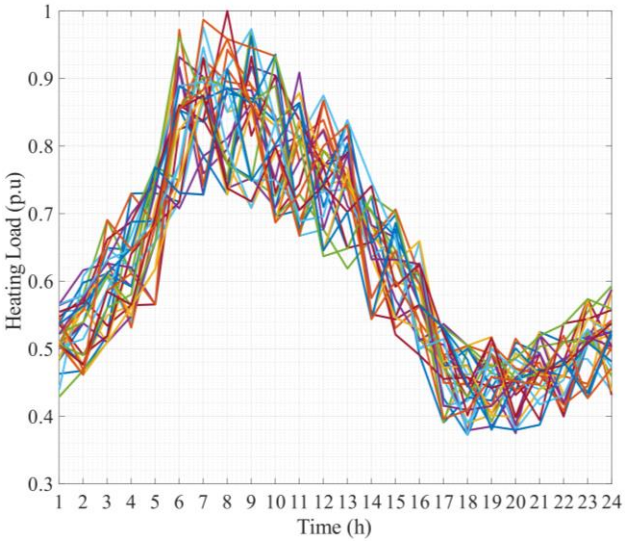

(g) Heating load

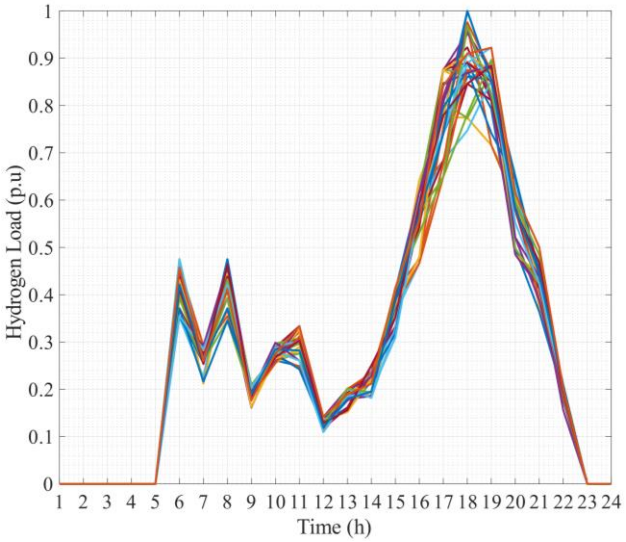

(h) Hydrogen load (Refueling Stations)

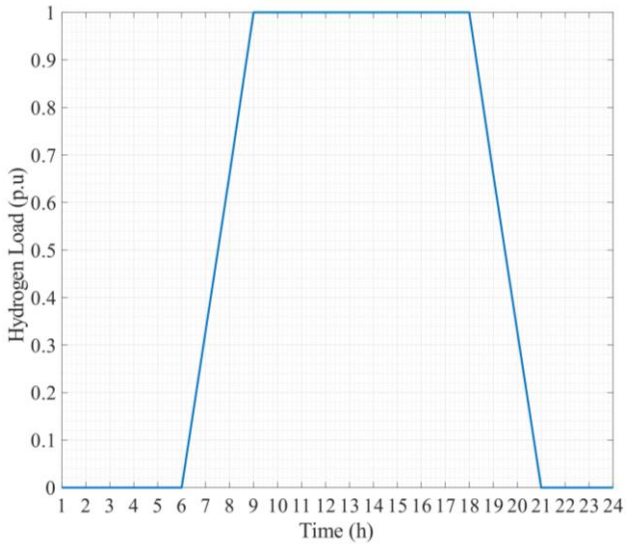

(i) Hydrogen load (Industrial Usage)

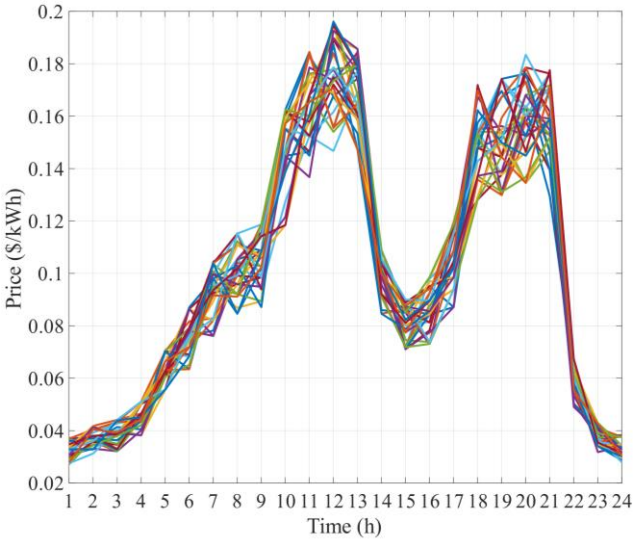

(j) Electricity market settlement price

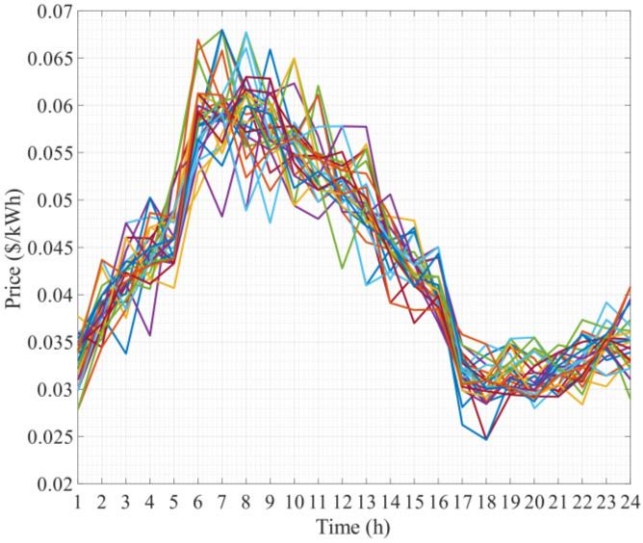

(k) Heating market settlement price

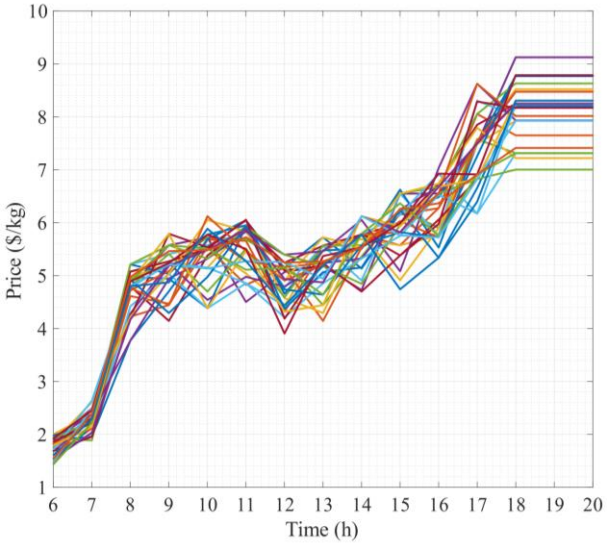

(l) Hydrogen market clearing price

Fig. 5. Historical data associated with uncertain parameters

5.2. Results for Cases Studies 1 and 2

In this subsection, the proposed concept is tested in CS1 and CS2. In these CSs, DR schemes, residents' comfortable lifestyles, and EVs/ FCVs incentive schemes are not considered in the model, and their difference is in the modeling of risk of MEMGs' scheduling. In CS1, MEMGs do their scheduling through the risk-neutral strategy, while in CS2, they use a risk-averse strategy for scheduling. Tables 8 and 9 respectively tabulate the scheduling results in CS1 and CS2. Examining these tables reveals that the operators of MEMGs in CS2 have paid more money to increase scheduling robustness against

uncertainties by adopting the risk-averse strategy. The analysis of the numerical results reflects the impact of the risk-averse strategy on the 11.95% increase in the daily costs of MEMGs in CS2. Figures 6a-6h show the permissible ranges of deviation of uncertain parameters in the MEMG 6 from the predicted curves in risk-averse scheduling (CS2). It can be observed from these figures that despite the 11.95% cost increase in risk-averse scheduling, the uncertain parameters can fluctuate in a safe range without imposing more costs on the system. In Figs. 7a-7h, the operating point of the gas turbines placed in MEMGs is shown. As can be seen in risk-averse scheduling, gas turbines have a higher operating point and have produced more power, which is to increase the robustness of the scheduling against uncertainties caused by RGs and demands.

Table 8. Scheduling results for CS1

MEMGs	**Daily Costs ($/day)**						
	Components	**Energy Transactions**			**Smart Homes**	**Ch. / Ref. Stations**	**Sum**
		Electricity	**Heating**	**Hydrogen**			
MEMG 1	399.59	2962.59	-15000.59	-1310.73	3281.88	3085.38	-6581.88
MEMG 2	664.63	4269.85	36185.86	4829.2	4241.25	4140.11	54330.9
MEMG 3	1704.06	9292.97	84866.92	5064.94	9947.04	4557.73	115433.66
MEMG 4	1190.4	10144.53	-22985.17	4216.27	10898.56	3653.26	7117.85
MEMG 5	422.16	2541.44	24272.41	3556.19	2844.91	2575.71	36212.82
MEMG 6	1729.64	8900.66	-40205.59	-1562.22	9400.7	4619.39	-17117.42
Total	6110.48	38112.04	67133.84	14793.65	40614.34	22631.58	189395.93

Table 9. Scheduling results for CS2

MEMGs	**Daily Costs ($/day)**						
	Components	**Energy Transactions**			**Smart Homes**	**Ch. / Ref. Stations**	**Sum**
		Electricity	**Heating**	**Hydrogen**			
MEMG 1	399.59	3301.08	-13870.38	-1216.29	3281.88	3085.38	-5018.74
MEMG 2	664.63	4743.23	41513.86	5467.82	4241.25	4140.11	60770.9
MEMG 3	1704.06	10505.49	93560.65	5719.96	9947.04	4557.73	125994.93
MEMG 4	1190.4	11642.83	-21401.21	4723.51	10898.56	3653.26	10707.35
MEMG 5	422.16	2800.42	27085.55	4078.57	2844.91	2575.71	39807.32
MEMG 6	1729.64	10097.21	-38021.36	-1418.74	9400.7	4619.39	-13593.16
Total	6110.48	43090.26	88867.11	17354.83	40614.34	22631.58	218668.6

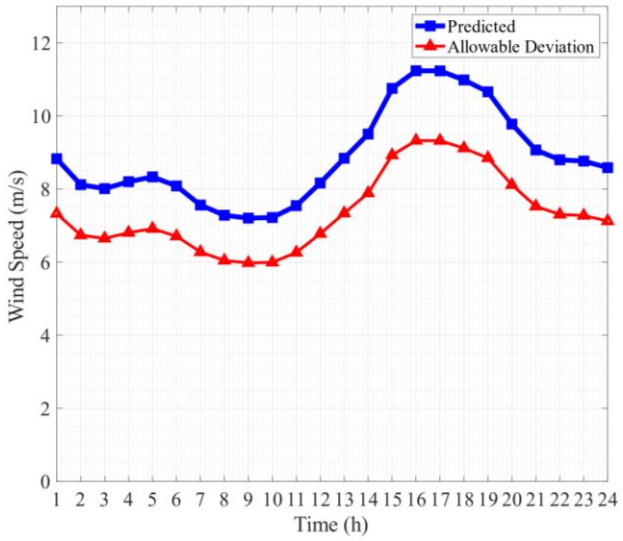

(a) Wind speed

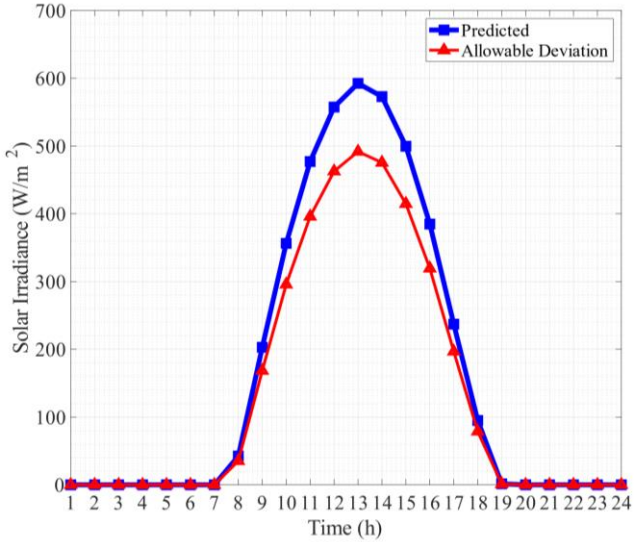

(b) Solar radiation

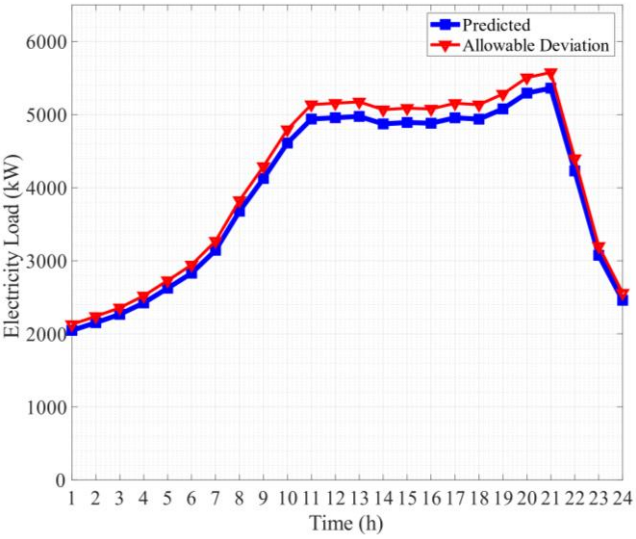

(c) Electricity load

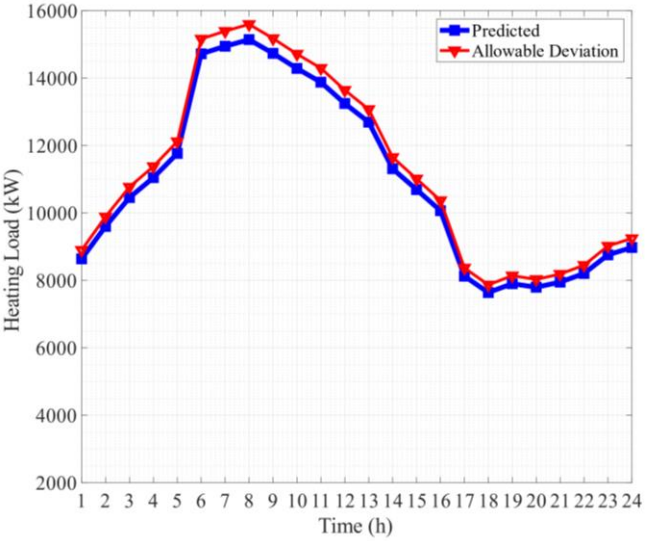

(d) Heating load

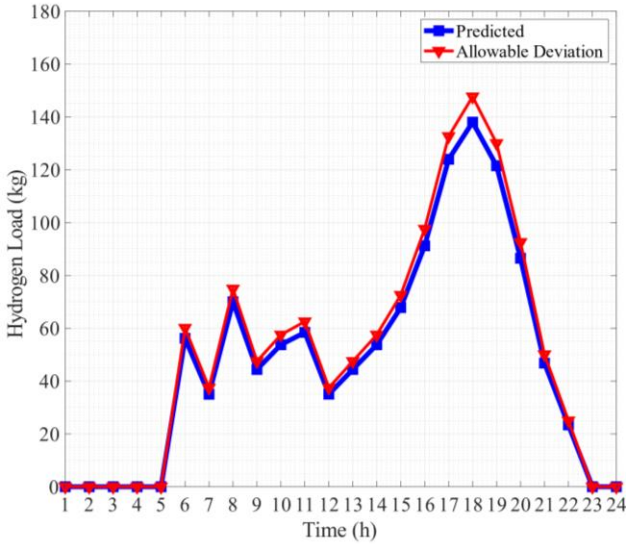

(e) Hydrogen load

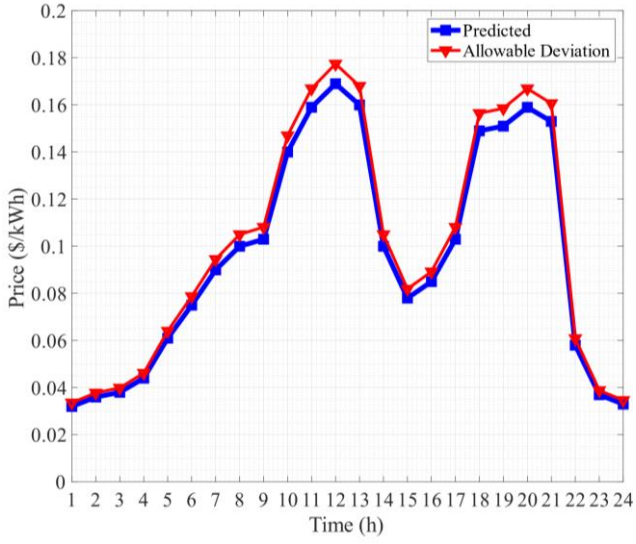

(f) Electricity market clearing price

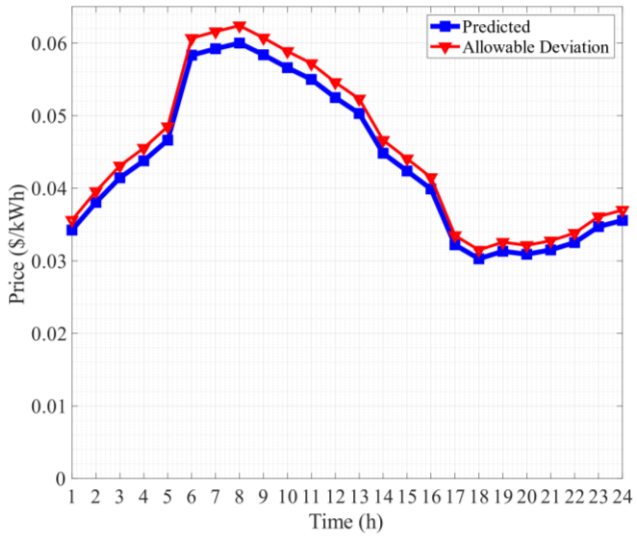

(g) Heating market clearing price

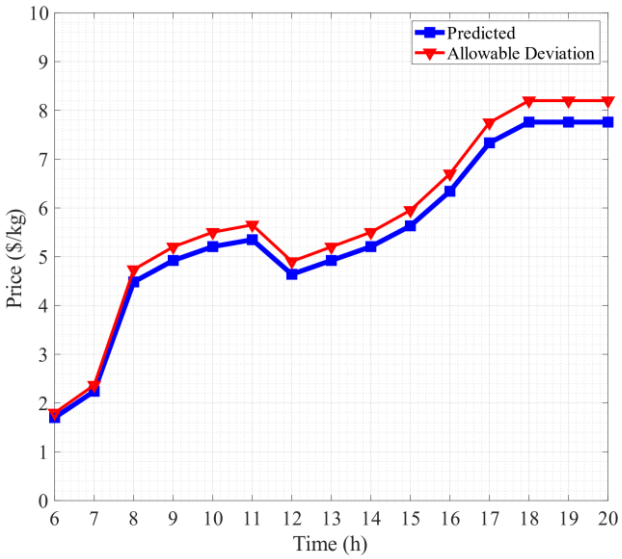

(h) Hydrogen market clearing price

Fig. 6. The permissible range of deviation from the predicted curves in risk-averse scheduling

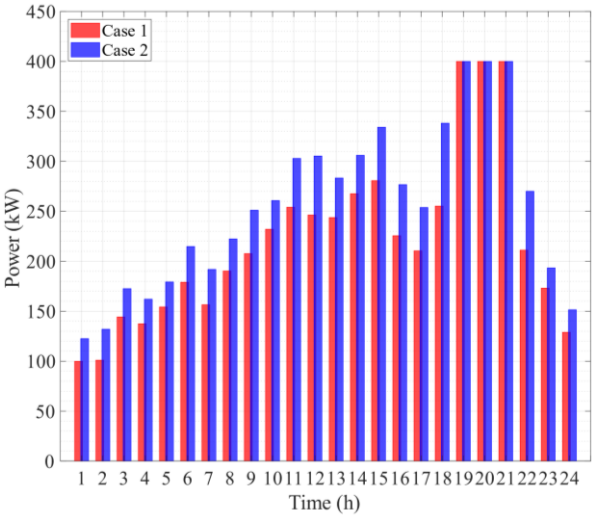

(a) Gas turbines of MEMG 1

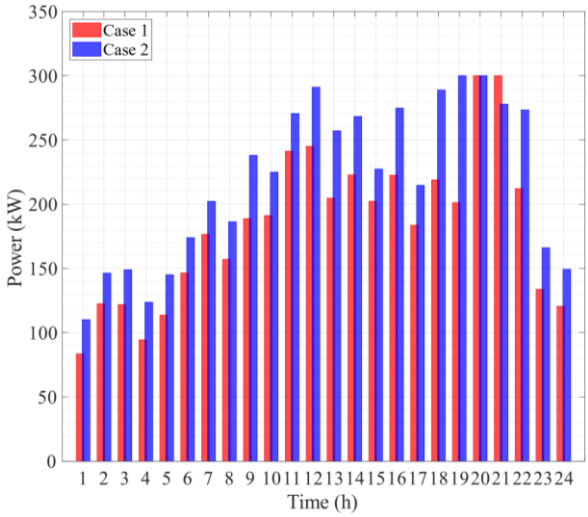

(b) Gas turbines of MEMG 2

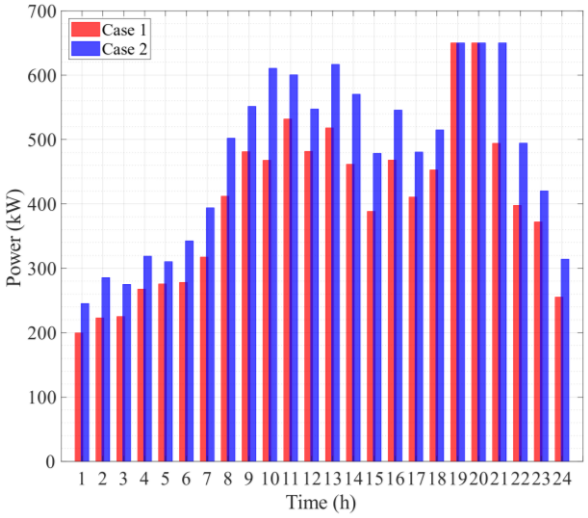

(c) Gas turbines of MEMG 3

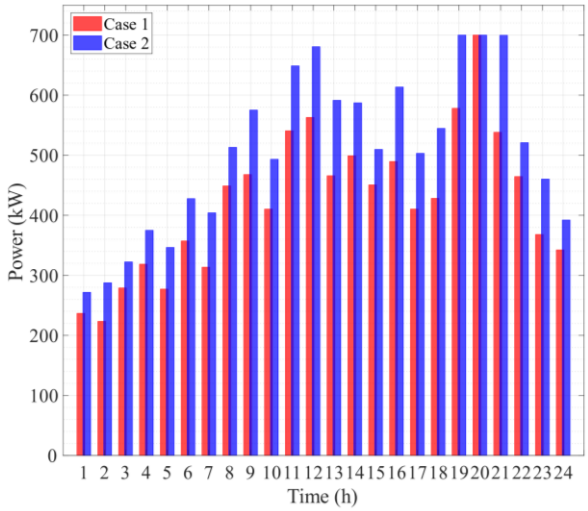

(d) Gas turbines of MEMG 4

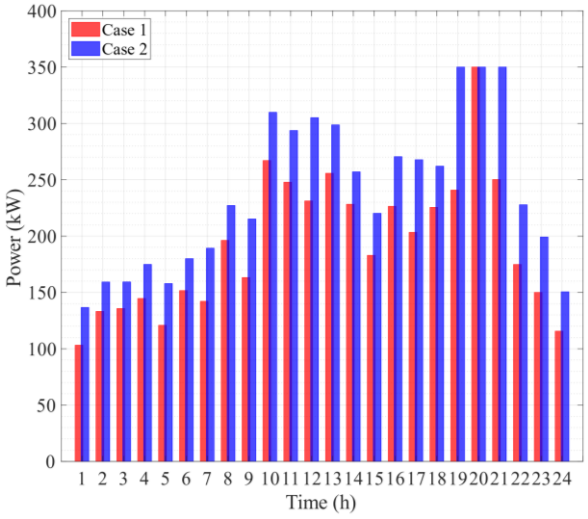

(e) Gas turbines of MEMG 5

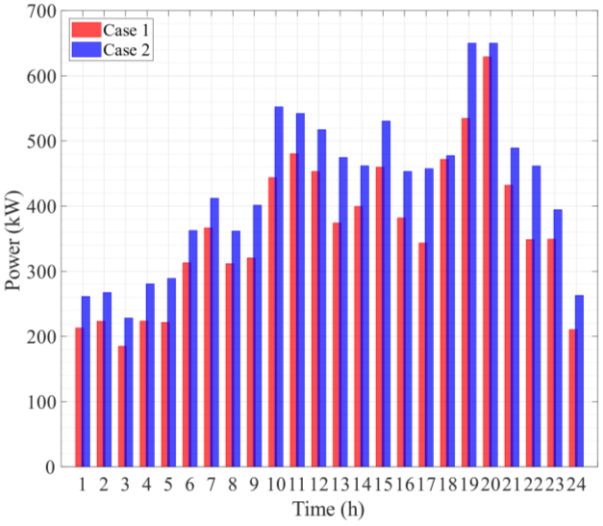

(f) Gas turbines of MEMG 6

Fig. 7. The operating point of gas turbines: CS1 and CS2

5.3. Results for Case Study 3

The third case is the same as the second case except that electrical and thermal DR schemes are considered in the model. It should be noted that these schemes are designed by the operator of MEMGs and according to the behavior of customers, so that different rewards are assigned to them per hour. Table 10 is provided to show the scheduling results of CS3. According to these results, participation in DR schemes has reduced the daily costs of smart homes and MEMGs by 12.35% and 12.20%, respectively, which is due to the change in consumption behavior of smart customers. Figures8-8c are presented to

evaluate the consumption behavior of customers in CS2 and CS3. These figures reveal that electrical and heating consumptions have decreased in peak periods and moved to valley periods. Figure 8c shows that despite the non-implementation of the DR scheme on the gas network, the consumption pattern of this network has also improved, which is due to the modification of electrical and heating consumption patterns. This point reveals the mutual effects of different networks.

Figures 9a-9b depict the amount of hydrogen production of P2H units placed in MEMGs. According to these figures, P2H units are at their maximum operating point between 10:00 and 17:00, which is due to the high production of solar panels connected to them during this period. It can also be seen that the operating point of P2H units between 18:00 and 09:00 has dropped significantly, which is due to the decrease in the production level of solar panels during this period. Note that P2H units are also connected to wind turbines in addition to solar panels to ensure the continuity of their production throughout the day and night. Table 11 presents the schedules obtained for hydrogen trucks in CS3. These results illustrate that the loading, traveling and unloading times of trucks are different and depend on hydrogen exchange contracts. It should be noted that the time required to travel between the hydrogen production and consumption points is assumed to be 1 hour while the time required for loading / unloading is considered 30 minutes. Moreover, the results of Table 10 reveal that the most trips were made between 10:00 and 16:00, as the hydrogen level of the hydrogen tanks placed in the consumption points must be at a high level to meet the peak demand (between 17:00 and 19:00).

Figures 10 and 11 compare the marginal prices obtained for electricity and heat in each MEMG in CS2 and CS3, which reveal that these prices are much lower during peak periods in CS3. Figures 12a and 12b depict the clearing prices of electricity and heat markets, respectively. These figures reflect that the lower marginal prices of MEMGs have led to lower clearing prices in markets. Figures 13a and 13b are provided to compare the voltage and gas pressure of MES in CS2 and CS3. These curves are related to the peak hour and confirm that the decrease in the demand level in this hour has led to the improvement of the voltage and pressure levels in the electricity and gas networks, respectively. Overall, the results

obtained in the third case confirm the significant impact of the implementation of DR schemes on improving the technical and economic indicators of MES.

Table 10. Scheduling results for CS3

MEMGs	Daily Costs ($/day)						
	Components	Energy Transactions			Smart Homes	Ch. / Ref. Stations	Sum
		Electricity	Heating	Hydrogen			
MEMG 1	434.41	2835.24	-15133.61	-1416.29	2940.22	3085.38	-7254.65
MEMG 2	750.36	4207.63	36887.39	5467.82	3776.69	4140.11	55230
MEMG 3	1848.92	9276.38	84177.29	5719.96	8731.94	4557.73	114312.22
MEMG 4	1344.09	10387.61	-22788.97	4723.51	9298.57	3653.26	6618.07
MEMG 5	472.34	2411.31	23393.65	4078.57	2421.25	2575.71	35352.83
MEMG 6	1927.38	8624.96	-40071.75	-1618.74	8429.78	4619.39	-18088.98
Total	6777.5	37743.13	66464	16954.83	35598.45	22631.58	186169.49

Table 11. Obtained schedules for hydrogen transport trucks

Origin (Bus)		Destination (Bus)	Operation Time	
MEMG 1 (27)	**MEMG 6 (112)**		**Start of Loading (h)**	**End of Unloading (h)**
✓	×	MEMG 1 (16)	9:00	10:00
✓	×	MEMG 2 (17)	15:00	17:00
✓	×	MEMG 2 (51)	16:00	18:00
✓	×	MEMG 3 (42)	12:00	14:00
×	✓	MEMG 3 (62)	15:00	17:00
×	✓	MEMG 4 (72)	11:00	13:00
×	✓	MEMG 4 (87)	16:00	18:00
×	✓	MEMG 5 (95)	12:00	14:00
×	✓	MEMG 6 (111)	8:00	9:00
×	✓	MEMG 6 (113)	11:00	12:00

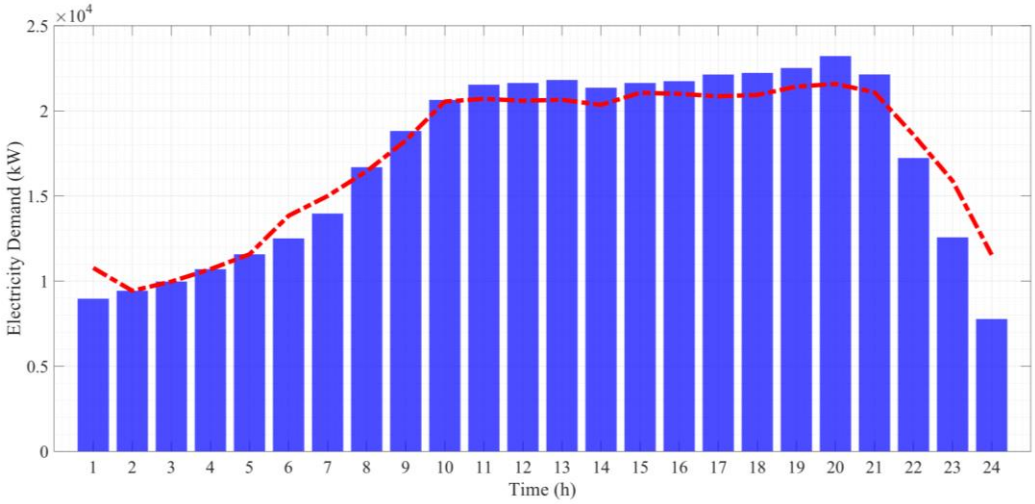

(a) Electricity demand

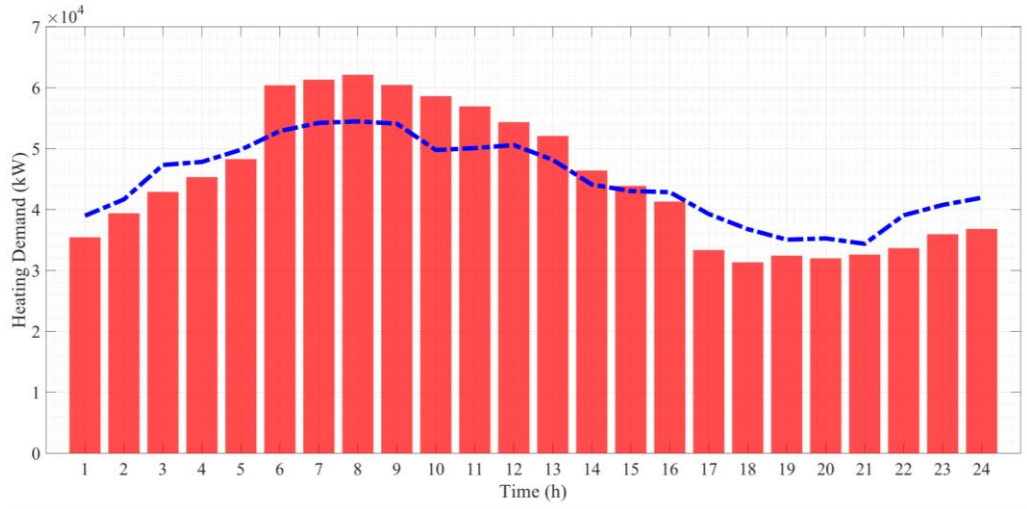

(b) Heating demand

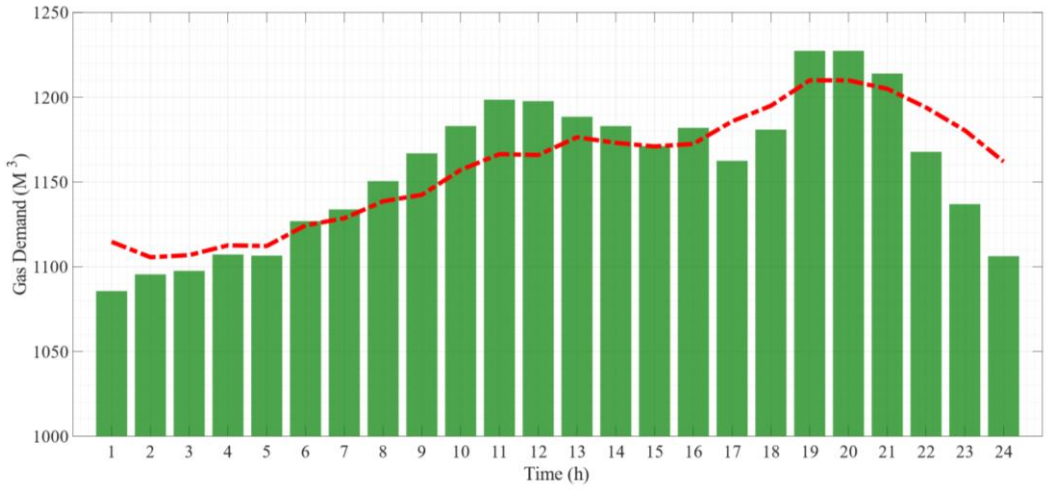

(c) Gas demand

Fig. 8. Consumption pattern of different carriers: CS2 and CS3

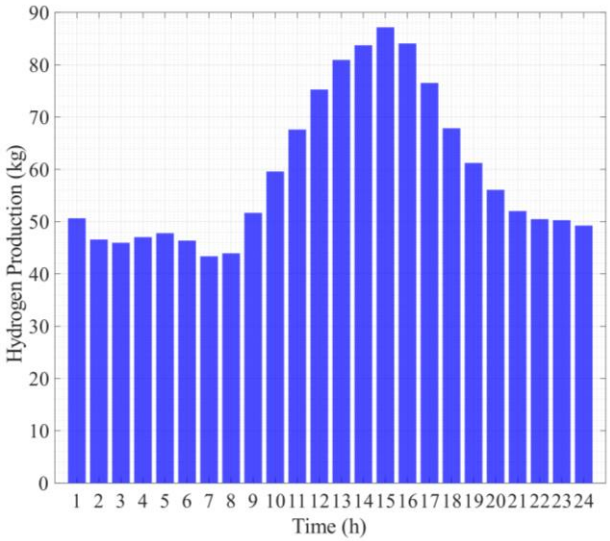

(a) P2H unit located in MEMG 1

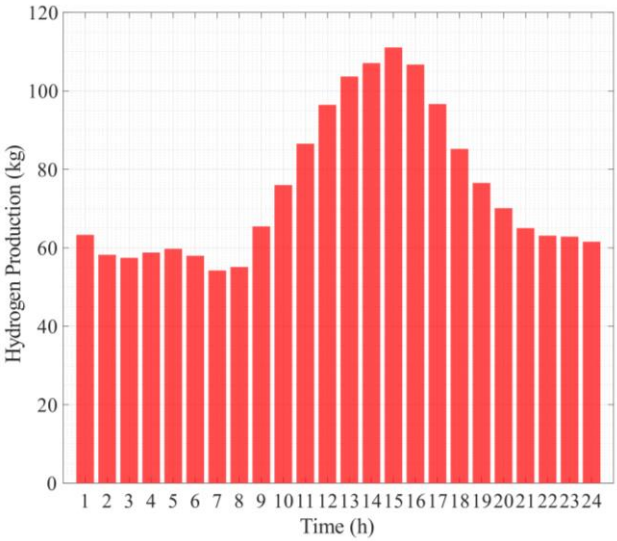

(b) P2H unit located in MEMG 6

Fig. 9. Hydrogen production rate of P2H units

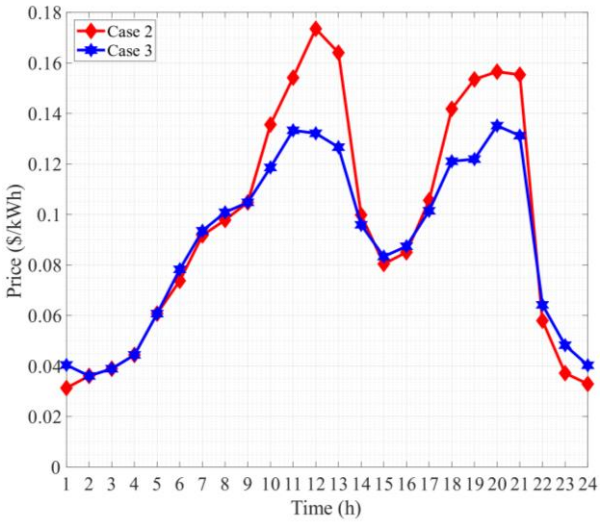

(a) MEMG 1

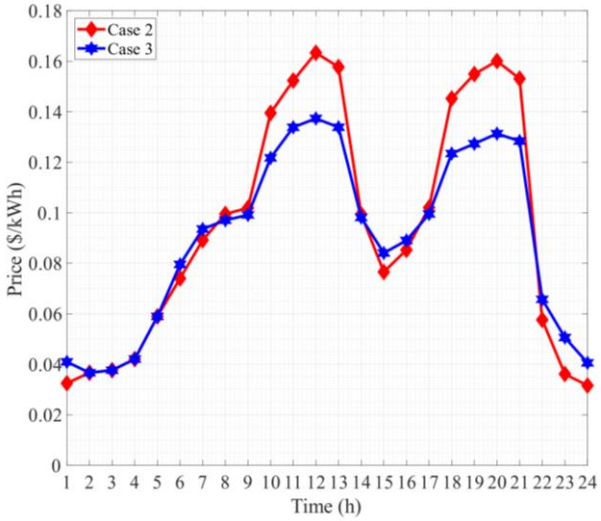

(b) MEMG 2

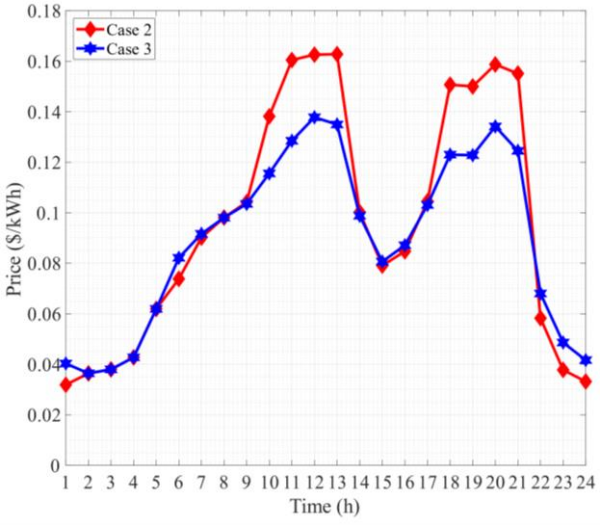

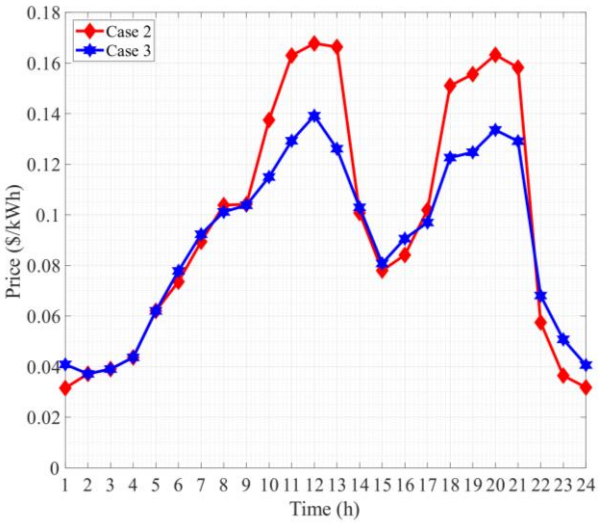

(c) MEMG 3

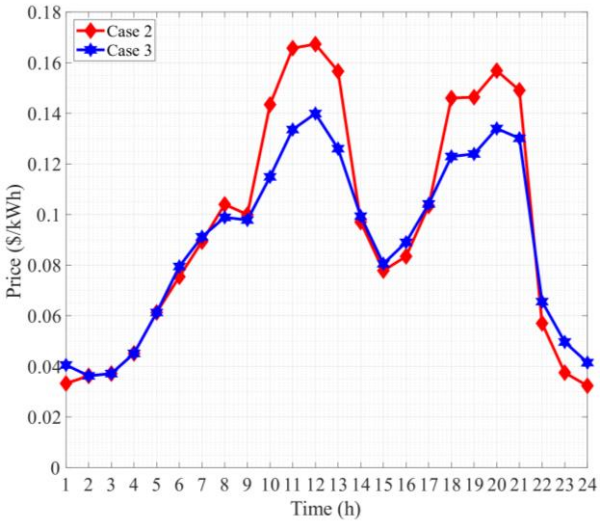

(d) MEMG 4

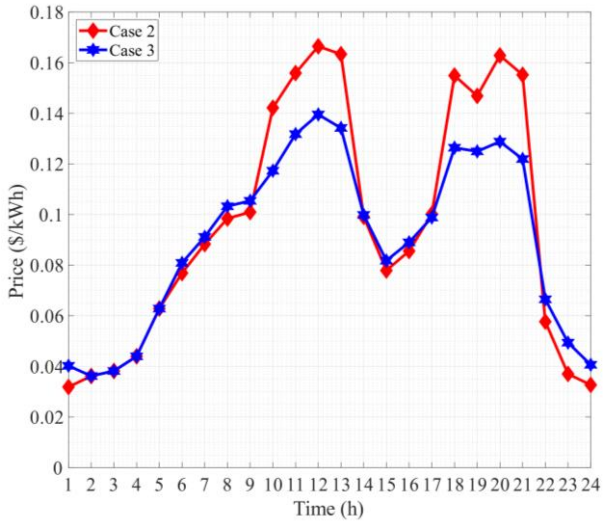

(e) MEMG 5

(f) MEMG 6

Fig. 10. Marginal prices of electricity in MEMGs: CS2 and CS3

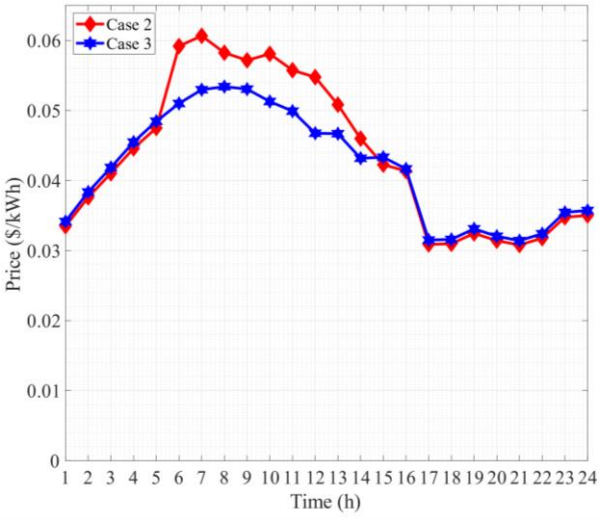

(a) MEMG 1

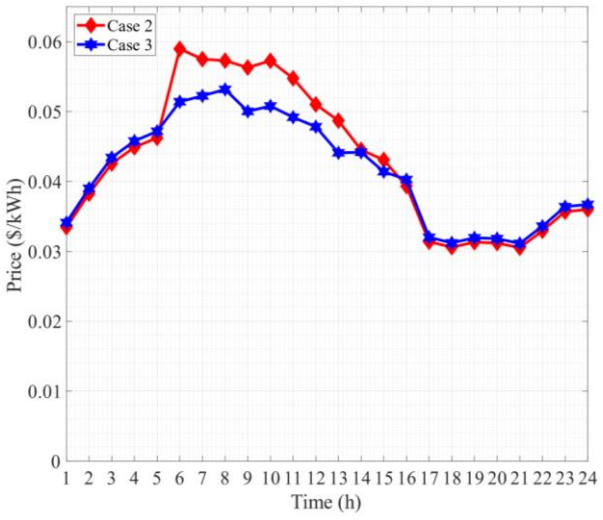

(b) MEMG 2

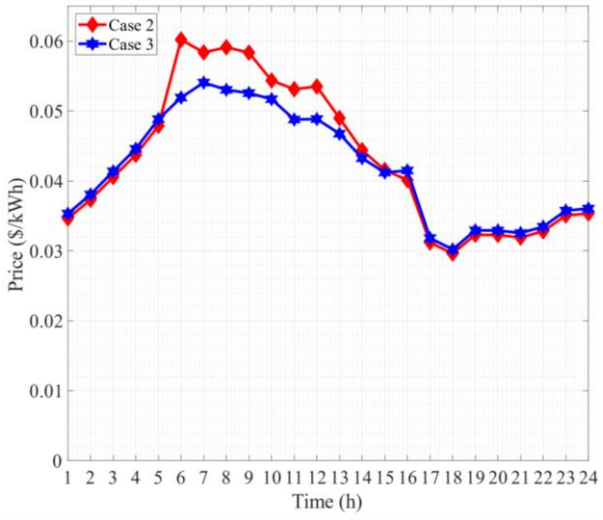

(c) MEMG 3

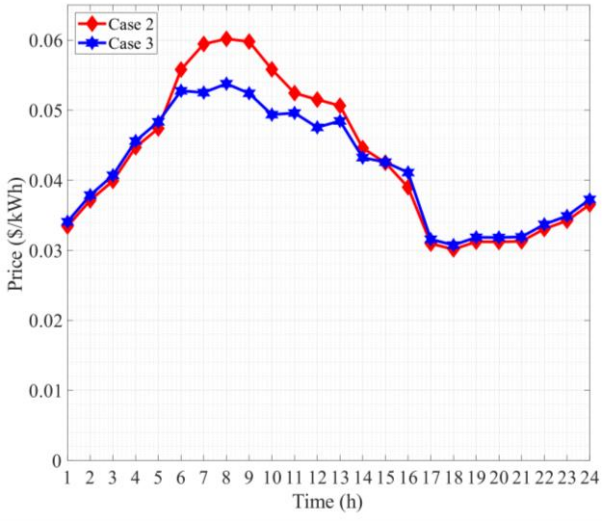

(d) MEMG 4

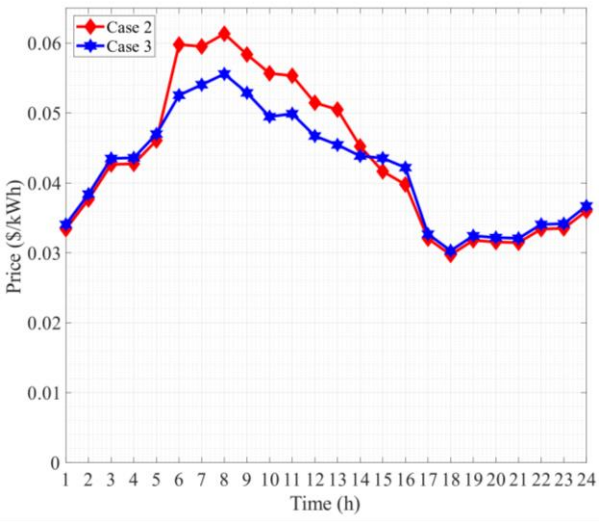

(e) MEMG 5

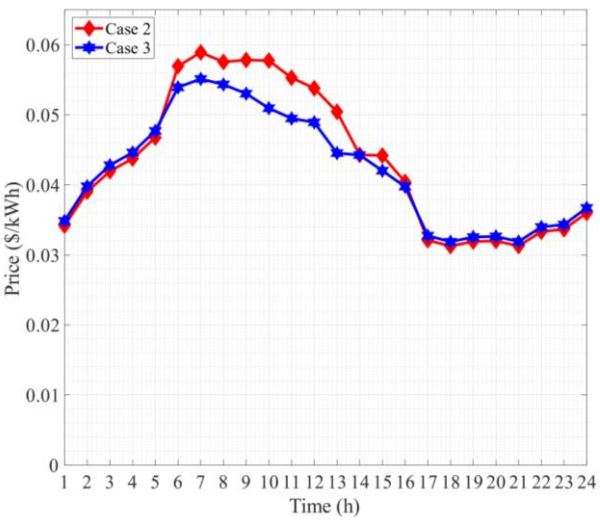

(f) MEMG 6

Fig. 11. Marginal prices of heat in MEMGs: CS2 and CS3

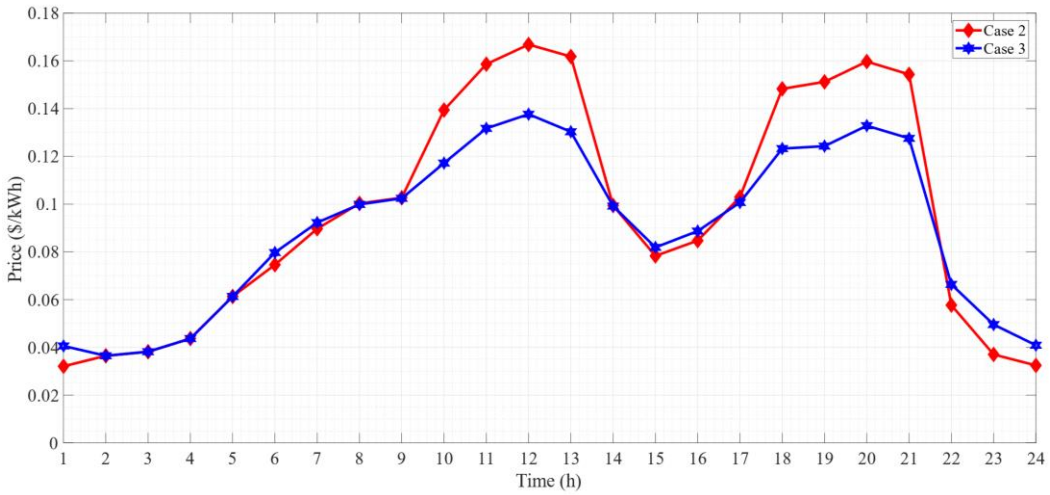

(a) Electricity market

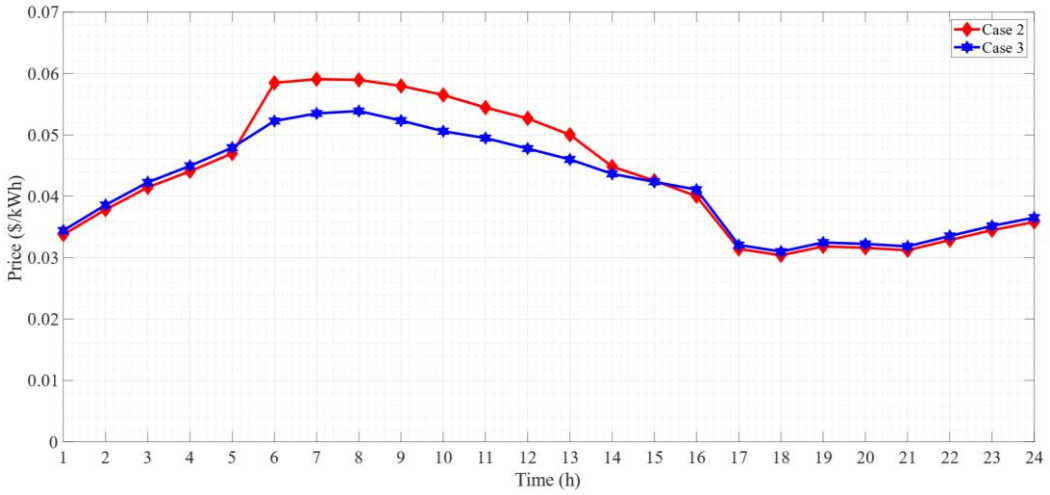

(b) Heat market

Fig. 12. Clearing prices in different markets: CS2 and CS3

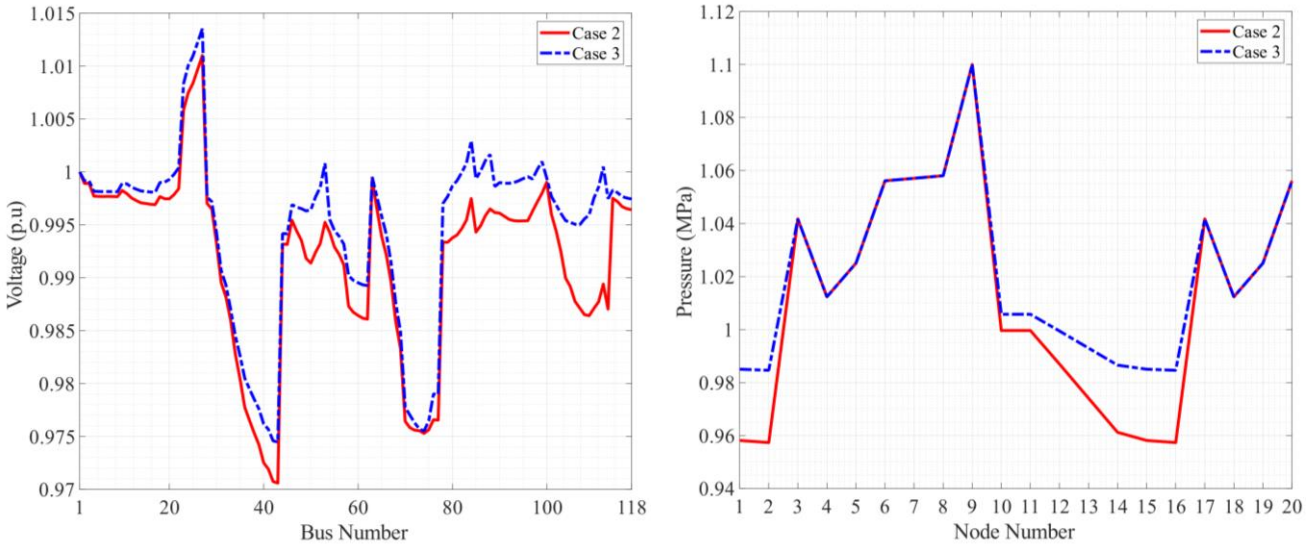

(a) Voltage magnitude at 21:00 (b) Gas pressure at 22:00

Fig. 13. Voltage magnitude and gas pressure in electricity and gas networks: CS2 and CS3

5.4. Results for Case Study 4

In the fourth case, smart charging and hydrogen refueling stations also participate in DR schemes in addition to other customers. To this end, smart stations receive DR schemes from MEMGs operators and send incentive schemes to the EV/ FCV users based on them. The results of this case are tabulated in Table 12, the analysis of which illustrates a reduction in the daily costs of MEMGs. In addition, the results reveal that the daily costs of the stations are also lower in CS4 compared to CS3, which is due to the change in the behavior of their EV / FCV users and also receiving rewards from MEMGs operators. Figures 14 and 15 depict the programs of smart charging and hydrogen refueling stations in CS3 and CS4. As can be seen, providing incentive schemes in CS4 changed the behavior of EV / FCV users, so that much fewer vehicles were charged during peak period. Note that the peak demands of hydrogen and electricity are at 18:00 and 20:00, respectively. Figures 16a and 16b are provided to analyze the impact of changing the behavior of EVs / FCVs on the clearing prices of the electricity and hydrogen markets. These figures reveal that the change in the EVs /FCVs charging schedule has led to a reduction in clearing

prices in the electricity and hydrogen markets during the peak period. In addition, Figs. 17a and 17b reveal that changing EVs / FCVs schedules has led to improved voltage and gas pressure levels in electricity and gas networks, respectively. The increase in the voltage level is due to the decrease in the power demand of the smart charging stations during the peak period, while the increase in the gas pressure level is due to the decrease in the gas demand of the gas turbines during this period.

Table 12. Scheduling results for CS4

MEMGs	Daily Costs ($/day)						
	Components	Energy Transactions			Smart Homes	Ch. / Ref. Stations	Sum
		Electricity	Heating	Hydrogen			
MEMG 1	429.33	2434.52	-15133.61	-1405.19	2940.22	2594.5	-8140.23
MEMG 2	739.83	3681.37	36887.39	4191.82	3776.69	3730.37	53007.47
MEMG 3	1829.31	7904.29	84177.29	4400.66	8731.94	4160.33	111203.82
MEMG 4	1323.51	8834.5	-22788.97	3557.72	9298.57	3527.6	3752.93
MEMG 5	465.47	2134.12	23393.65	3142.54	2421.25	2502.13	34059.16
MEMG 6	1898.29	7669.31	-40071.75	-1668.4	8429.78	4133.36	-19609.41
Total	6685.74	32658.11	66464	12219.15	35598.45	20648.29	174273.74

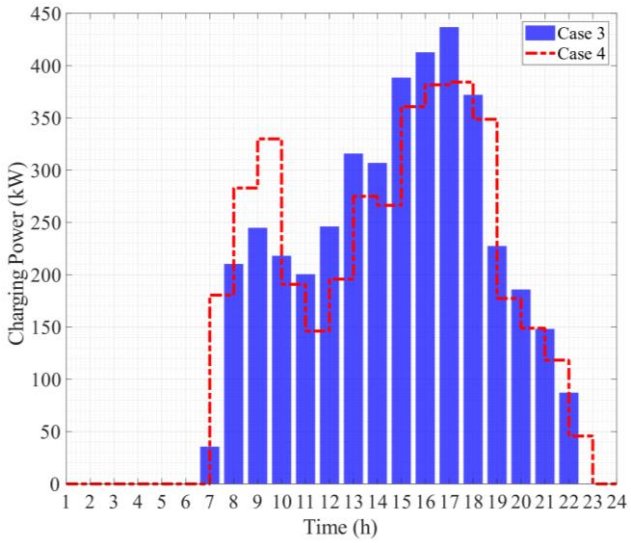

(a) MEMG 1

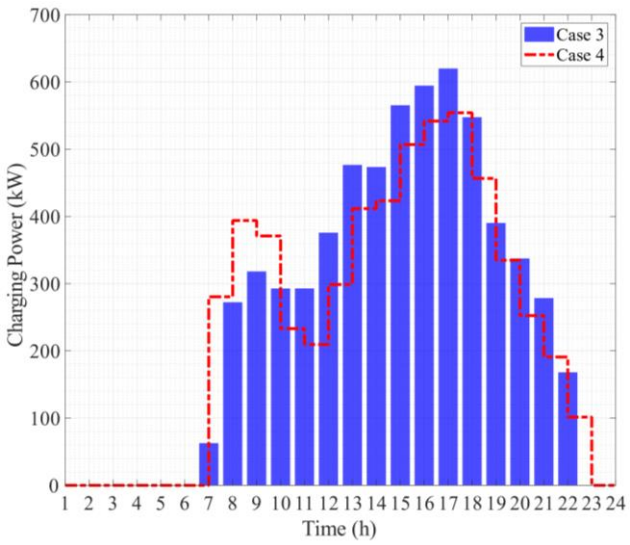

(b) MEMG 2

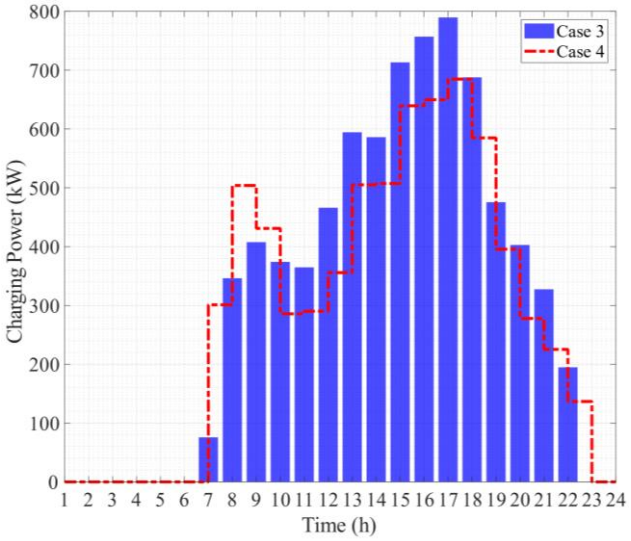

(c) MEMG 3

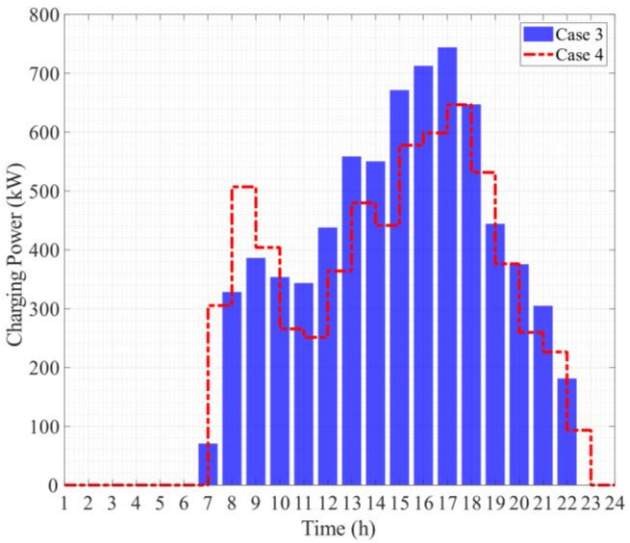

(d) MEMG 4

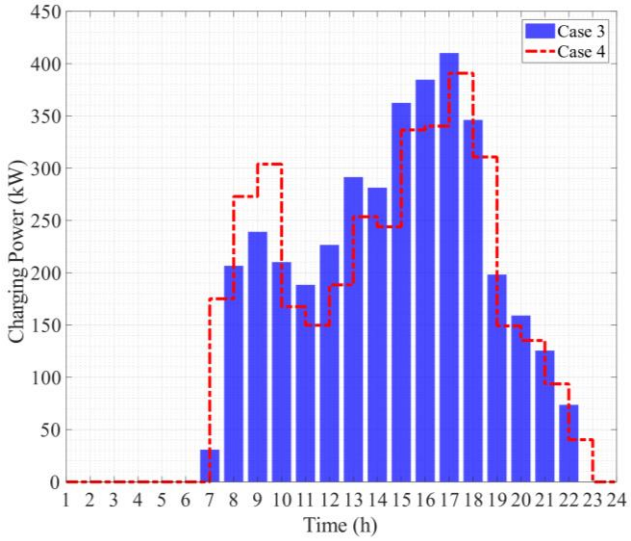

(e) MEMG 5

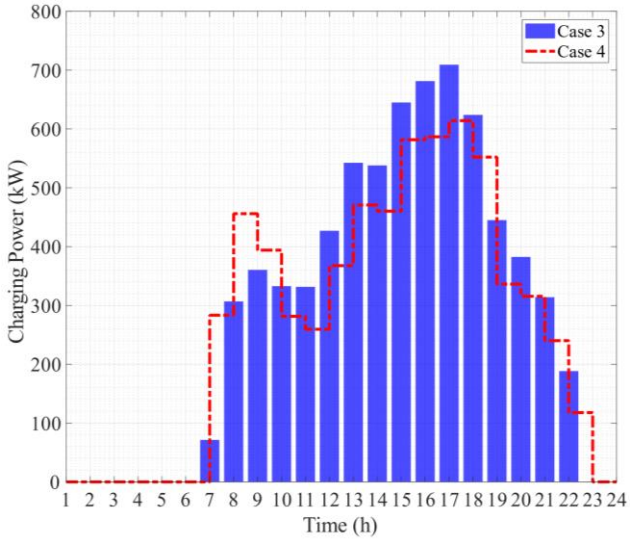

(f) MEMG 6

Fig. 14. The operating point of the charging stations: CS3 and CS4

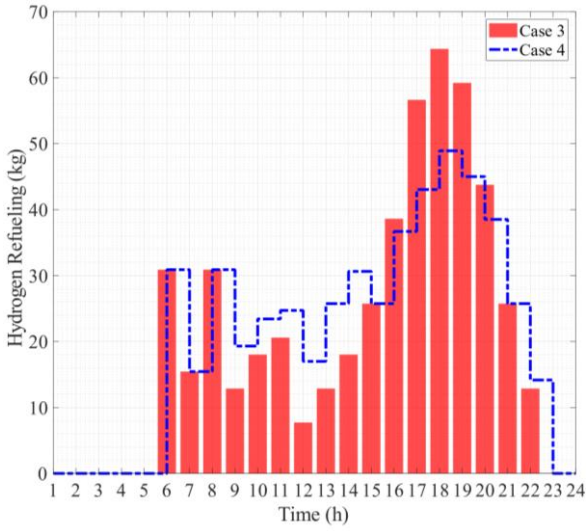

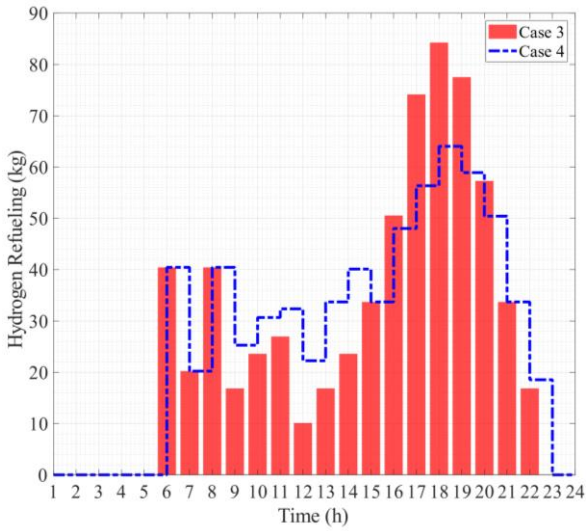

(a) MEMG 1

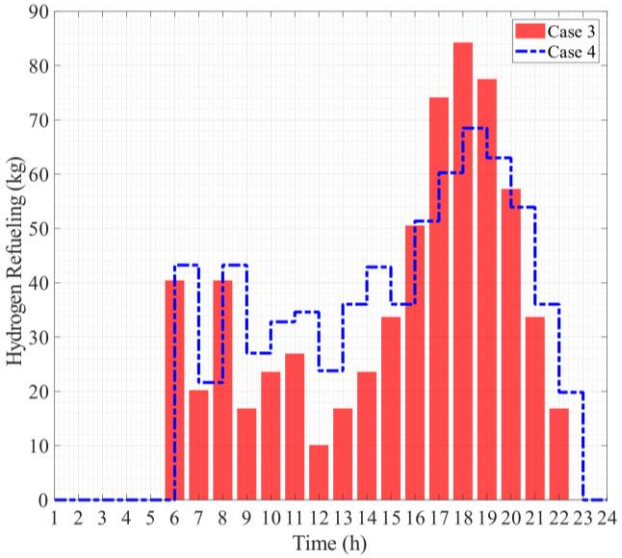

(b) MEMG 2

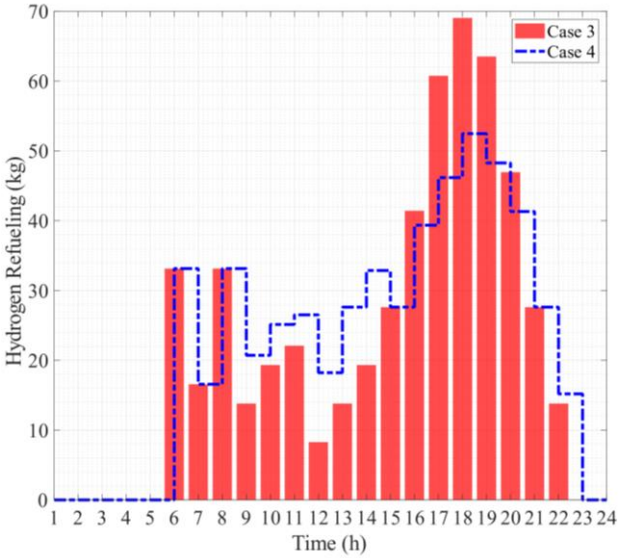

(c) MEMG 3

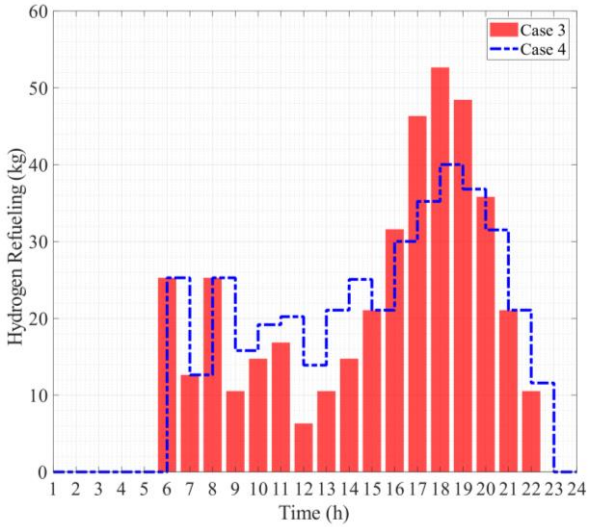

(d) MEMG 4

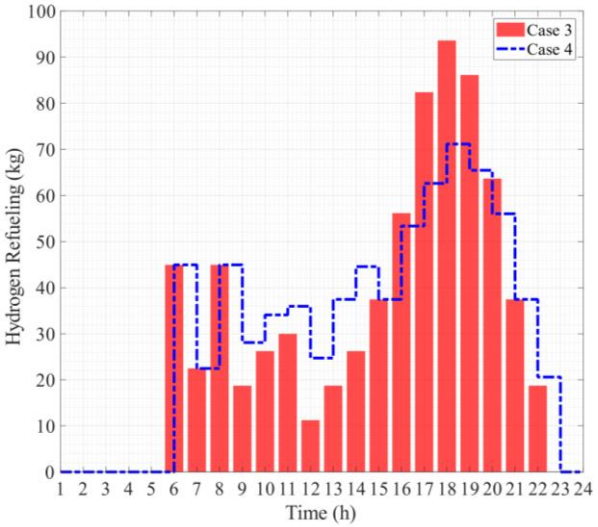

(e) MEMG 5

(f) MEMG 6

Fig. 15. The operating point of the hydrogen refueling stations: CS3 and CS4

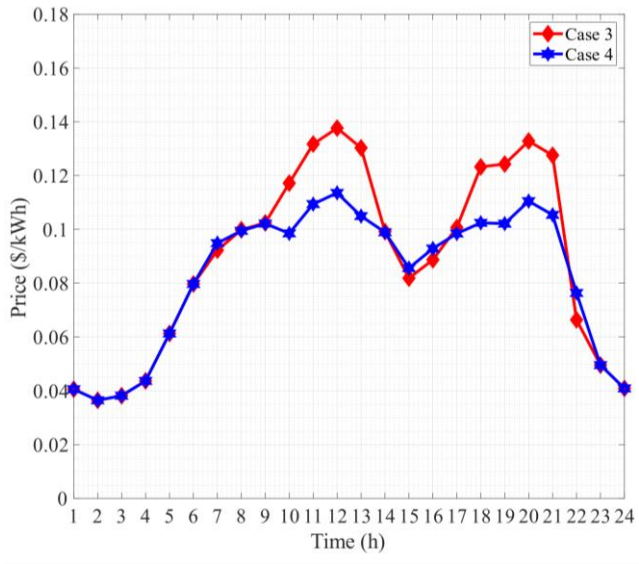

(a) Clearing price in the electricity market

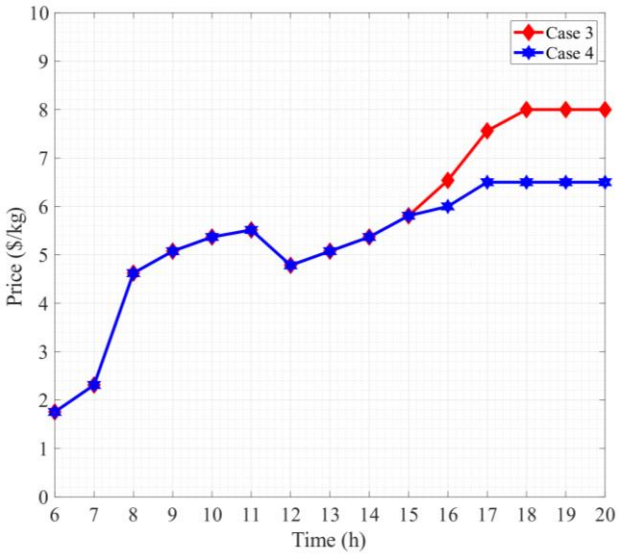

(b) Clearing price in the hydrogen market

Fig. 16. Market-clearing prices in electricity and hydrogen markets: CS3 and CS4

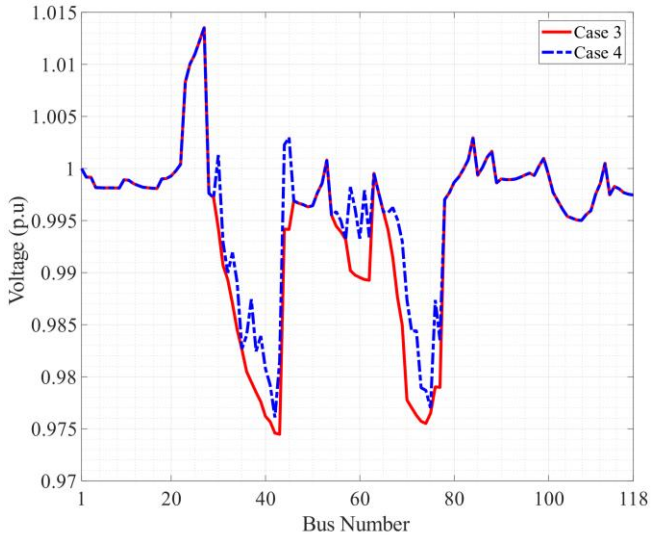

(a) Voltage magnitude at 21:00

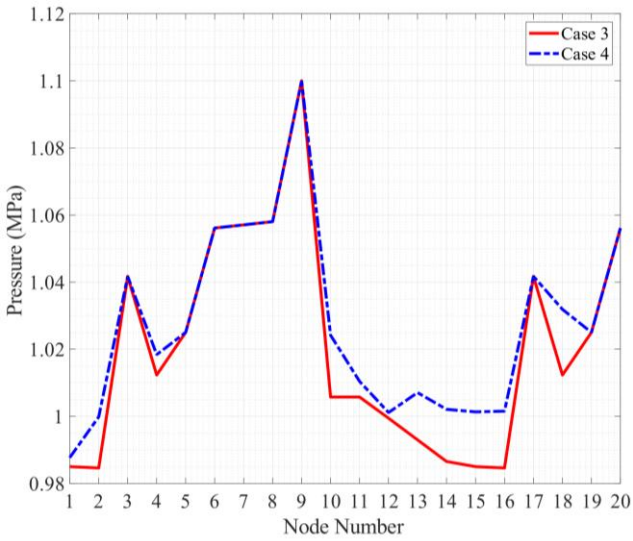

(b) Gas pressure at 22:00

Fig. 17. Voltage magnitude and gas pressure in electricity and gas networks: CS3 and CS4

5.5. Results for Case Study 5

In CS5, smart home scheduling is done considering the residents' comfortable lifestyle. To this end, the upper limit of the residents' dissatisfaction index is set at 15%. The results of this case are presented in Table 13, the evaluation of which shows the increase in the daily costs of smart homes and MEMGs.

Numerical results reveal that the total daily costs of smart homes in CS5 have increased by 6.43% compared to CS4, which is due to the reduction of the participation of these customers in DR schemes. In other words, limiting the residents' dissatisfaction index does not allow smart homes to deviate much from their preferred schedules. Figure 18 compares the residents' dissatisfaction index in Case studies 4 and 5, which confirms the decrease of this index in CS5. Figures 19a and 19b depict the clearing prices of electricity and heat markets in Cases 4 and 5. Analysis of these figures confirms that the comfortable lifestyle of smart homes in CS5 has led to increased clearing prices in the abovementioned markets.

Table 13 presents the schedules obtained for IoT-based appliances of a smart home placed in MEMG 6. According to this table, the schedules obtained for this customer in CS1 and CS2 are the same, which is due to the absence of DR schemes in these cases. It should be stated that due to the absence of DR schemes in these cases, smart homes did not change the operation time of their appliances, and therefore all appliances were activated in their preferred time range. The results of Table 14 also reveal that the participation of smart homes in DR schemes in CS3 and CS4 has led to the activation of seven appliances outside of their preferred time range. Note that the activation of these appliances outside the preferred time range of residents leads to an increase in the dissatisfaction index. Lastly, it can be observed from Table 13 that in CS5, where residents' comfortable lifestyle is considered in the model, more appliances are activated within the preferred time range of customers compared to CS3 and CS4, and subsequently, their dissatisfaction index has decreased. In other words, the results reflect that considering the residents' comfortable lifestyle in CS5, has led to lower participation of smart houses in DR schemes than in CS3 and CS4.

Table 13. Scheduling results for CS5

MEMGs	**Daily Costs ($/day)**						
	Components	**Energy Transactions**			**Smart Homes**	**Ch. / Ref. Stations**	**Sum**
		Electricity	**Heating**	**Hydrogen**			
MEMG 1	441.2	2677.4	-13925.46	-1405.19	3147.27	2594.5	-6470.28
MEMG 2	759.42	3882.79	39069.77	4191.82	4074.78	3730.37	55708.95
MEMG 3	1885.63	8379.18	90103.17	4400.66	9286.32	4160.33	118215.29
MEMG 4	1360.27	9510.9	-20749.51	3557.72	9952.07	3527.6	7159.05
MEMG 5	480.66	2334	25624.39	3142.54	2560.62	2502.13	36644.34

MEMG 6	1960.17	8358.81	-36315.95	-1668.4	8866.91	4133.36	-14665.1
Total	6887.35	35143.08	83806.41	12219.15	37887.97	20648.29	196592.25

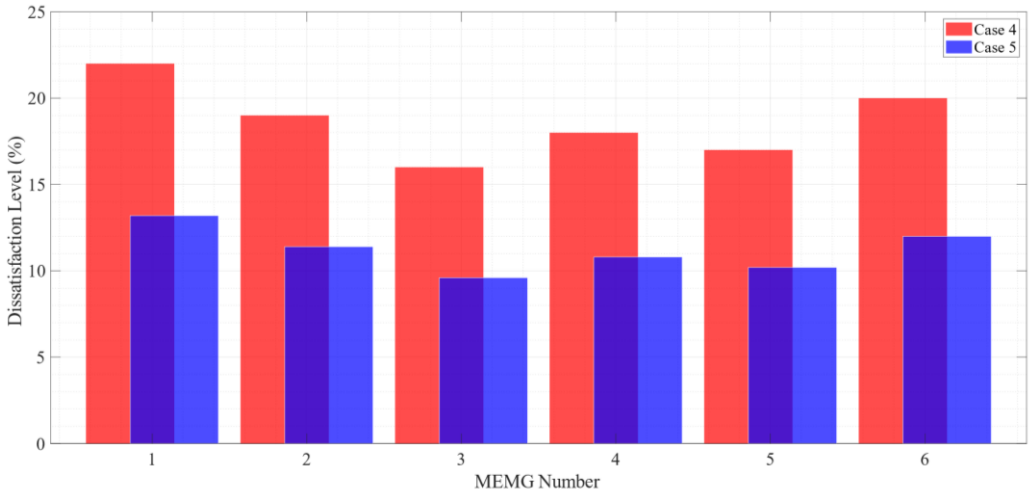

Fig. 18. Dissatisfaction level of smart homes residents: CS4 and CS5

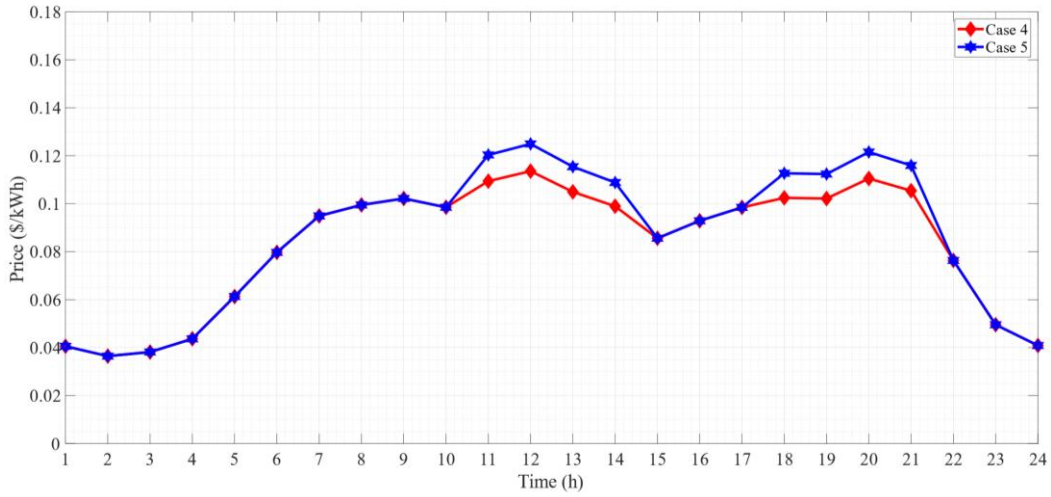

(a) Electricity market

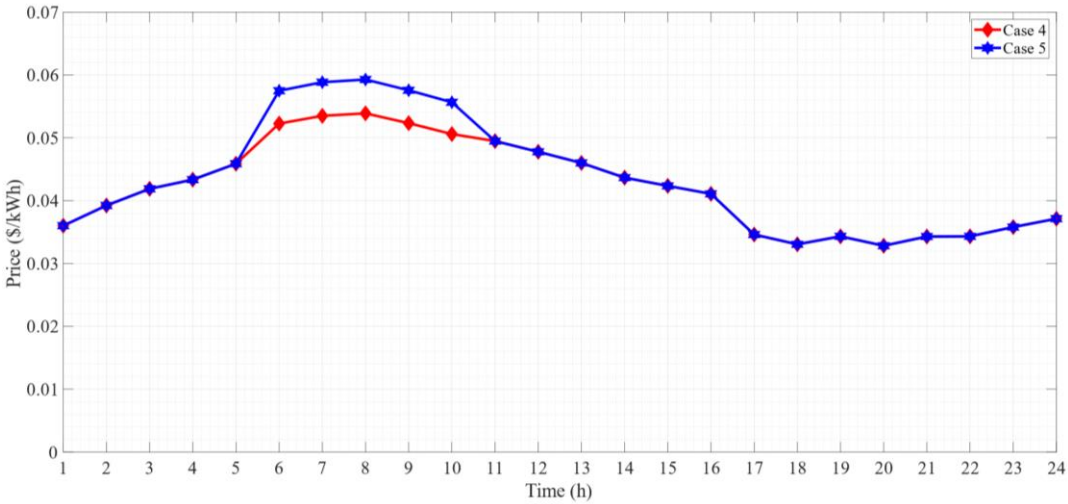

(b) Heating market

Fig. 19. Clearing prices in different markets: CS4 and CS5

Table 14. The programs obtained for the appliances of a smart home in the MEMG 5

Appliances	Preferred Time (h)		CS1	CS2	CS3	CS4	CS5
	Start	End					
Washing Machine	10	11	10-11	10-11	1-2	1-2	10-11
Clothes Dryer	12	13	12	12	3-4	3-4	13
Dishwasher	15	16	15-16	15-16	16-17	16-17	11-12
Refrigerator	1	24	1-24	1-24	1-24	1-24	1-24
Television	18	22	17-20	17-20	17-20	17-20	17-20
Lights	8	24	8-23	8-23	8-23	8-23	8-23
Rice Cooker	12	13	13	13	14	14	12
Kettle	7	8	7-8	7-8	6-7	6-7	7-8
Toaster	7	7	7	7	7	7	8
Microwave	11	13	12-13	12-13	21-22	21-22	20-21
Iron	6	6	1	1	1	1	8

6. Conclusion

A hierarchical framework for simultaneous management of fully competitive electricity, heat and hydrogen markets considering smart prosumers was introduced in this work. In the proposed model, MEMGs made their market strategy in a decentralized framework and according to the schedules of smart prosumers including smart homes, smart charging stations and smart hydrogen refueling stations. The proposed MILP model was tested under several case studies, and its noticeable results are summarized as follows:

- An IGDT risk-averse strategy was utilized to manage the scheduling risk of MEMGs, and the simulation results revealed that this strategy secured the scheduling against uncertainties despite increasing the daily costs by 11.95%. The results mirrored that in the risk-averse scheduling, uncertain parameters can fluctuate in a safe area without imposing more costs on the system.
- A novel prediction-based mechanism for designing DR schemes adapted to prosumers behavior was presented, which implementation on electrical and heating loads reduced the clearing prices of electricity and heat markets by 17.5% and 8.78% during peak hours, respectively. The results also confirmed that modifying the behavior of EVs / FCVs through incentive schemes improved the technical and economic indicators of MES.

- The results revealed that smart homes can provide significant flexibility for MES by controlling their IoT-based appliances. Although the results showed that providing a comfortable lifestyle for these customers caused a relative increase in the clearing prices of electricity and heat markets.
- A transport system-based structure for hydrogen exchange between MEMGs was introduced, and simulation results proved its ability to be implemented in modern competitive markets. Analysis of the results also illustrated that this system handled all hydrogen exchanges during the peak period.

Overall, the results substantiated that the proposed hierarchical concept, by taking advantage of the potential of smart prosumers, has high flexibility for optimal and sustainable management of the competitive markets of electricity, heat, and hydrogen.

Acknowledgment

This work is supported by DTE Network+ funded by EPSRC grant reference EP/S032053/1.

References

[1] Good N, Martínez Ceseña EA, Zhang L, Mancarella P. Techno-economic and business case assessment of low carbon technologies in distributed multi-energy systems. Appl Energy 2016;167:158–72. https://doi.org/https://doi.org/10.1016/j.apenergy.2015.09.089.

[2] Klemm C, Vennemann P. Modeling and optimization of multi-energy systems in mixed-use districts: A review of existing methods and approaches. Renew Sustain Energy Rev 2021;135:110206. https://doi.org/https://doi.org/10.1016/j.rser.2020.110206.

[3] Zhang X, Bauer C, Mutel CL, Volkart K. Life Cycle Assessment of Power-to-Gas: Approaches, system variations and their environmental implications. Appl Energy 2017;190:326–38. https://doi.org/https://doi.org/10.1016/j.apenergy.2016.12.098.

[4] Xi Y, Fang J, Chen Z, Lund H, Thomsen SM, Dyrelund A, et al. Integrated Flexible Resources

and Energy Markets in the Danish Multi-energy System. 2019 IEEE Innov. Smart Grid Technol. - Asia (ISGT Asia), 2019, p. 3099–103. https://doi.org/10.1109/ISGT-Asia.2019.8881491.

[5] Hemmati R, Mehrjerdi H, Nosratabadi SM. Resilience-oriented adaptable microgrid formation in integrated electricity-gas system with deployment of multiple energy hubs. Sustain Cities Soc 2021;71:102946. https://doi.org/https://doi.org/10.1016/j.scs.2021.102946.

[6] Kostelac M, Pavić I, Zhang N, Capuder T. Uncertainty modelling of an industry facility as a multi-energy demand response provider. Appl Energy 2022;307:118215. https://doi.org/https://doi.org/10.1016/j.apenergy.2021.118215.

[7] Mansouri SA, Ahmarinejad A, Javadi MS, Nezhad AE, Shafie-Khah M, Catalão JPS. Demand response role for enhancing the flexibility of local energy systems. In: Graditi G, Di Somma MBT-DER in LIES, editors. Distrib. Energy Resour. Local Integr. Energy Syst. Optim. Oper. Plan., Elsevier; 2021, p. 279–313. https://doi.org/10.1016/B978-0-12-823899-8.00011-X.

[8] Hemmati R, Faraji H. Identification of cyber-attack/outage/fault in zero-energy building with load and energy management strategies. J Energy Storage 2022;50:104290. https://doi.org/https://doi.org/10.1016/j.est.2022.104290.

[9] Qolomany B, Al-Fuqaha A, Gupta A, Benhaddou D, Alwajidi S, Qadir J, et al. Leveraging Machine Learning and Big Data for Smart Buildings: A Comprehensive Survey. IEEE Access 2019;7:90316–56. https://doi.org/10.1109/ACCESS.2019.2926642.

[10] Mehrjerdi H, Hemmati R, Mahdavi S, Shafie-Khah M, Catalão JPS. Multicarrier Microgrid Operation Model Using Stochastic Mixed Integer Linear Programming. IEEE Trans Ind Informatics 2022;18:4674–87. https://doi.org/10.1109/TII.2021.3121333.

[11] Mansouri SA, Nematbakhsh E, Jordehi AR, Tostado-Veliz M, Jurado F, Leonowicz Z. A Risk-Based Bi-Level Bidding System to Manage Day-Ahead Electricity Market and Scheduling of Interconnected Microgrids in the presence of Smart Homes. 2022 IEEE Int. Conf. Environ. Electr. Eng. 2022 IEEE Ind. Commer. Power Syst. Eur. (EEEIC / I&CPS Eur., 2022, p. 1–6.

https://doi.org/10.1109/eeeic/icpseurope54979.2022.9854685.

[12] Coelho A, Iria J, Soares F. Network-secure bidding optimization of aggregators of multi-energy systems in electricity, gas, and carbon markets. Appl Energy 2021;301:117460. https://doi.org/https://doi.org/10.1016/j.apenergy.2021.117460.

[13] Bao S, Yang Z, Yu J. Decomposition and analysis of marginal prices in multi-energy systems. Energy 2021;221:119814. https://doi.org/https://doi.org/10.1016/j.energy.2021.119814.

[14] Najafi A, Pourakbari-Kasmaei M, Jasinski M, Lehtonen M, Leonowicz Z. A max–min–max robust optimization model for multi-carrier energy systems integrated with power to gas storage system. J Energy Storage 2022;48:103933. https://doi.org/https://doi.org/10.1016/j.est.2021.103933.

[15] Mokaramian E, Shayeghi H, Sedaghati F, Safari A, Alhelou HH. A CVaR-Robust-Based Multi-Objective Optimization Model for Energy Hub Considering Uncertainty and E-Fuel Energy Storage in Energy and Reserve Markets. IEEE Access 2021;9:109447–64. https://doi.org/10.1109/access.2021.3100336.

[16] Zhu X, Sun Y, Yang J, Dou Z, Li G, Xu C, et al. Day-ahead energy pricing and management method for regional integrated energy systems considering multi-energy demand responses. Energy 2022;251:123914. https://doi.org/https://doi.org/10.1016/j.energy.2022.123914.

[17] Mirzaei MA, Ahmadian A, Mohammadi-Ivatloo B, Zare K, Elkamel A. A mixed conditional value-at-risk/information gap decision theory framework for optimal participation of a multi-energy distribution system in multiple energy markets. J Clean Prod 2022:133283. https://doi.org/https://doi.org/10.1016/j.jclepro.2022.133283.

[18] Tostado-Véliz M, Kamel S, Hasanien HM, Turky RA, Jurado F. A mixed-integer-linear-logical programming interval-based model for optimal scheduling of isolated microgrids with green hydrogen-based storage considering demand response. J Energy Storage 2022;48:104028. https://doi.org/10.1016/j.est.2022.104028.

[19] Bahmanyar D, Razmjooy N, Mirjalili S. Multi-objective scheduling of IoT-enabled smart homes for energy management based on Arithmetic Optimization Algorithm: A Node-RED and NodeMCU module-based technique. Knowledge-Based Syst 2022;247:108762. https://doi.org/https://doi.org/10.1016/j.knosys.2022.108762.

[20] Ramadan R, Huang Q, Bamisile O, Zalhaf AS. Intelligent home energy management using Internet of Things platform based on NILM technique. Sustain Energy, Grids Networks 2022;31:100785. https://doi.org/https://doi.org/10.1016/j.segan.2022.100785.

[21] Chaouch H, Çeken C, Arı S. Energy management of HVAC systems in smart buildings by using fuzzy logic and M2M communication. J Build Eng 2021;44:102606. https://doi.org/https://doi.org/10.1016/j.jobe.2021.102606.

[22] Esmaeel Nezhad A, Rahimnejad A, Gadsden SA. Home energy management system for smart buildings with inverter-based air conditioning system. Int J Electr Power Energy Syst 2021;133:107230. https://doi.org/https://doi.org/10.1016/j.ijepes.2021.107230.

[23] Mansouri SA, Ahmarinejad A, Nematbakhsh E, Javadi MS, Jordehi AR, Catalão JPS. Energy management in microgrids including smart homes: A multi-objective approach. Sustain Cities Soc 2021;69:102852. https://doi.org/10.1016/j.scs.2021.102852.

[24] Mansouri SA, Ahmarinejad A, Nematbakhsh E, Javadi MS, Esmaeel Nezhad A, Catalão JPS. A sustainable framework for multi-microgrids energy management in automated distribution network by considering smart homes and high penetration of renewable energy resources. Energy 2022:123228. https://doi.org/https://doi.org/10.1016/j.energy.2022.123228.

[25] Alabi TM, Aghimien EI, Agbajor FD, Yang Z, Lu L, Adeoye AR, et al. A review on the integrated optimization techniques and machine learning approaches for modeling, prediction, and decision making on integrated energy systems. Renew Energy 2022;194:822–49. https://doi.org/https://doi.org/10.1016/j.renene.2022.05.123.

[26] Xuan W, Shouxiang W, Qianyu Z, Shaomin W, Liwei F. A multi-energy load prediction model

based on deep multi-task learning and ensemble approach for regional integrated energy systems. Int J Electr Power Energy Syst 2021;126:106583. https://doi.org/https://doi.org/10.1016/j.ijepes.2020.106583.

[27] Zhou B, Meng Y, Huang W, Wang H, Deng L, Huang S, et al. Multi-energy net load forecasting for integrated local energy systems with heterogeneous prosumers. Int J Electr Power Energy Syst 2021;126:106542. https://doi.org/https://doi.org/10.1016/j.ijepes.2020.106542.

[28] Zhang G, Bai X, Wang Y. Short-time multi-energy load forecasting method based on CNN-Seq2Seq model with attention mechanism. Mach Learn with Appl 2021;5:100064. https://doi.org/https://doi.org/10.1016/j.mlwa.2021.100064.

[29] Zhang H, Chen Y, Liu K, Dehan S. A novel power system scheduling based on hydrogen-based micro energy hub. Energy 2022;251:123623. https://doi.org/10.1016/j.energy.2022.123623.

[30] Mansouri SA, Nematbakhsh E, Ahmarinejad A, Jordehi AR, Javadi MS, Matin SAA. A Multi-objective dynamic framework for design of energy hub by considering energy storage system, power-to-gas technology and integrated demand response program. J Energy Storage 2022;50:104206. https://doi.org/10.1016/j.est.2022.104206.

[31] Mei J, Zuo Y, Lee CHT, Wang X, Kirtley JL. Stochastic optimization of multi-energy system operation considering hydrogen-based vehicle applications. Adv Appl Energy 2021;2:100031. https://doi.org/10.1016/j.adapen.2021.100031.

[32] Xu Y-P, Liu R-H, Tang L-Y, Wu H, She C. Risk-averse multi-objective optimization of multi-energy microgrids integrated with power-to-hydrogen technology, electric vehicles and data center under a hybrid robust-stochastic technique. Sustain Cities Soc 2022;79:103699. https://doi.org/https://doi.org/10.1016/j.scs.2022.103699.

[33] Godazi Langeroudi AS, Sedaghat M, Pirpoor S, Fotouhi R, Ghasemi MA. Risk-based optimal operation of power, heat and hydrogen-based microgrid considering a plug-in electric vehicle. Int J Hydrogen Energy 2021;46:30031–47. https://doi.org/10.1016/j.ijhydene.2021.06.062.

[34] Zhou L, Zhang F, Wang L, Zhang Q. Flexible hydrogen production source for fuel cell vehicle to reduce emission pollution and costs under the multi-objective optimization framework. J Clean Prod 2022;337:130284. https://doi.org/10.1016/j.jclepro.2021.130284.

[35] Lai C-M, Teh J. Comprehensive review of the dynamic thermal rating system for sustainable electrical power systems. Energy Reports 2022;8:3263–88. https://doi.org/https://doi.org/10.1016/j.egyr.2022.02.085.

[36] Teh J, Lai C-M. Reliability impacts of the dynamic thermal rating and battery energy storage systems on wind-integrated power networks. Sustain Energy, Grids Networks 2019;20:100268. https://doi.org/https://doi.org/10.1016/j.segan.2019.100268.

[37] Lai C-M, Teh J. Network topology optimisation based on dynamic thermal rating and battery storage systems for improved wind penetration and reliability. Appl Energy 2022;305:117837. https://doi.org/https://doi.org/10.1016/j.apenergy.2021.117837.

[38] Lawal OA, Teh J. Assessment of dynamic line rating forecasting methods. Electr Power Syst Res 2023;214:108807. https://doi.org/https://doi.org/10.1016/j.epsr.2022.108807.

[39] Jimada-Ojuolape B, Teh J. Impacts of Communication Network Availability on Synchrophasor-Based DTR and SIPS Reliability. IEEE Syst J 2021:1–12. https://doi.org/10.1109/JSYST.2021.3122022.

[40] Jimada-Ojuolape B, Teh J. Composite Reliability Impacts of Synchrophasor-Based DTR and SIPS Cyber–Physical Systems. IEEE Syst J 2022;16:3927–38. https://doi.org/10.1109/JSYST.2021.3132657.

[41] Jimada-Ojuolape B, Teh J. Surveys on the reliability impacts of power system cyber–physical layers. Sustain Cities Soc 2020;62:102384. https://doi.org/https://doi.org/10.1016/j.scs.2020.102384.

[42] Zhang D, Fu Z, Zhang L. An improved TS algorithm for loss-minimum reconfiguration in large-scale distribution systems. Electr Power Syst Res 2007;77:685–94.

https://doi.org/10.1016/j.epsr.2006.06.005.

[43] Li X, Li W, Zhang R, Jiang T, Chen H, Li G. Collaborative scheduling and flexibility assessment of integrated electricity and district heating systems utilizing thermal inertia of district heating network and aggregated buildings. Appl Energy 2020;258:114021. https://doi.org/https://doi.org/10.1016/j.apenergy.2019.114021.

[44] Gu C, Zhang Y, Wang J, Li Q. Joint planning of electrical storage and gas storage in power-gas distribution network considering high-penetration electric vehicle and gas vehicle. Appl Energy 2021;301:117447. https://doi.org/https://doi.org/10.1016/j.apenergy.2021.117447.

[45] Subbiah SS, Chinnappan J. Deep learning based short term load forecasting with hybrid feature selection. Electr Power Syst Res 2022;210:108065. https://doi.org/https://doi.org/10.1016/j.epsr.2022.108065.

[46] Ma S, Su L, Wang Z, Qiu F, Guo G. Resilience Enhancement of Distribution Grids Against Extreme Weather Events. IEEE Trans Power Syst 2018;33:4842–53. https://doi.org/10.1109/TPWRS.2018.2822295.

[47] Mansouri SA, Nematbakhsh E, Ahmarinejad A, Jordehi AR, Javadi MS, Marzband M. A hierarchical scheduling framework for resilience enhancement of decentralized renewable-based microgrids considering proactive actions and mobile units. Renew Sustain Energy Rev 2022;168:112854. https://doi.org/10.1016/j.rser.2022.112854.

[48] Mansouri SA, Ahmarinejad A, Javadi MS, Catalão JPS. Two-stage stochastic framework for energy hubs planning considering demand response programs. Energy 2020;206:118124. https://doi.org/10.1016/j.energy.2020.118124.

[49] Wu X, Qi S, Wang Z, Duan C, Wang X, Li F. Optimal scheduling for microgrids with hydrogen fueling stations considering uncertainty using data-driven approach. Appl Energy 2019;253:113568. https://doi.org/https://doi.org/10.1016/j.apenergy.2019.113568.

[50] Kim HJ, Kim MK. Risk-based hybrid energy management with developing bidding strategy and

advanced demand response of grid-connected microgrid based on stochastic/information gap decision theory. Int J Electr Power Energy Syst 2021;131:107046. https://doi.org/https://doi.org/10.1016/j.ijepes.2021.107046.